Final Technical Report

Project Title: Critical Research for Cost-Effective Photoelectrochemical Production of Hydrogen

Project Period: April 1, 2005 to July 31, 2014
Reporting Period: April 1, 2005 to July 31, 2014
Date of Report: October 29, 2014
Award Number: DE-FG36-05GO15028
Recipient: Midwest Optoelectronics, LLC (MWOE)
Xunlight Corporation (Xunlight)
University of Toledo (UT)
National Renewable Energy Laboratory (NREL)

Project Participants: MWOE: L. Xu, A. Abken, W. Du, S. Cao

Xunlight: A. Vijh

UT: X. Deng, W. Ingler, C. Chen, X. Liao, Q. Fan, L. Anderson, Y. Yan,

R. Collins, D. Giolando, A. Compaan

NREL: J. Turner

Principal Investigator: Liwei Xu - MWOE

Main Contact: Liwei Xu (Primary Contact)

2600 Dorr Street, Toledo, Ohio 43606
Ph: (419) 215-8583
E-mail: xu@mwoe.com

Addresses: Midwest Optoelectronics, LLC, 2600 Dorr Street, Toledo, Ohio 43606
Contact: Liwei Xu; E-mail: xu@mwoe.com
Ph: (419) 215-8583

University of Toledo, 2801 W. Bancroft St. Toledo, Ohio 43606
Contact: Yanfa Yan.; E-mail: Yanfa.Yan@utoledo.edu
Ph: (419) 530-5335; Fax: (419) 530-2723;

National Renewable Energy Lab, 1617 Cole Blvd, Golden, CO
Contact: John Turner; E-mail: jturner@nrel.gov
Ph: (303) 275-4270; Fax: (303) 275-3033;

DOE Managers: Eric Miller, DOE HQ Technology Manager

David Peterson, DOE Field Project Officer

Table of Contents

List of Figures

List of Tables

1. Executive Summary

The objective of this project is to develop critical technologies required for cost-effective production of hydrogen from sunlight and water using a-Si triple junction solar cell based photo-electrodes.

In this project, Midwest Optoelectronics, LLC (MWOE) and its collaborating organizations utilize triple junction a-Si thin film solar cells as the core element to fabricate photoelectrochemical (PEC) cells. Triple junction a-Si/a-SiGe/a-SiGe solar cell is an ideal material for making cost-effective PEC system which uses sun light to split water and generate hydrogen. It has the following key features: 1) It has an open circuit voltage (V_{oc}) of ~ 2.3V and has an operating voltage around 1.6V. This is ideal for water splitting. There is no need to add a bias voltage or to inter-connect more than one solar cell. 2) It is made by depositing a-Si/a-SiGe/aSi-Ge thin films on a conducting stainless steel substrate which can serve as an electrode. When we immerse the triple junction solar cells in an electrolyte and illuminate it under sunlight, the voltage is large enough to split the water, generating oxygen at the Si solar cell side (for SS/n-i-p/sunlight structure) and hydrogen at the back, which is stainless steel side. There is no need to use a counter electrode or to make any wire connection. 3) It is being produced in large rolls of 3ft wide and up to 5000 ft long stainless steel web in a 25MW roll-to-roll production machine. Therefore it can be produced at a very low cost.

However, the a-Si thin film solar cell is not sufficiently stable in the electrolyte which is usually acidic or basic. Without proper protection, it would be corroded by the electrolyte, especially under working conditions. In order to develop a PEC system with the triple junction a-Si solar cells as electrodes, we need to develop a coating which can be applied onto the solar cell surface, and which has the following features: 1) Transparent, so that the light can pass through the coating and reach the solar cells, 2) Conducting, so that the voltage generated by the solar cell under sun light can be applied to the electrolyte-electrode interface to split water, generating hydrogen and oxygen, 3) Corrosion Resistant, so that it can protect the solar cell surface not being corroded in the electrolyte, and 4) can be deposited onto the solar cell surface at 200-250^{o}C or lower, since the solar cell would be damaged if the temperature is higher than 250^{o}C. In addition, it would be very helpful that it can also act as an efficient oxygen evolution catalyst (OER).

After several years of research with many different kinds of material, we have developed promising transparent, conducting and corrosion resistant (TCCR) coating material; we carried out extensive research on oxygen and hydrogen generation catalysts, developed methods to make PEC electrode from production-grade a-Si solar cells; we have designed and tested various PEC module cases and carried out extensive outdoor testing; we were able to obtain a solar to hydrogen conversion efficiency (STH) about 5.7% and a running time about 480 hrs, which are very promising results; we have also completed a techno-economic analysis of our PEC system, which indicates that a projected hydrogen generation cost of $2/gge is achievable with a 50 Ton-per-day (TPD) scale under certain conditions.

Renewable hydrogen generation from sunlight and water is very important for our economy. It helps reduce our dependence on fossil fuels; it reduces emission and global warming; it improves our quality of life by reducing emission from vehicle. Cost effective production of hydrogen from sunlight make it economically feasible for large scale use. Low-cost hydrogen generation is essential for zero-emission fuel cell vehicles to become a reality.

2. Comparison of the Actual Accomplishments with the Goals and Objectives of the Project

We have accomplished the following goals and objectives of this project.

1) We have carried out extensive research on TCCR material and developed high quality TCCR materials, for example, Co_3O_4, with extended stability up to 1,000 hours; it can be deposited at 250 °C or lower; at 70nm, it has a transparency ≥ 90%, and a voltage drop ≤0.15V across the TCCR layer for the TCCR/PV-cell stack under typical PEC device operating conditions.
2) We have carried out extensive research on the hydrogen generation and oxygen generation catalyst materials and developed highly promising catalyst material.
3) We have developed procedures for the fabrication of PEC cells from production-grade a-Si triple junction solar cells. We were able to achieve an initial direct Solar-to-Hydrogen (STH) conversion efficiency of 5.7%, which is, to the best of our knowledge, the highest ever achieved for direct STH efficient for PEC system made using low cost thin film materials without electrical bias.
4) We have successfully transferred the sputtering method to coat Co_3O_4 on solar cells from lab to a proto-type 2 MW roll-to-roll production machine and were able to make PEC electrode on a 91cm wide web.
5) We have designed various types of immersion-type PEC modules, with electrode size vary from 2”x2” to 4”x4”; and carried out extensive outdoor testing.
6) Using Department of Energy (DOE)’s H2A model, we have performed preliminary techno-economic analysis of the immersion-type PEC system based on the concept design. The result indicates that with 50 TPD production scale, generation cost of $2/gge is achievable.
7) During the course of this project, four PCT patent applications and two provisional patent applications have been filed.
8) We have worked with many outside industry and university labs, contributed triple-junction solar cells for the collaborative PEC research, and provided technical support to facilitate the progress of the overall PEC field.
9) We have studied immersion type PEC cells in which one of the voltage-generating junctions is a semiconductor-electrolyte rectifying junction, which is deposited on two semiconductor junctions to produce sufficient voltage for water splitting.
10) We have studied substrate-type PEC cells in which only the SS substrate was in direct contact with electrolyte.

3. Summary of Project objectives, Technical Barriers and Approaches

3.1. Overall Objectives

To develop critical technologies required for cost-effective production of hydrogen from sunlight and water using thin film (tf)-Si based photoelectrodes.

3.2. Technical Barriers

This project addresses the following technical barriers from Section 3.1.5 of the Hydrogen, Fuel Cells and Infrastructure Technologies Program Multi-Year Research, Development and Demonstration Plan:

- AE. Materials Efficiency
- AF. Materials Durability
- AG. Integrated device configuration
- AI: Auxiliary Material
- AJ. Synthesis and manufacturing

3.3. Approaches

Two approaches were taken for the development of efficient and durable photoelectrodes for immersion-type photoelectrochemical cells. In the first approach, shown in Figure 1, triple-junction tf-Si based solar cells (a-Si/a-SiGe/a-SiGe) are used to generate the voltage bias and a transparent, conducting and corrosion resistant (TCCR) coating is deposited on top to protect the semiconductor layer from corrosion while forming an ohmic contact with the electrolyte.

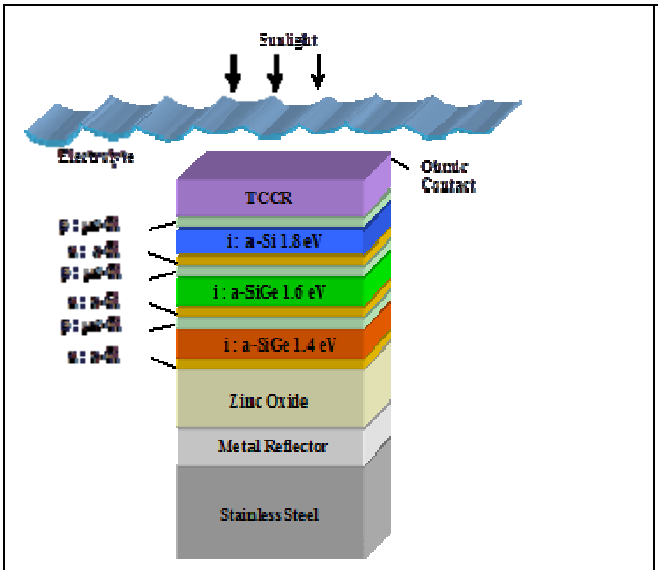

Figure 2: Schematic of PEC electrode with TCCR layer on top of an a-Si triple cell

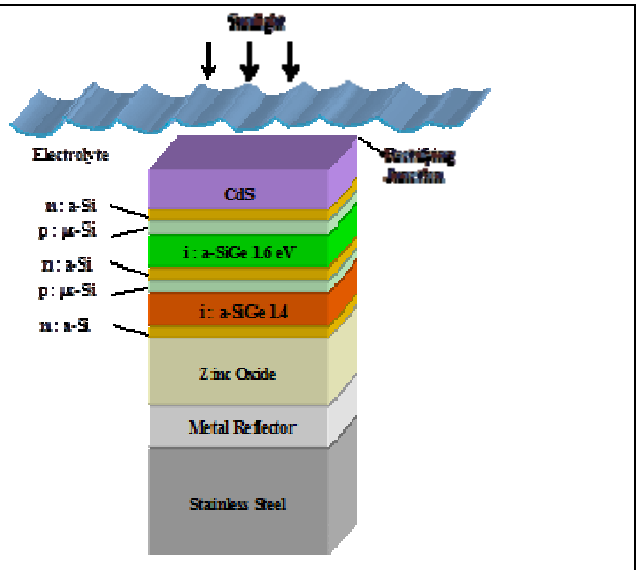

Figure 3: Schematic of hybrid PEC electrode with a photoactive electrode that forms a liquid junction with electrolyte

In the second approach, shown in Figure 2, we used a hybrid structure in which two tf-Si based junctions (middle and bottom junctions of the present triple-junction tf-Si cell) provide a voltage bias (around 1.1V), and a third junction (the top junction) is a rectifying junction between a photo-active semiconductor and the electrolyte.

We also studied and developed substrate-type PEC devices in which only one surface of the PEC cell (the back surface) is in direct contact with the electrolyte and the voltage from the front contact is brought to the back via conducting wires.

Five technical tasks were performed in this project toward the objectives:

Task 1: Transparent, conducting and corrosion resistant coating for triple-junction tf-Si based photoelectrode.

Task 2: Hybrid multi-junction PEC electrode having semiconductor-electrolyte junction.

Task 3: Understanding and characterization of photoelectrochemistry.

Task 4: Fabrication of low-cost, durable and efficient immersion-type PEC cells and systems.

Task 5: Fabrication of substrate-type PEC panels.

4. Summary of Project and Technical Research Activities

4.1. Development of TCCR material

4.1.1 Small-Area Deposition of TCCR Layer

In order for the TCCR layer to work properly for the immersion type PEC cells, it has to meet the following conditions: 1) It has to be corrosion resistant in electrolyte in order to protect the a-Si in the PEC cell assembly to ensure reliable performance for thousands of hours; 2) It can be deposited on top of the a-Si device at temperatures of 250°C or lower in order to avoid any damage of a-Si layer during TCCR deposition; 3) It has to provide transparency of 90% or greater so that most of the light can reach the solar cell; and 4) it has to provide sufficient lateral electrical conductivity for efficient electrolysis of water into hydrogen and oxygen.

Our lab-scale studies covered a variety of oxide materials with the potential of meeting these requirements, including: a) cobolt oxide (Co_3O_4), b) fluorine-doped tin oxide, c) In_2O_3-Fe_2O_3, 4) In_2O_3-$InFe_2O_4$. These materials were deposited in our lab using rf-sputtering.

In a short summary, extensive experiments in our laboratory show that: a) cobolt oxide (Co_3O_4) coatings, when optimized, gives excellent current density and stability; good transparency except in the UV region; and can be made at below 300^{o}C; b) fluorine-doped tin oxide coating did not show good stability in the electrolyte; c) In_2O_3-Fe_2O_3 coating gives short-term stability, excellent conductivity, but its transmission needs improvement; 4) In_2O_3-$InFe_2O_4$ is quite stable under initial trials, shows excellent conductivity, but its transmission needs improvement. Out of all these materials studied, Co_3O_4 seems to be the most promising material. Co_3O_4 has a low band gap of 1.52 eV, it absorbs significant visible light unless the film thickness is kept low. For use as the oxygen evolution catalyst layer, alloying of Co_3O_4 with NiO seems to provide higher current densities without increasing unwanted absorption. Using Co_3O_4 based TCCR materials requires fabricating thin, uniform and void-free Co_3O_4 layer. It is observed that the light-enhancing texture of the back-reflector layer in the a-Si device affects the surface roughness which consequently affects the growth conditions of oxide layer on top. High degree of light-enhancing texture in the a-Si device surface could lead to the formation of voids and defects in the TCCR layer. Therefore, careful optimization is needed in the formation of back reflector and the growth of Co_3O_4 layer so that uniform and void-free Co_3O_4 films can be prepared using rf sputtering on textured a-Si device surface.

For the deposition of Co_3O_4 films, we use a 2" cobalt oxide target purchased from Kurt J. Lesker Company for TCCR layer deposition. Table 1 summarizes the experimental conditions used for small-area Co_3O_4 sputter deposition.

Table 1: Co_3O_4 sputtering conditions

Run	RF power (kW)	sputtering pressure (mTorr)	Ar flow (sccm)	sputtering time (min)
ST986	0.1	8	8	60
ST987	0.1	8	8	30
ST988	0.1	8	8	10
ST990	0.1	8	8	12.5

Borosilicate and TEC15 glass substrates were used for sputtering Co_3O_4 at 250°C; various sputtering times were used as experimental parameter. This experiment was done in order to study the effect of the TCCR layer thickness on transmission and corrosion resistance of Co_3O_4 in electrolyte.

The Co_3O_4 film thickness was determined by using a Dektak^3 ST Surface Profiler (Veeco Instruments Inc); the results from Dektak measurements for Samples ST986 through ST990 are shown in Table 2.

Table 2: Thickness of Co_3O_4 layer

Sample #	sputtering power (kW)	sputtering time (min)	d (nm)
ST986	0.1	60	200
ST987	0.1	30	120
ST988	0.1	10	45
ST990	0.1	12.5	40

Figure 3 shows the UV-vis transmission measurements obtained for Sample ST986 to ST988.

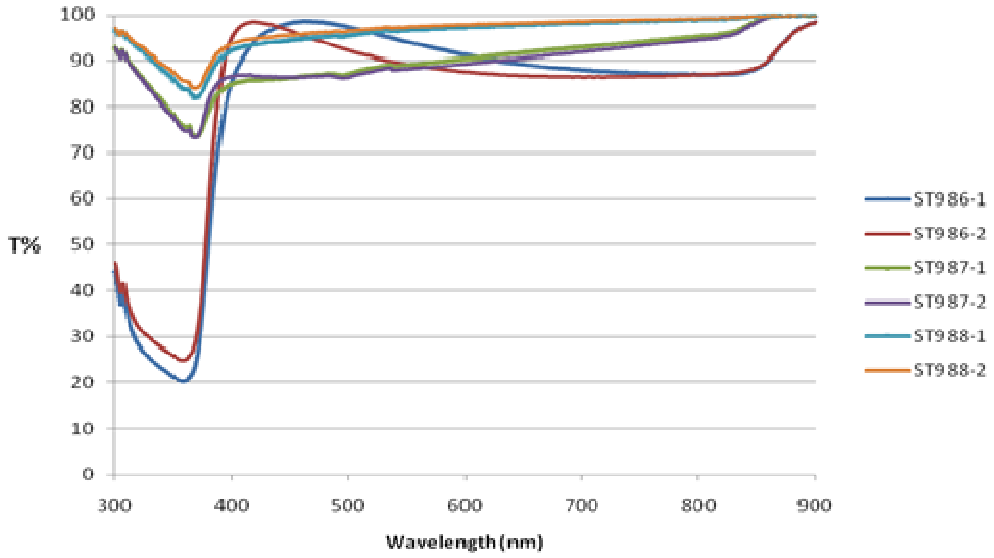

Figure 4: UV-vis transmission vs. wavelength for Co_3O_4 samples (on ITO) with different thickness

From the UV-vis scans, it is observed that all of the films have a desirable high transmission for $\lambda > 400$nm, which is the bulk of photons being absorbed by a-Si solar cells. The reduced absorption for thicker Co_3O_4 films at $\lambda < 400$nm hurts the blue response of the a-Si solar cells and therefore would reduce solar to hydrogen conversion efficiency.

Sample ST988 with a Co_3O_4 thickness of 45 nm shows reduced absorption in the blue region compared to the thicker films, as anticipated. It also has a similar thickness as the

underlying ITO layer (typically 70nm thick). In this study, ST988 was used as a standard reference film for corrosion stability tests and for surface morphology studies.

Co_3O_4 samples sputtered onto TEC glass were immersed into 30% KOH solution, which is a common electrolyte. Sample ST988 was tested for corrosion stability: the stress test in electrolyte uses a bias voltage of 1.8V, which reassembles the voltage at the maximum power point (Vmp) of the PEC electrode under operating conditions; this test was conducted to find out whether the Co_3O_4 TCCR coating is stable for at least 1000hrs, which is the DOE target.

JV-measurements were performed using a Voltalab PGZ 301 Potentiostat and the scans were recorded as a function of biasing time. The current density increases after biasing the sample in electrolyte (see Fig.4): only the first JV-measurement for Co_3O_4 layers before the bias test shows lower current densities than the JV-measurements recorded after biasing the Co_3O_4 in electrolyte. This effect maybe explained by the oxidation of residual Co, which could be incorporated into the Co_3O_4 film during sputtering from a Co_3O_4 (Co) target: Co is oxidized in the electrolyte under biasing conditions. On the other hand, JV-measurements taken after 500, 750, and 1000hrs of biasing do not show significant differences. This indicates that the Co_3O_4 TCCR layer is corrosion resistant under operating conditions of a PEC cell.

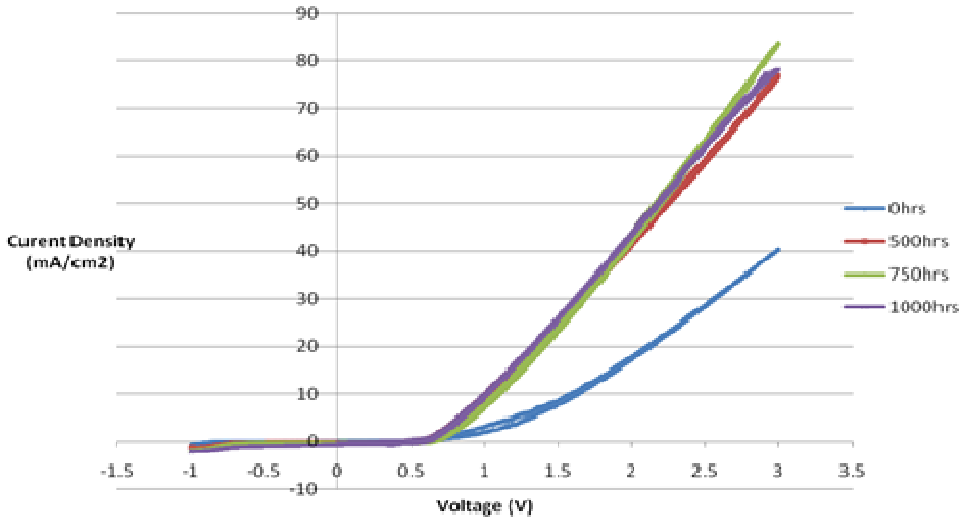

Figure 5: Current density (mA/cm^2) vs. applied voltage (V) for Co_3O_4 TCCR deposited onto TEC15 glass: Sample ST988 after 0, 500, 750 and 1000hrs of biasing;

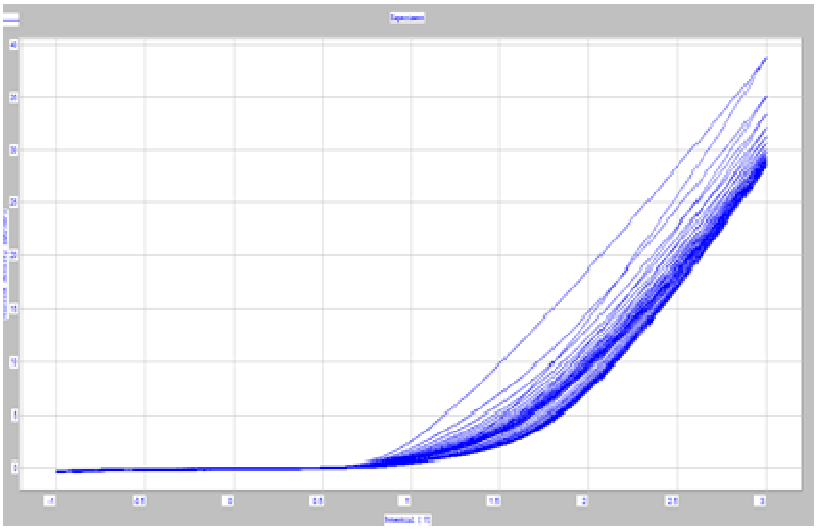

Figure 6: Current density (mA/cm^2) vs. applied voltage (V) for a FTO (TEC 15) sample: 30 scans

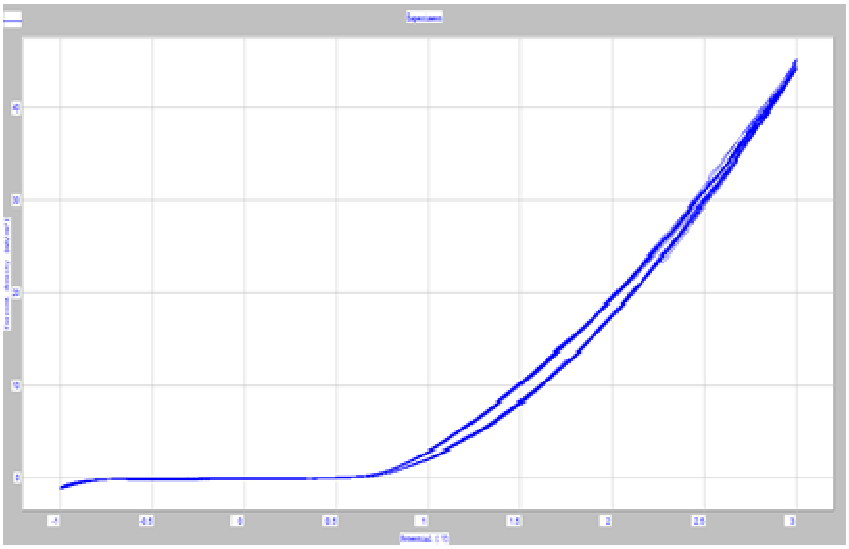

Figure 7: Current density (mA/cm^2) vs. applied voltage (V) for Sample ST988 (Co_3O_4 on TEC15) after biasing in electrolyte for 1000hrs: 30 scans**.**

JV-measurements were recorded for a TEC15 and a Co_3O_4/TEC15 sample, which was biased in electrolyte for 1000hrs; 30 JV-scans were recorded for each sample (see Fig.5 & Fig.6).

JV-measurements of TEC15 (fluorine-doped tin oxide, or, FTO) and Co_3O_4/TEC15 samples show significant differences: the TEC15 sample (Fig. 5) shows noticeable differences in the JV-curve during forward and reverse sweep, which maybe caused by reduction of Sn(+IV) to Sn(+II) (or even to Sn(0)) as TEC15 consists of F:SnO_2 as the TCO layer. Reaction products from the corrosion process are ablated from the glass surface; the corrosion effect leads to a decrease in current density with the increasing JV-sweep number. The experiment was repeated by using multiple sweeps (up to 30 scans), which demonstrates the continuous corrosion of the F:SnO_2 layer. JV-measurements recorded for the Co_3O_4 sample (Fig. 6) do not show any drift or difference between forward and reverse sweep as the Co_3O_4 layer remains stable during the whole cycle.

Noteworthy is, that the Co_3O_4 sample is still corrosion resistant after 1000hrs of biasing in electrolyte.

Comparing the JV-curves obtained for TEC15 and Co_3O_4/TEC15 samples in a range of 1.5-2.0V shows that Co_3O_4 layers provide a much higher current density at the operating voltage of the PEC cell (~1.8V) than TEC15, which uses F:SnO_2 as the TCO layer.

AFM Measurements:

Atomic Force Microscopy (AFM) images of Co_3O_4 layer for Sample ST988 were recorded using Picoscan, before and after biasing the sample in electrolyte for 1000hrs (see Fig.7a and Fig.7b). The scans show comparable roughness of the Co_3O_4 features, which is about 0-20 nm. However, Co_3O_4 features of the biased sample seem to become "smoother" compared to the features observed for a Co_3O_4 sample as grown, while a TEC15 control sample shows a higher micro-roughness of the surface compared to the Co_3O_4/TEC15 samples (see Fig. 8). This smoothening effect might be caused by erosive oxidation or it might be that the incorporated elemental Co is oxidized and, the reaction products are filling up any voids in the Co_3O_4 film. SEM imaging will reveal how the grain structure of the Co_3O_4 layer changes due to biasing in electrolyte.

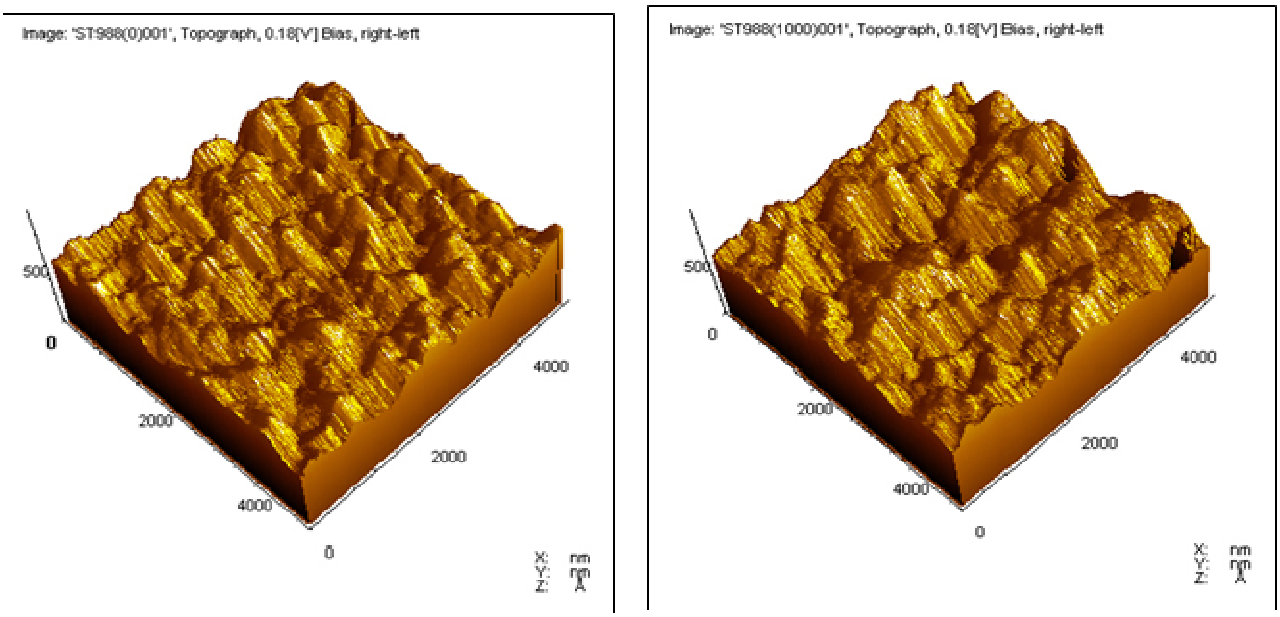

Figure 8: 3D AFM image of Co_3O_4/TEC15 film (Sample ST988): a) as grown (left); and b) after 1000 hrs of biasing (right)

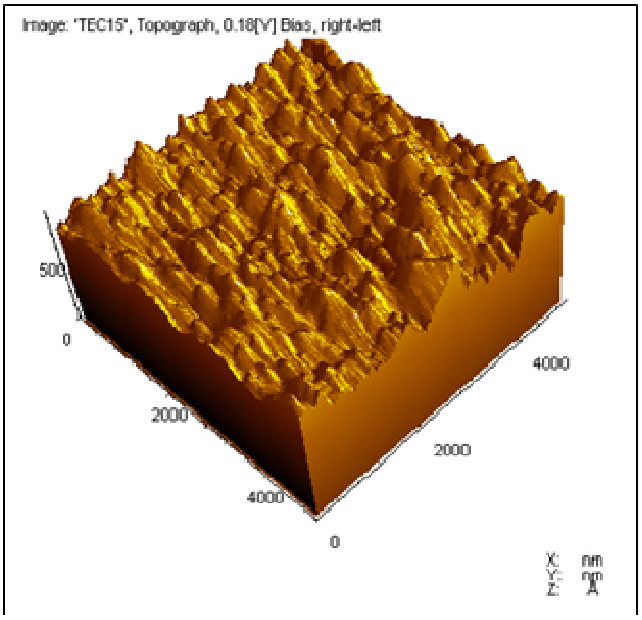

Figure 9: 3D AFM image of FTO (TEC15);

XRD Measurements:

XRD measurements were carried out for the Co_3O_4 sample at the end of 1000 hrs of biasing in the electrolyte. The XRD scan-time was increased to 4 hrs in order to suppress the noise in the measurement. The comparison of the XRD scans taken initially from the Co_3O_4 sample which was normalized and that taken after 500 and 1000 hrs of biasing in the electrolyte, shows that Co_3O_4 films as-grown show peaks of CoO and these peaks disappear after biasing. Since Co_3O_4 is a mixed valence compound, CoO (c) and Co_2O_3 (b) peaks together, as labeled in the Figure 9, is the evidence of Co_3O_4.

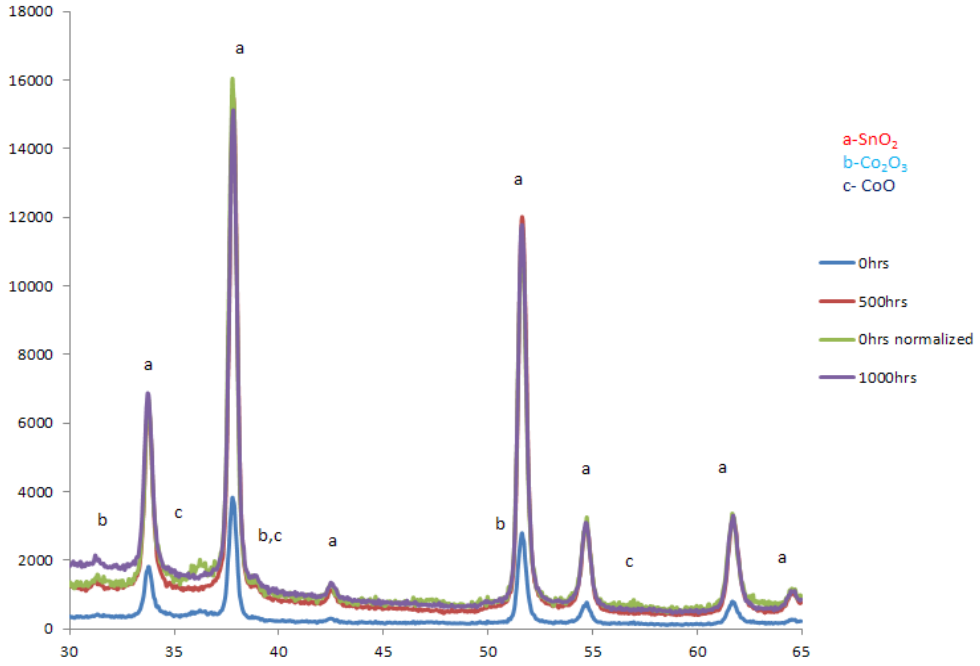

Figure 10: XRD measurements for Sample ST 988 at 0, 500, and 1000 hrs of biasing in the electrolyte;

SEM Measurements:

Scanning Electron Microscopy (SEM) imaging reveals how the grain structure of the Co_3O_4 layer changes due to biasing in electrolyte. As shown in Figure 10, SEM images of the Co_3O_4 layer for Sample ST988 were recorded using a Hitachi S-4800, before and after being put under a voltage (biasing) in electrolyte for 1000 hrs. EDS measurements taken for ST988 after biasing in the electrolyte for 1000 hrs, (shown in Fig. 11) proves the existence of Co_3O_4 layer deposited onto the fluorine doped tin oxide FTO ($F:SnO_2$). Even after stressing the sample in the electrolyte under bias for 1000 hrs, peaks measured from Sn, Co and O are found.

While relatively more detailed description of a variety of measurements, including J-V characteristics, AFM, XRD, SEM and EDS measurements, taken before and after 1000 hours bias, is provided above for only one sample (ST988), these measurements were carried out for a large number of samples for different groups of materials under this research. These studies show that Co_3O_4 materials has most desirable characteristics for use as TCCR layer among the group of materials studied.

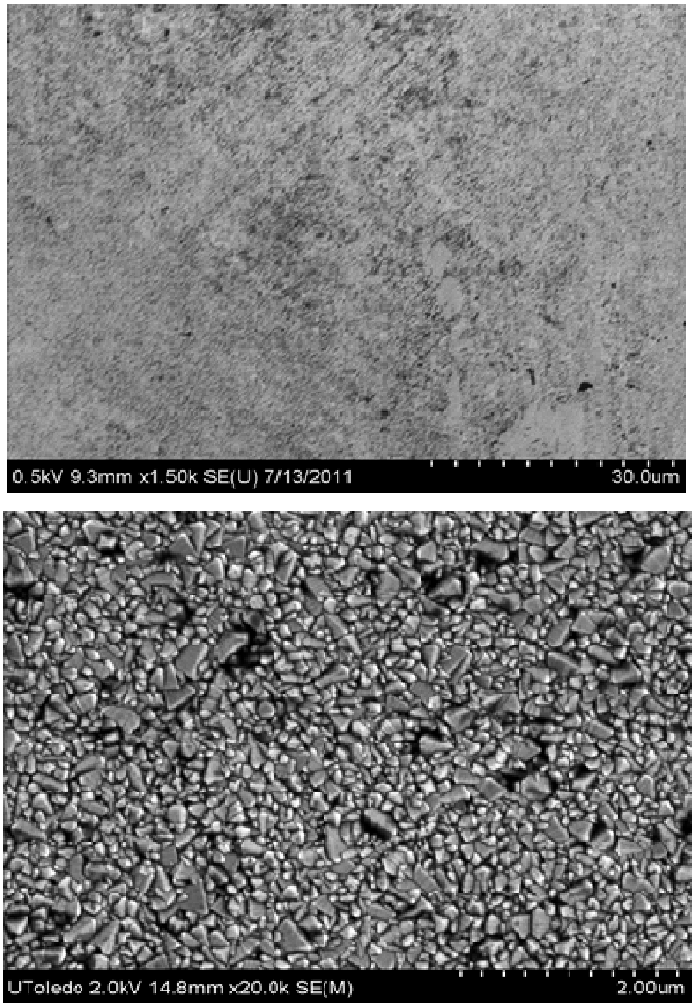

Figure 11: SEM micrograph of Co_3O_4/TEC15 film ST988 as grown (top) and after 1000 hrs of biasing (bottom);

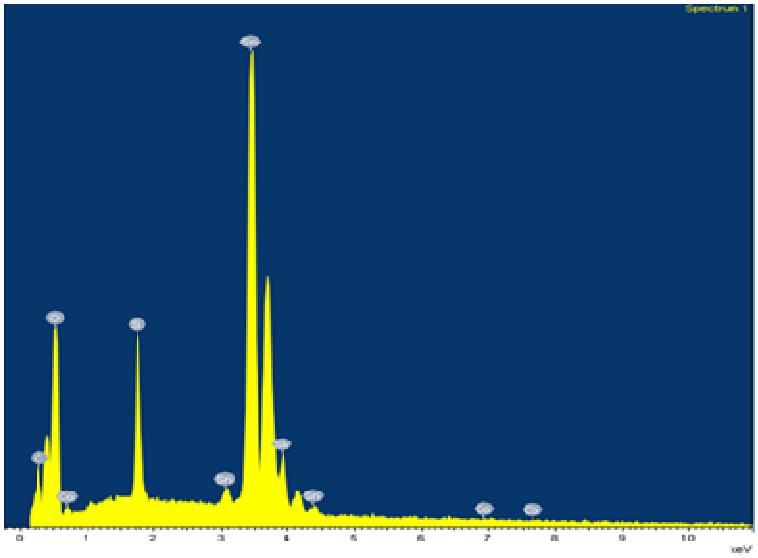

Figure 12: EDS for ST 988 after stressing in the electrolyte for 1000 hrs;

4.1.2 Large-area Deposition of TCCR layer

We have carried out numerous studies on lab-scale equipment to investigate potential TCCR materials for immersion-type triple-junction a-Si PEC cells. These studies have shown many promising results as we described above. However, there are some restrictions for small scale experiment, for example, the edge effect for sputtering may affect the uniformity of the TCCR coating; and the small samples obtained from the lab scale deposition machine prevents us from making commercial size PEC cells. Based on the extensive lab results and the availability of a large scale roll-to-roll machine at Xunlight Corporation, which was formed initially as a wholly owned subsidiary of MWOE, we have worked on the fabrication of TCCR coating on large area a-Si electrodes. The prototype 2MW roll-to-roll machine has the capability of both PECVD coating and RF sputtering integrated in the same roll-to-roll machine, and is perfect for this purpose. With this machine, we can make PEC electrodes which are 3 ft wide and thousands of feet long. This system simulates processing conditions which are comparable to a manufacturing environment. The system allows depositing of back-reflector, semiconductor and TCCR layers continuously and without the need for breaking the vacuum. For TCCR layer optimization, parameters such as line-speed, layer thickness, sputtering power and O_2 gas flow are tested and optimized. We have used a 6 inch x 42" linear Co_3O_4 sputtering target (99%) for the fabrication of the TCCR layer. The film thickness is controlled by the rf power, process gas, pressure and the process line speed. for example, at a a line speed of 6"/min, every spot of the substrate would take 1 min to travels through the 6" linear target so the total deposition time is 1 min at this line speed.

Figure 12 below provides a view into the opened pay-out chamber of the 2MW machine after carrying out the experiment: the 36" wide stainless steel web is coated with back reflector, semiconductor solar cells and Co_3O_4 layers.

Dektak (thickness) measurements show that Co_3O_4 layers obtained under these experimental conditions have a thickness in a range between 200 nm - 275 nm. Figure 13 shows that the Co_3O_4 layer thickness decreases with increasing argon/oxygen flow during sputtering. These data is used for an optimization experiment targeting the required TCCR layer thickness of ~ 30-70 nm. Increasing the line speed and lowering the sputtering power significantly decreases the Co_3O_4 layer thickness. The argon/oxygen flow speed used during sputtering has a noticeable effect on the expected film thickness as well, as shown in Figure 13.

The transparency of TCCR films was measured using Co_3O_4 layer sputtered onto glass slides: the glass slides were attached to the web and were moved through Co_3O_4 sputtering station using the roll-to-roll transport system.

With the thicknesses of the Co_3O_4 layers in the 200 to 275 nm region, the transparency is quite low in the wavelength range between 300 nm - 900 nm (see Fig. 14). However, with reduced Co_3O_4 thickness, the transparency will increase.

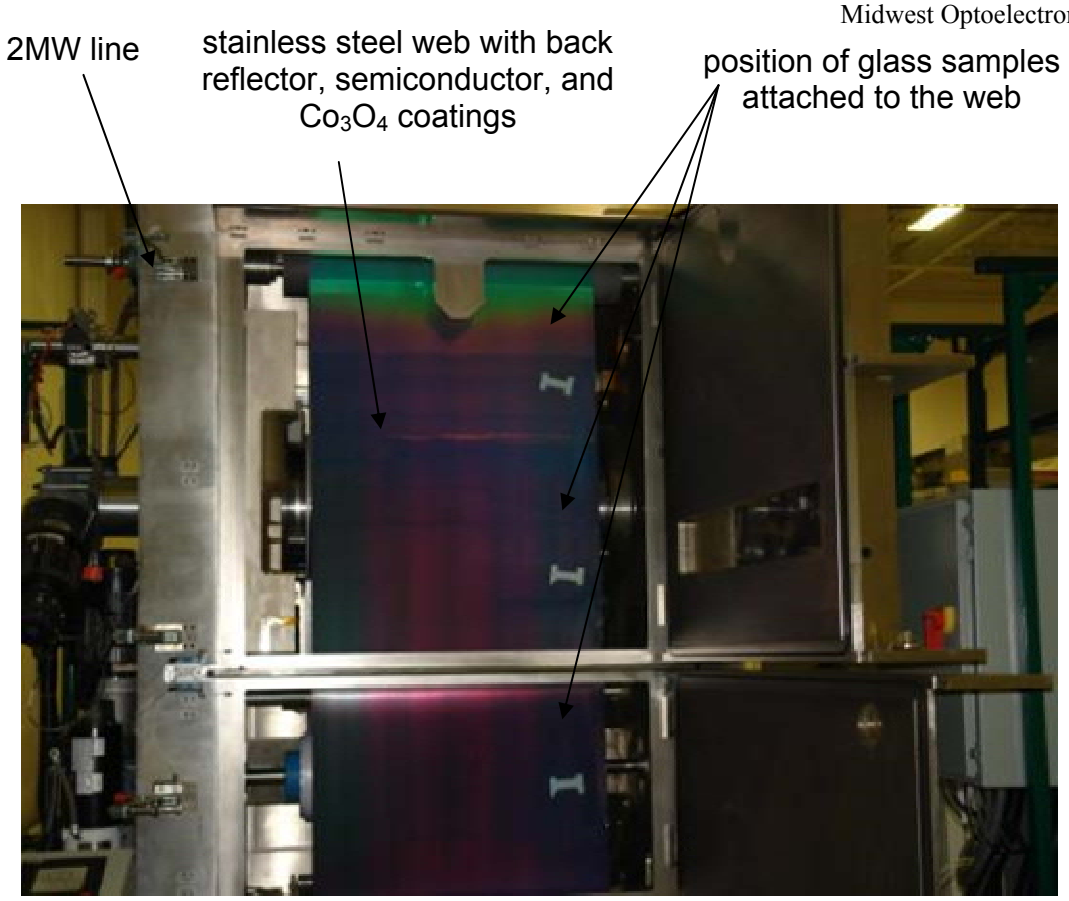

Figure 13: Opened pay-out chamber of 2MW roll-to-roll machine with inserted stainless steel web after Co_3O_4 sputtering;

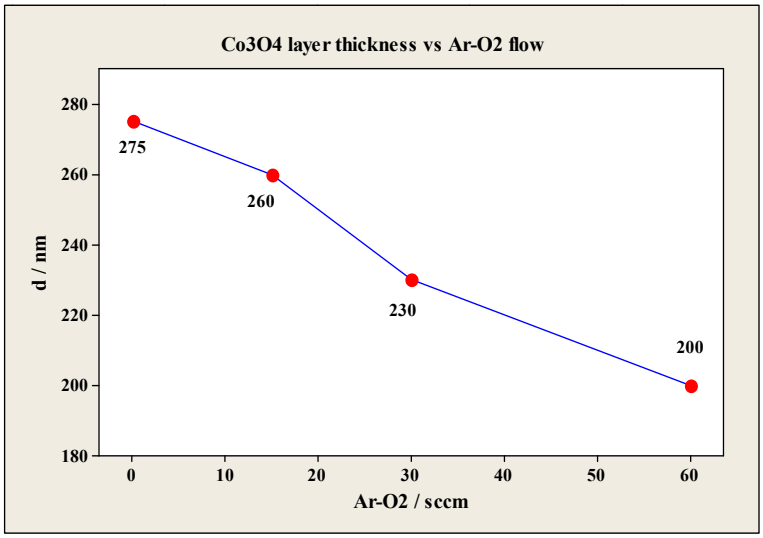

Figure 14: Co_3O_4 thickness vs. Argon/Oxygen flow

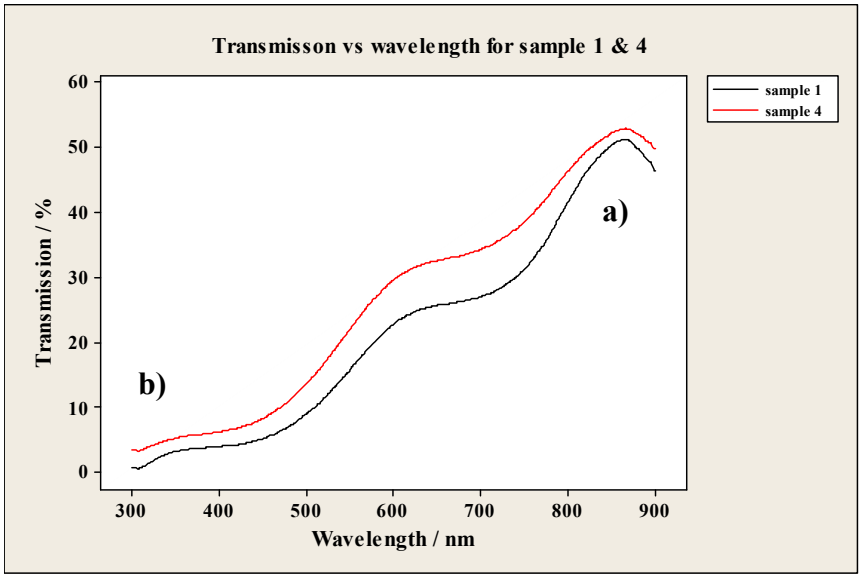

Figure 15: Transmission vs. wavelength for Co_3O_4 coatings with different thickness: a) 275 nm, b) 200 nm

Next, the optimization work was focused on obtaining thinner Co_3O_4 layer in order to increase the transparency of the TCCR material. Table 3 summarizes the experimental conditions used for Co_3O_4 sputtering.

Table 3: Co_3O_4 sputtering conditions

Run, exp. #	**material**	**pulsed DC power**	**sputtering pressure**	**Ar/Ar-O_2 flow**	**line speed**
Run 2, exp. 5	Co_3O_4	3 kW	6.5 mTorr	80 sccm / 60 sccm	1 " / min
Run 2, exp. 6	Co_3O_4	3 kW	6.5 mTorr	60 sccm / 80 sccm	1 " / min
Run 2, exp. 7	Co_3O_4	3 kW	6.5 mTorr	40 sccm / 100 sccm	1 " / min
Run 2, exp. 8	Co_3O_4	3 kW	6.5 mTorr	20 sccm / 120 sccm	1 " / min
Run 3, exp. 9	Co_3O_4	3 kW	6.5 mTorr	40 sccm / 100 sccm	6 " / min
Run 3, exp. 10	Co_3O_4	3 kW	6.5 mTorr	20 sccm / 120 sccm	6 " / min
Run 3, exp. 11	Co_3O_4	3 kW	6.5 mTorr	10 sccm / 130 sccm	6 " / min
Run 3, exp. 12	Co_3O_4	3 kW	6.5 mTorr	0 sccm / 120 sccm	6 " / min
Run 4, exp. 13	Co_3O_4	1.5 kW	6.5 mTorr	40 sccm / 100 sccm	6 " / min

Run 4, exp. 14	Co_3O_4	1.5 kW	6.5 mTorr	20 sccm / 120 sccm	6 " / min
Run 4, exp. 15	Co_3O_4	1.5 kW	6.5 mTorr	10 sccm / 130 sccm	6 " / min
Run 4, exp. 16	Co_3O_4	1.5 kW	6.5 mTorr	0 sccm / 140 sccm	6 " / min

Run 2 uses 3kW as sputtering power and 1"/min as line speed; and we experimented with increased argon/oxygen level in the sputtering gas. Run 3 uses a faster line speed than that used for Run 2; the argon/oxygen flow was increased. For Run 4 the sputtering power was reduced and the line speed was kept at the high setting of 6 "/min. This run uses settings for the sputtering gas flow comparable to Run 3. The Co_3O_4 film thickness was determined by using Dektak^3 ST Surface Profiler (Veeco Instruments Inc); the results from Dektak measurements for samples from Run 2 - Run 4 are summarized in Table 4 and displayed in Fig. 15. The 80 sccm / 60 sccm for Ar/Ar-O_2(20%) flow means there is a flow of 80 sccm of pure Ar gas and 60 sccm of a mixture of Ar/O_2 gas with 20% O_2 in the mixture flowing into the deposition chamber. The total flow is maintained at 140 sccm.

Table 4: Co_3O_4 layer thickness;

sample #	sputtering power	Ar-ArO2(20%) flow	d / nm
E5	3KW	80 sccm / 60 sccm	281
E6	3KW	60 sccm / 80 sccm	*)
E7	3KW	40 sccm / 100 sccm	272
E8	3KW	20 sccm / 120 sccm	258
E9	3KW	40 sccm / 100 sccm	120
E10	3KW	20 sccm / 120 sccm	135
E11	3KW	10 sccm / 130 sccm	148
E12	3KW	0 sccm / 120 sccm	129
E13	1.5KW	40 sccm / 100 sccm	129
E14	1.5KW	20 sccm / 120 sccm	121
E15	1.5KW	10 sccm / 130 sccm	140
E16	1.5KW	0 sccm / 140 sccm	151

*) sample not measurable;

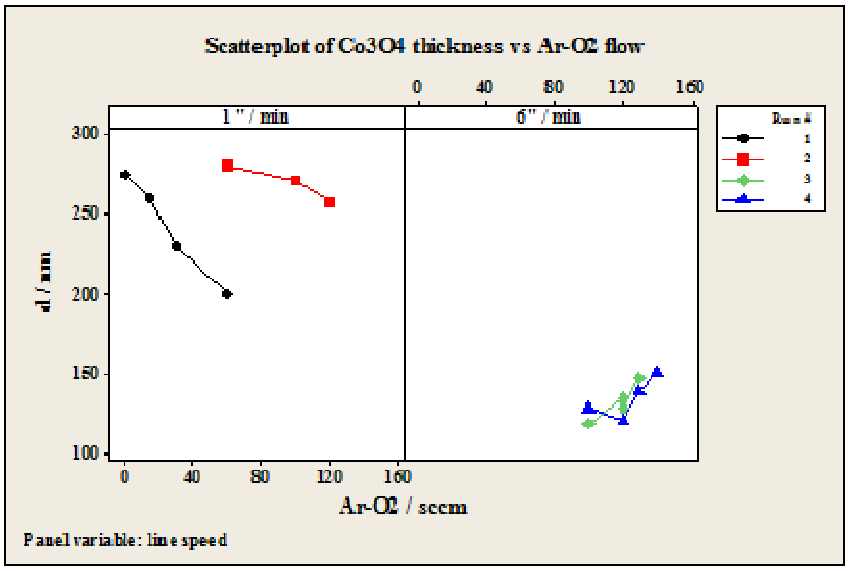

Figure 16: Co_3O_4 layer thickness for samples from Run 1 - Run 4 vs. Argon/Oxygen flow

The Co_3O_4 layer thickness obtained for Run 1 and 2 are in a range of 280 nm - 200 nm; here, the layer thickness decreases with increasing oxygen level in the sputtering gas. As discussed earlier, the Co_3O_4 layer thickness for samples from Run 1 and Run 2 is too high in order to obtain the required transparency for the TCCR layer: the target thickness for Co_3O_4 TCCR layer is suggested to be below 30 nm. Run 3 and Run 4 use a much higher line speed for Co_3O_4 layer deposition, which decreases the Co_3O_4 layer thickness significantly down to a range of 120 nm - 150 nm. For samples from Run 3 and Run 4 a small increase in layer thickness with increasing oxygen level in the sputtering gas is found. On the other hand, the decrease in sputtering power from 3 kW to 1.5 kW does not seem to impact the obtained Co_3O_4 layer thickness.

UV-vis spectra of Co_3O_4 samples coated onto plain borosilicate glass were measured using a UV/VIS/NR-Cary 5 Diode Array (HP8452A). The percentage transmission data obtained were corrected by using an uncoated borosilicate glass slide for a baseline measurement.

Figure 16 shows the UV-vis transmission measurements obtained for samples from Run 1, Run 2 and Run 4. The data show that decreasing the Co_3O_4 layer thickness from 200 nm - 270 nm (Run 1) to 100 nm - 150 nm (Run 3) significantly improves the transparency. The samples from Run 4 show higher transmission than samples from Run 3 although the Co_3O_4 layer thickness is within 120 nm - 150 nm, comparable to the samples from Run 3. The sputtering power was decreased from 3 kW (Run 1-3) to 1.5 kW for Run 4. Noteworthy is that the transmission of the Co_3O_4 layer does not change with the oxygen flow in the sputtering gas; this is observed for samples from Run 3 and Run 4. It should be noted here that the transmission was obtained by taking the ratio of the film on glass to the reference measurment on glass. The transmission of the reference glass is not 100% due to the two air/glass interfaces. However, the estimate is sufficiently close for the purpose in this study. It should also be noted that the transparency is not necessary a bulk effect as the film is very thin and tranmission coefficient at different sublayer may not be the same.

We further studied the effect of the sputtering power on film thickness and transparency. The transmission data and layer thicknesses obtained from Co_3O_4 samples obtained from Runs 1-4 showed that lowering the sputtering power is beneficial for improving the transparency of the TCCR material in a wavelength range of 300-900nm. For Run 5 the sputtering power was

decreased even further from 1.5kW to 0.8kW; the parameter settings for sputtering pressure, Argon/Argon-Oxygen flow and line-speed were kept at values comparable to the settings used for Run 4. The experimental parameter settings used for sputtering Co_3O_4 TCCR layer for Run 5 are summarized in Table 5.

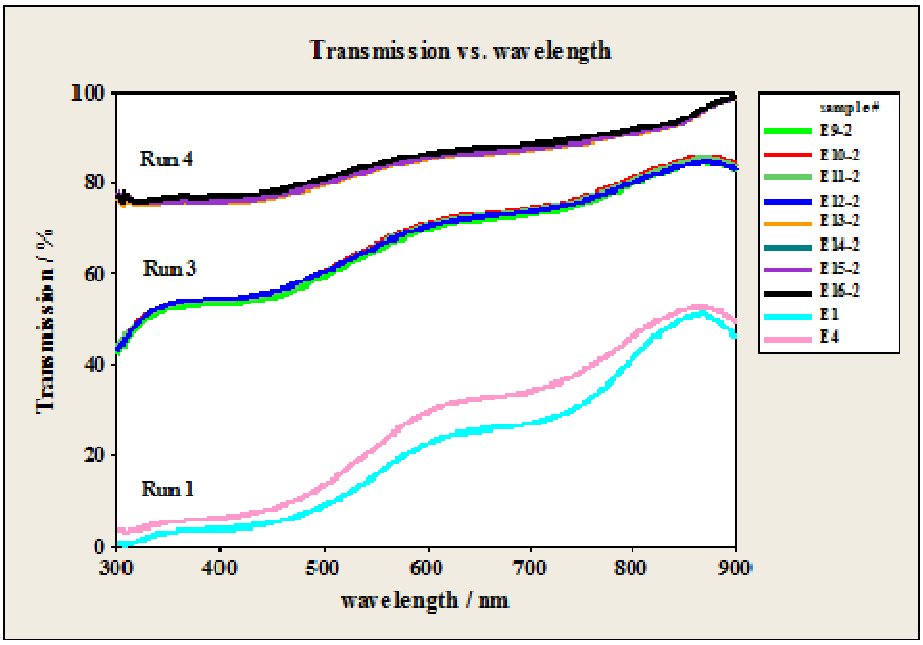

Figure 17: UV-vis transmission vs. wavelength for Co_3O_4 samples (on glass) from Run 1, Run 3 and Run 4;

Table 5: **Co_3O_4 sputtering conditions**

Run, exp. #	material	pulsed DC power	sputtering pressure	Ar/Ar-O_2 flow	line speed
Run 5, exp. 17	Co_3O_4	0.8 kW	6.5 mTorr	40 sccm / 100 sccm	6 " / min
Run 5, exp. 18	Co_3O_4	0.8 kW	6.5 mTorr	20 sccm / 120 sccm	6 " / min
Run 5, exp. 19	Co_3O_4	0.8 kW	6.5 mTorr	10 sccm / 130 sccm	6 " / min
Run 5, exp. 20	Co_3O_4	0.8 kW	6.5 mTorr	0 sccm / 140 sccm	6 " / min

Co_3O_4 layer were sputtered onto borosilicate glass slides for thickness and transmission measurements. The Co_3O_4 film thickness was determined by using Dektak® ST Surface Profiler; the data from Run 5 are summarized in Table 6 and displayed in Fig. 17. For comparison, the data obtained previously for Run 4 are displayed in the same graph.

The data show that lowering the sputtering power from 1.5kW to 0.8kW reduced the Co_3O_4 thickness from 121-151 nm to 68-82 nm; the thickness values obtained for Run 5 are closer to the thickness demonstrated on small-area samples reported in the earlier section..

Table 6: Co_3O_4 layer thickness

sample #	sputtering power	Ar/Ar-O_2 flow	d / nm
E17	0.8kW	40 sccm / 100 sccm	68
E18	0.8kW	20 sccm / 120 sccm	72
E19	0.8kW	10 sccm / 130 sccm	82
E20	0.8kW	0 sccm / 140 sccm	78

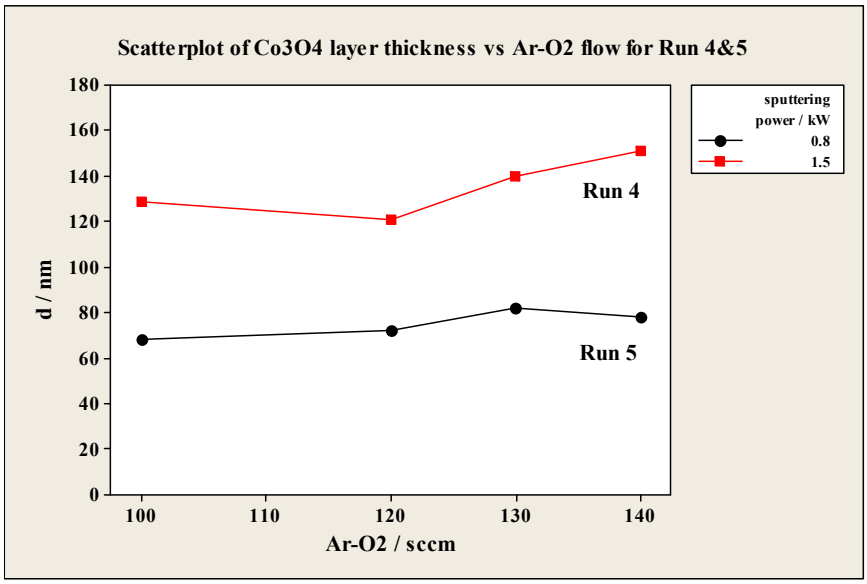

Figure 18: Co_3O_4 layer thickness for samples from Run 4 and Run 5 vs. Argon/Oxygen flow;

Fig. 18 compares the transmission data of Co_3O_4 layer obtained from Run 4 with the data obtained from samples from Run 5. The data suggest that the transparency of the Co_3O_4 layer is significantly improved for samples obtained in Run 5 compared to samples from Run 4. The transparency of the TCCR is >90% in a wavelength range of 300-900nm; these results indicate that the TCCR transparency is acceptable. Noteworthy is, that the transmission of the Co_3O_4 layer does not change with the oxygen flow in the sputtering gas; this is observed so far for samples from all runs. We therefore have used the condition in Run 5 as our default condition for making Co_3O_4 TCCR layers.

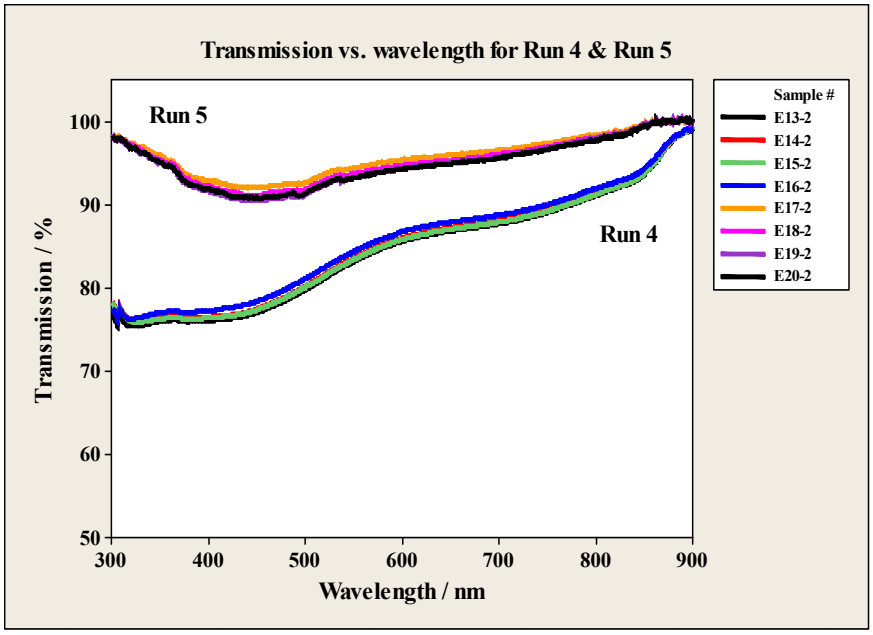

Figure 19: UV-vis transmission vs. wavelength for Co_3O_4 samples (on glass) from Run 4 and Run 5;

Voltage Drop across the TCCR layer:

One of the key metrics presented in the scope of work of this project is the possible voltage drop caused by the TCCR layer. If the TCCR layer, Co_3O_4, causes too much a voltage drop, then we may not have enough voltage for water splitting. In the following we will describe our efforts in measuring the voltage drop across the Co_3O_4 layer. Co_3O_4 TCCR layers were sputtered onto a-Si material. The voltage drop across the TCCR layer is determined by the difference between the open circuit voltages of an a-Si sample with ITO and an a-Si sample with ITO and Co_3O_4 layer measured in electrolyte under 1 sun from a 150 W Xenon lamp using the set-up shown in Fig.19 here.

The open circuit voltages are measured in electrolyte (pH 9 buffer solution) using a 2-electrode set-up:

- Working electrode: (1) a-Si with ITO, or (2) a-Si with ITO and Co_3O_4
- Counter electrode: (1) Stainless steel back-sheet of solar cell; or (2) Platinum Gauze;

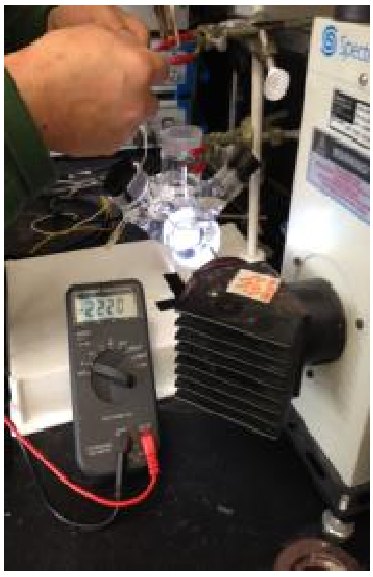

Figure 20: A setup to measure the voltage drop.

As we can see from the results in Table 7, the voltage drop across the Co_3O_4 layer is very minimal, well within the 0.35 V voltage drop limit that MWOE had proposed.

Table 7: Voltage drop across the Co_3O_4 layer, by comparing the voltage between (1) a-Si with ITO, and (2) a-Si with ITO/ Co_3O_4 .

Full Module response

a-Si (front) vs SS (back)	open circuit voltage
a-Si with ITO	2.118 V
a-Si with Co_3O_4/ITO	2.220 V
difference	(-) 0.102 V

Anodic response

a-Si (front) vs Pt	open circuit voltage
a-Si with ITO	0.997 V
a-Si with Co_3O_4/ITO	0.845 V
difference	0.152 V

Cathodic response

SS(Back) vs Pt	open circuit voltage
a-Si with ITO	1.121 V
a-Si with Co_3O_4/ITO	1.316 V
difference	(-) 0.195 V

In summary, the film properties were further optimized in the 2MW roll-to-roll deposition system. This prototype production system allows large-area PEC electrode fabrication, including the deposition of TCCR layer. Cobalt oxide has been sputtered on a-Si triple junction solar cells at 200°C. Reducing the sputtering power from 1.5kW (Run 4) to 0.8 kW (Run 5) leads to transmission values of 90-100% in a wavelength range between 300-900nm. The average thickness of these Co_3O_4 layer is ~ 70 nm. The oxygen flow was varied between 100-140 sccm and it seems that the transmission of the Co_3O_4 layer does not change with the oxygen flow in the sputtering gas. Under one-sun condition, the voltage drop on the cobalt oxide layer is only 0.086 V, which is excellent since this indicates that almost all the voltage generated by the solar cell can be used for water splitting and hydrogen generation. All of the above performance metrics meet or exceed the proposed DOE project goals and MWOE project goals. Cobalt oxide films deposited on FTO (TEC 15) have been shown to be electrochemically stable for over 1000 hrs under an applied bias of 1.8 V which reassembles the operating conditions for an immersion-type PEC cell assembly. With the roll-to-roll deposition system, not only can we optimize the deposition conditions for cobalt oxide, we can also adjust the solar cell deposition conditions and optimize the solar cell and TCCR layer deposition parameters for PEC performance, instead for solar-to-electricity performance. This is a great advantage that we have comparing to many other groups that have to rely on commercially available solar cells which are always optimized for solar to electricity performance. An additional benefit for making the PEC electrode using a roll-to-roll system is the uniformity. In each experiment, we produce several square meters of uniform coating, and these can then be made available to many different laboratories for comparison. One set of such PEC electrodes were supplied to Dr. Dan Nocera's lab at MIT and highly efficient PEC hydrogen production was observed using MWOE/Xunlight produced PEC cells.

4.2. Development of Hydrogen Generation Catalyst – Porous Nickel

Effort under this task is to develop various hydrogen generation catalysts in order to improve the Solar to hydrogen conversion efficiency. We have studied several material for this purpose, such as Platinum, Ruthium, Nickel and so on. Platinium and Ruthium give very good results, but they are precious metal, therefore the cost is quite high. Nickel is a much inexpensive alternative if we can improve its performance. We made significant research effort to develop porous nickel as a hydrogen generation catalyst. Below are some of the detailed results.

We carried out many experiments optimizing the conditions for making electro-plated Ni coating. The goal is to be able to apply it to the back side of our PEC electrode and to achieve high solar to hydrogen (STH) efficiency and durability.

We make the porous Ni coating on stainless steel substrates. First, we clean and roughen the substrate so that the coating can have a strong adhesion to the substrate surface. Then we put the substrate in a Ni/Zn solution to electro-plate Ni/Zn mixtures on the surface. Then we put it in KOH solution to leach out Zn to create a porous structure. The following are the detailed procedures to make porous Ni coating:

1) Preparation of Ni electrolyte
2) Etching of the stainless steel substrate
3) Electro-deposition of Ni and Ni/Zn on the substrate
4) Leaching in KOH solution
5) Testing the porous Nickel electrodes

Step 1: Preparation of the Ni electrolyte

Ni electrolyte is prepared using the following chemicals. The chemicals are mixed in a conical flask with water and stirred for approximately an hour.

Chemicals:	Composition
$NiSO_4 \cdot 6H_2O$ (Nickel Sulphate Hexahydrate)	330g/l
$NiCl_2 \cdot 6H_2O$ (Nickel Chloride Hexahydrate)	45g/l
H_3BO_3 (Boric Acid)	37g/l

Step 2: Etching the stainless steel substrate

The 4”×4”stainless steel substrate is cleaned in an ultrasonic bath for 30 min and then cleaned with acetone to remove any surface impurities. It is then put into an electrolytic cell and is chemically etched with 50% HCl solution for 10 min. The purpose of this step is to roughen the substrate surface in order to increase the adhesion of Ni coating to it. After that, the electrode is cleaned with DI water thoroughly to remove any trace of HCl.

Step 3: Electro-plating of the Ni and Ni/Zn

The next step is to electro-deposit Ni onto the substrate. The anode is a piece of Ni foil and the cathode is the stainless steel substrate that was cleaned in Step 2. The Ni foil is about the size of 2"×6", and is cleaned in an ultrasonic bath for 30 min, and then cleaned with acetone before rinsing. Then it is ready to be used as the anode. The deposition is carried out at a constant temperature of 60°C.

The Ni electrolyte solution prepared in Step 1 is poured into the electrolytic cell and heated to 60°C, ready for the electro-deposition. The first phase of the electro-deposition of Ni is carried out at a current density about 19 mA/cm^2 for 45 min.

In the second phase of the electro-deposition, Zinc Chloride ($ZnCl_2$) solution is added as a precursor. The concentration of $ZnCl_2$ used here is 5% by weight. $ZnCl_2$ solution is gradually added to the Ni electrolyte solution at the rate of 0.2 ml/min for 30 min. The second phase is carried out at a current density about 24 mA/cm^2. The electro-deposited stainless steel substrate is then taken out of the cell and ready for the next step -- leaching.

Step 4: Leaching in KOH solution

The purpose of this step is to create some porous structure in the plated Ni layer in order to increase the surface area and catalytic efficiency. 33% KOH solution is used for leaching Zn out of the plated Ni layer. The samples are allowed to leach for 48 hours, after that they are cleaned with DI water thoroughly. A sample of the electroplated porous Ni is shown in Fig. 20 and an SEM image is shown in Fig. 21.

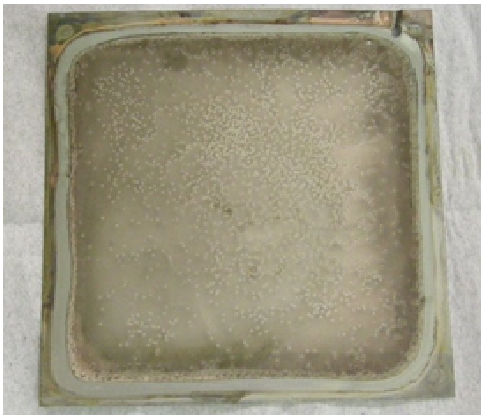

Figure 21: Electroplated porous Ni coating

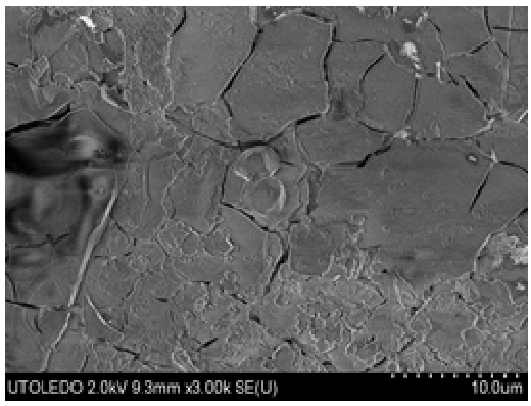

Figure 22: a SEM image of the porous Ni coating

In addition to $ZnCl_2$, We have worked with a wide range of pre-cursor material, such as $MnCl_2 \cdot 6H_2O$, $(NH_4)_2SO_4$, $CuSO_4$, or $Zn(NO_3)_2$ with the goal of obtaining higher STH efficiency.

Figs. 22-24 summarize the J-V curves obtained from using the porous Ni-catalyst electrode as anode or cathode; the Ni catalyst was fabricated using the same electro-deposition procedure but with different precursor salts. The Ni-electrode used as anode or cathode was placed at different distances (1-3 cm) from the Pt-mesh electrode. This simulates the conditions in a PEC cell assembly for H_2 generation. A significant difference in the J-V curves can be observed when the Ni electrode acts as the cathode with different precursor salt such as $MnCl_2$, $(NH_4)_2SO_4$, $CuSO_4$, $ZnCl_2$, or $Zn(NO_3)_2$, indicating that the precursor salt has a significant effect on the surface area, structure and furthermore the porosity of the Ni catalyst. So far the highest current density was obtained using $(NH_4)_2SO_4$.

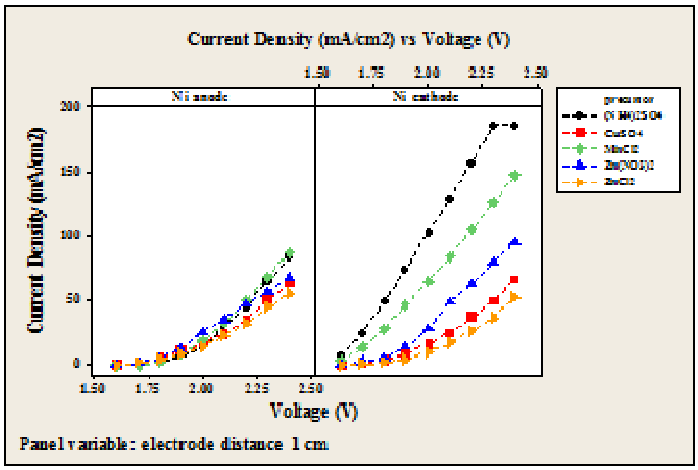

Figure 23: J-V curves for porous Ni-electrode made with various precursor salts such as $CuSO_4$, $ZnCl_2$, $Zn(NO_3)_2$, $MnCl_2$ and $(NH_4)_2SO_4$; electrode distance: 1 cm;

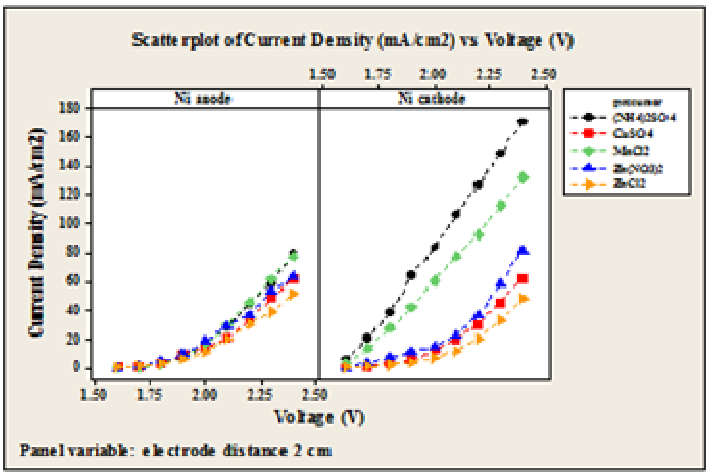

Figure 24: J-V curves for porous Ni-electrode made with various precursor salts such as $CuSO_4$, $ZnCl_2$, $Zn(NO_3)_2$, $MnCl_2$ and $(NH_4)_2SO_4$; electrode distance: 2 cm;

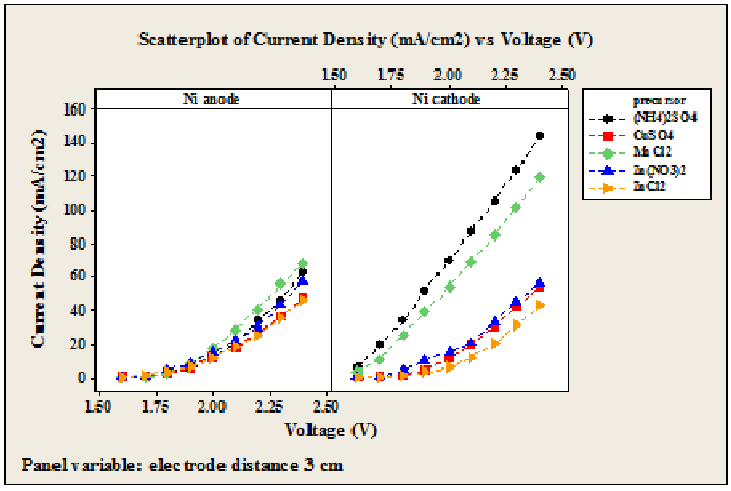

Figure 25: J-V curves for porous Ni-electrode made with various precursor salts such as $CuSO_4$, $ZnCl_2$, $Zn(NO_3)_2$, $MnCl_2$ and $(NH_4)_2SO_4$; electrode distance: 3 cm;

A porous Ni-plated electrode and an SEM image with $(NH_4)_2SO_4$ as precursor is shown in Fig 25 below.

Figure 26: A picture (left) and a SEM image (right) of a porous Ni-plated electrode with $(NH_4)_2SO_4$ as precursor

4.3. Fabrication of PEC Electrodes with TCCR Layer and the Effect of the ITO Layer

The deposition conditions for sputtering Co_3O_4 TCCR layer onto production quality a-Si solar cell material in a prototype production machine were previously optimized (see Section 4.1.2 for details). Normally, production quality a-Si solar cells all have an ITO (Indium Tin Oxide) coating, which serves as a transparent, conducting layer on top of a-Si solar cells. Another function of the ITO layer is the photo-electrochemical passivation of electrical shunts by converting the ITO nearby the electrical shunts into insulator. Since Co_3O_4 TCCR layer also serves as a Transparent, Conducting (in additional to Corrosion Resistant) layer, one natural question would be: "Can we save some cost by eliminating the ITO layer when making photo-electrode and replace it with Co_3O_4 TCCR layer or by using a thinner ITO layer beneath Co_3O_4 layer?" To answer that question, we have studied the effect of the ITO layer thickness underneath the Co_3O_4 TCCR layer on PEC electrode performance. Normally, to measure the degree of electrical shunt, the low light V_{OC} (LLVOC) values of a solar cell is a routine measurement to determine whether the solar cell are shunted, which would directly affect the performance of the solar cell or the photo-electrodes. Therefore, we have been using the LLVOC measurement to determine the effect of ITO layer thickness on the performance of the photo-electrodes.

Usually, there are tiny defects and defect clusters associated with manufacturing of a-Si PV material which sometimes lead to shunts in the PV material, and affect the performance of PV cells. For photo-electrodes this would reduce the voltage of the devices below the values which are necessary for water splitting. The routine process to resolve the shunt issue is to do a light assisted shunt passivation process. With this process, the electrically conductive ITO layer on top of the shunted area is selectively converted into non-conductive material, therefore leading to an electrical isolation of the shunted area.

We made some solar cell without the ITO layer, but coated directly with Co_3O_4 layer. When we tried to carry out the shunt passivation on these samples, it was not successful -- Co_3O_4 simply does not respond to the light-assisted shunt passivation process as ITO does. The resulting LLVOC for these samples turned out to be very low because the existing shunt could not be isolated. We have also tried to start with the ITO coated solar cell but skip the shunt passivation process, and apply the Co_3O_4 layer. The resulting photo-electrodes also gave very low LLVOC values. These two experiments indicated that an ITO coating and the shunt passivation process for the solar cells are essential for isolating the shunt and achieve a reasonable voltage for water splitting.

The next set of experiments we carried out is to determine relationship between the thickness of the ITO layer and the photo-electrode performance.

Amorphous-Si triple junction solar cells were coated with different ITO thicknesses ranging from 0nm - 70nm. Material that had an ITO top layer was then passivated using light-assisted shunt passivation process. These samples were then coated with Co_3O_4 using the deposition conditions that we have optimized previously (see Section 4.1.2). From each sample set, 4 small-area (1.5"x1.5") PEC electrodes were fabricated and low-light VOC (LLVOC) measurements (4 readings per sample) were taken. The individual data are shown in Fig. 26 and, Table 8 summarizes the average, stand deviation (stddev.) and median values for this experiment. The LLVOC measurements suggest that there is no strong correlation between LLVOC and ITO thickness when comparing the data for PEC electrodes with different ITO thickness. However, the sample with 70nm ITO layer shows the most consistent LLVOC measurement. The samples which do not comprise an ITO layer show very low LLVOC values. These samples are not shunt passivated as Co_3O_4 does not respond to the light-assisted shunt passivation process as the ITO layer does. From these series of experiments, it can be concluded that at least a thin layer of ITO, which can be as thin as 10 nm, underneath the Co_3O_4 TCCR coating, is required and the shunt passivation process is essential for the good performance of the PEC electrodes. The samples with 70 nm thickness ITO gave most consistent voltage results. Therefore we have decided to use this condition for our PEC electrode fabrication.

Table 8: LLVOC vs. ITO thickness for Co_3O_4 coated PEC electrodes;

ITO thickness	Co_3O_4	Average voltage	stddev	median
0	yes	0.24	0.10	0.24
10	yes	1.39	0.45	1.66
20	yes	1.08	0.52	1.13
20	yes	1.73	0.03	1.74
30	yes	1.74	0.04	1.75
45	yes	1.03	0.71	1.25
60	yes	0.54	0.73	0.15
70	yes	1.71	0.05	1.73

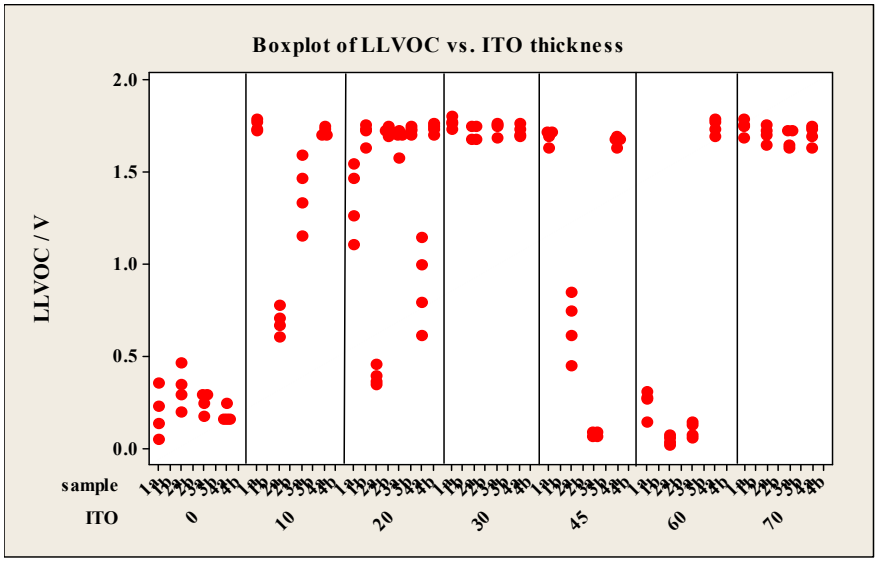

Figure 27: LLVOC measurements for PEC electrodes with different ITO thickness

Fig. 27 compares the LLVOC voltage of PEC electrodes with and without Co_3O_4 TCCR coating; these samples comprise a ~70 nm thick ITO layer. The data suggest an average low-light voltage loss of about 0.12V due to the presence of the Co_3O_4 TCCR layer (see Table 9), which is in the acceptable range.

Table 9: LLVOC for PEC electrodes with and without Co_3O_4 TCCR (all samples have an ITO layer of ~70nm)

ITO thickness	Co_3O_4	Average Voltage	stddev	median
70	no	1.83	0.03	1.84
70	yes	1.71	0.05	1.73

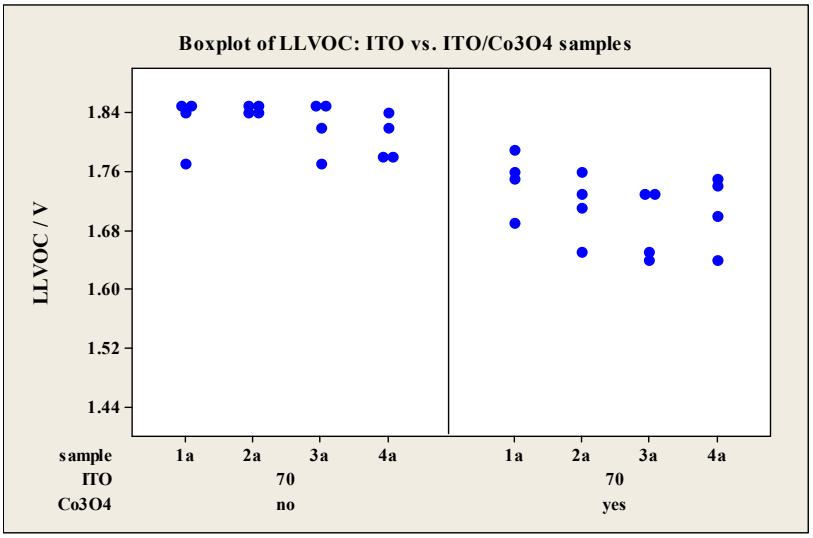

Figure 28: LLVOC for PEC electrodes with and without Co_3O_4 TCCR coating, both have an ITO layer of ~70nm;

4.4. Fabrication and characterization PEC electrodes for immersion type PEC system:

In this section, we will discuss extensive efforts we have carried out to prepare and characterize the PEC electrodes with TCCR layer for immersion type PEC system.

11"×17" standard size solar cells were shunt passivated and coated with Co_3O_4 TCCR layer in the 2MW roll-to-roll machine. It was then cut into 1"×1" pieces. Very often, after cutting, the positive and negative sides of the solar cells may be shorted at the edge, an edge isolation step is necessary to isolate the two sides of the electrodes. Phosphoric acid was applied to the edge of the cell to remove the ITO layers, and the cell was then placed in a furnace at 130ºC for 30 min and was rinsed thoroughly afterwards with D.I. water. Fig. 28 shows several PEC electrodes which have been edge isolated. A clear coat is applied to all edges of the samples to protect the edge of the solar cell from being corroded by electrolyte, as shown in Fig. 29. Then the samples are usually heated in an oven at 150°C for 30 min to cure the clear coating. Fig. 30 shows a typical I-V curve for a PEC cell after edge isolation. Normally, a good PEC cell made from a-Si triple junction solar cell would show room light V_{oc} of ~1.4V and AM1.5 V_{oc} of ~2.1 to 2.2 V.

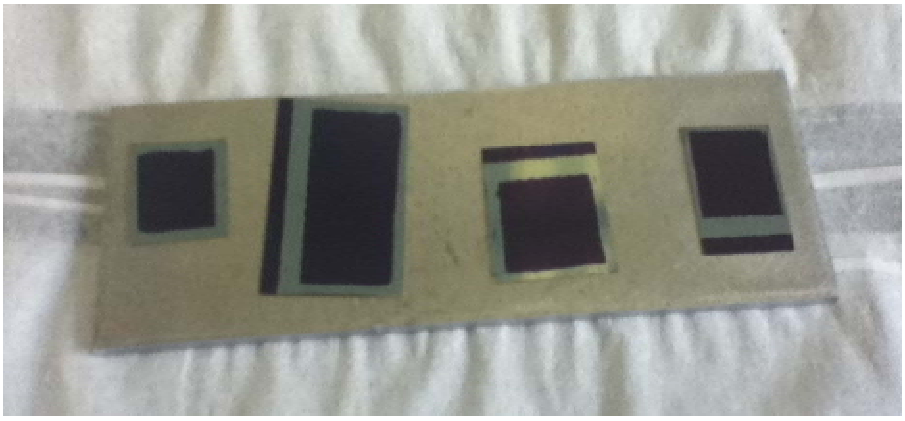

Figure 29: Various PEC cells for which edge isolation have been performed**;**

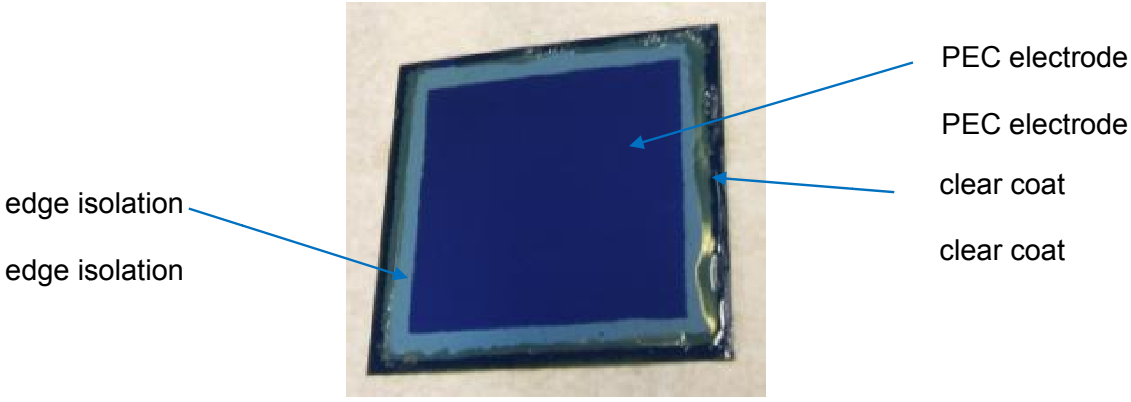

Figure 30: 1.5"x1.5" PEC electrode (front) with clear coat edge seal;

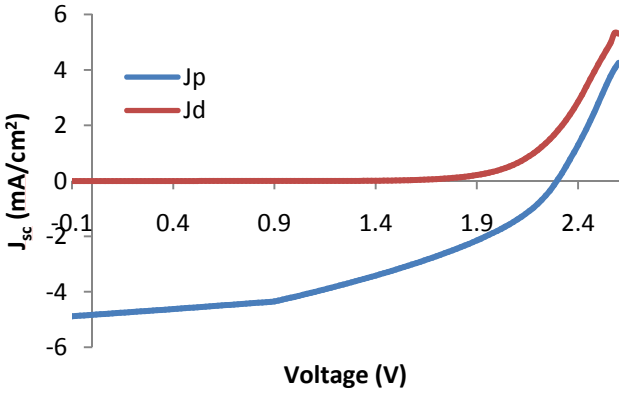

Figure 31: I-V data for a PEC cell after edge isolation: V_{oc}=2.295 V; Jd: dark current; Jp: photocurrent (under AM1.5).

After the PEC electrodes are prepared as described in previous paragraph, they are then placed in the electrolyte with a pH about 9. Initially, the STH conversion was quite low, indicating that we may need to also apply some hydrogen generation catalyst. That is where the porous Ni coating come into play. We would use silver epoxy to attach a porous Ni coated Ni sheet onto the back side of the PEC electrode, as shown in Fig. 31. The detailed procedures for preparing electroplated nickel molybdenum material and the optimized condition for porous Ni plating have been discussed earlier in Section 4.2.

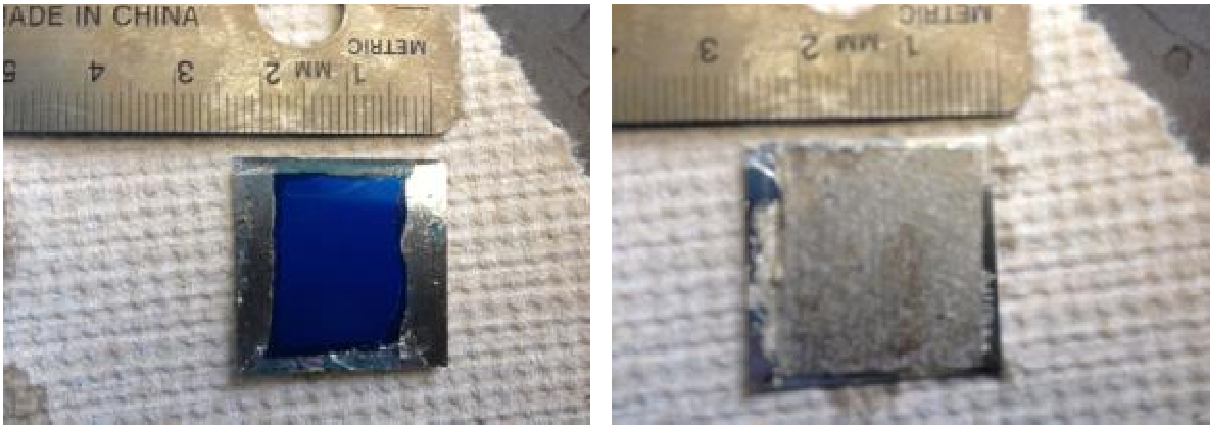

a. Front of the electrode b. Back of the electrode w. Ni catalyst

Figure 32: Photographs showing PEC electrodes after edge isolation, a) with clear coat treatment in the front and b) with porous Ni catalyst on the back

Solar to hydrogen conversion efficiency for immersion-type PEC cell:

The PEC electrodes were tested in the set-up shown in Fig. 32. This set-up consists of a Pyrex container modified with a quartz window attached to the side. A Teflon cylinder with a groove on one side is used to place the cells into an alignment with the quartz window; a 50 mL graduated cylinder is placed directly over the top of the PEC electrode to collect all gas produced off the front and the back of the electrode. A 150W Spectra Physics lamp is used to illuminate the PEC electrode sample with AM1.5 radiation (100 mW/cm^2) which was calibrated using a Si photodiode.

Figure 33: The experimental set-up for measuring the STH efficiency of the PEC electrodes;

Gas generation was observed on the electrode under light illumination. Table 10 summarizes the volume of hydrogen collected over time. These volumes were derived by taking 66% of the total volume assuming 2:1 ratio for hydrogen to oxygen generation. The calculated solar-to-hydrogen (STH) efficiency based on the volume of hydrogen generated for this system is shown in Table 10. The STH efficiency is calculated using the following equation:

$$STH = \frac{(mol\ of\ H_2/sec) \times (237\ kJ/mol\ [\Delta G\ for\ H_2])}{(P_{total}\ mW/cm^2) \times (Area\ of\ Cell\ cm^2)} \qquad (1)$$

where P_{total} is 100 mW/cm^2 and the area of the electrode is 2.696 cm^2. Fig. 33 shows a graphical representation of these results.

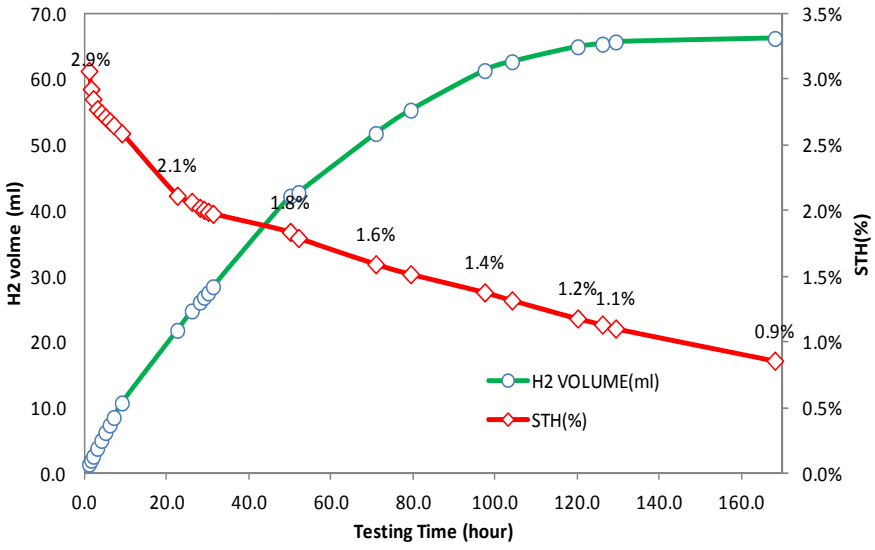

Figure 34: Volume of hydrogen produced and STH efficiency over time for an immersion type PEC electrode.

As shown in Table 10, we were able to achieve the initial Solar to hydrogen conversion efficiency of 3.1%. The electrolyte is a water solution with KOH and Boric acid at a PH about 9. This PEC electrode was able to run continuously for over 160 hours until the hydrogen generation speed slowed down to very low level. When we examined the electrode after the 160 hour run, the solar cell seems to be in good condition which indicates that corrosion resistant property of the PEC is appropriate in the electrolyte that we have used.

Table 10: Volume of hydrogen gas generated and average STH efficiency of an immersion type PEC cell;

TIME (hrs)	H_2 VOLUME (ml)	STH (%)	TIME (hrs)	H_2 VOLUME (ml)	STH (ml)
1.0	1.41	3.1%	29.0	26.80	2.0%
1.5	2.01	2.9%	30.0	27.47	2.0%
2.0	2.61	2.8%	31.2	28.41	2.0%
3.0	3.82	2.8%	50.0	42.21	1.8%
4.0	5.03	2.7%	52.0	42.75	1.8%
5.0	6.23	2.7%	70.8	51.72	1.6%
6.0	7.37	2.7%	79.3	55.28	1.5%
7.0	8.51	2.6%	97.3	61.31	1.4%
9.0	10.72	2.6%	104.0	62.65	1.3%
22.5	21.78	2.1%	120.0	64.92	1.2%
26.0	24.72	2.1%	129.3	65.66	1.1%
28.0	26.06	2.0%	168.0	66.20	0.9%

Testing of PEC electrodes in immersion-type modules outdoors:

Several PEC electrodes with an active area of 1.5”x1.5” were tested using the prototype PEC modules. The edges of the PEC electrode sample are typically insulated using a clear coat in order to prevent shorting of the device.

The H_2-evolution catalyst is attached to the backside of the PEC electrode. For the experiments presented here, we used electroplated Pt deposited onto stainless steel or porous-Ni as catalyst materials (see Fig. 34). The PEC electrodes are inserted into a sample holder with double O-ring edge seal (see Fig. 35 below) and, the sample insert is placed into the PEC module case.

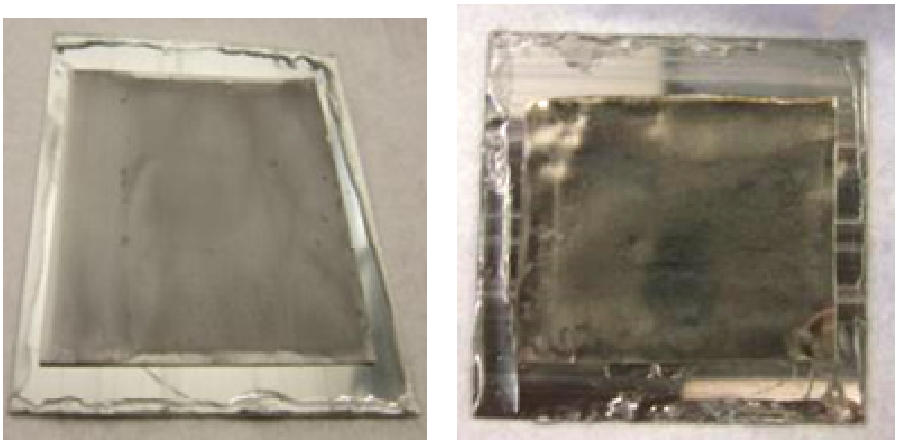

Figure 35: Electroplated Pt-catalyst on stainless steel (left) and Ni-foil (right) attached to the backside of PEC electrodes.

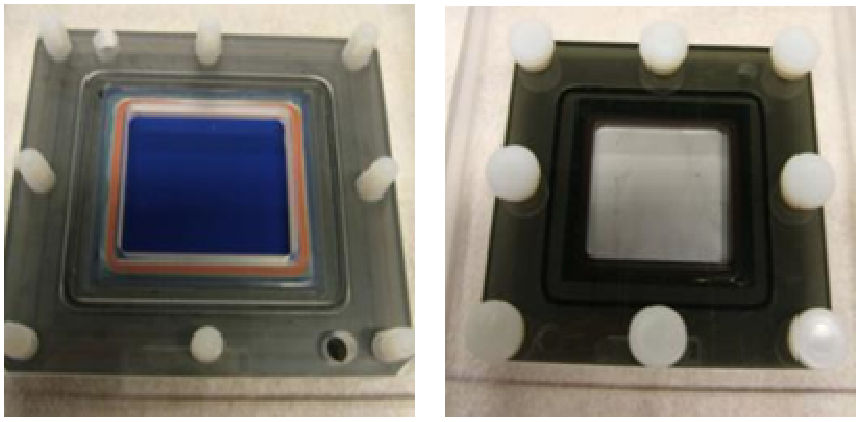

Figure 36: The front (left) and back (right) of the PEC electrode which is inserted in double O-ring seal sample holder which will be placed in a module case.

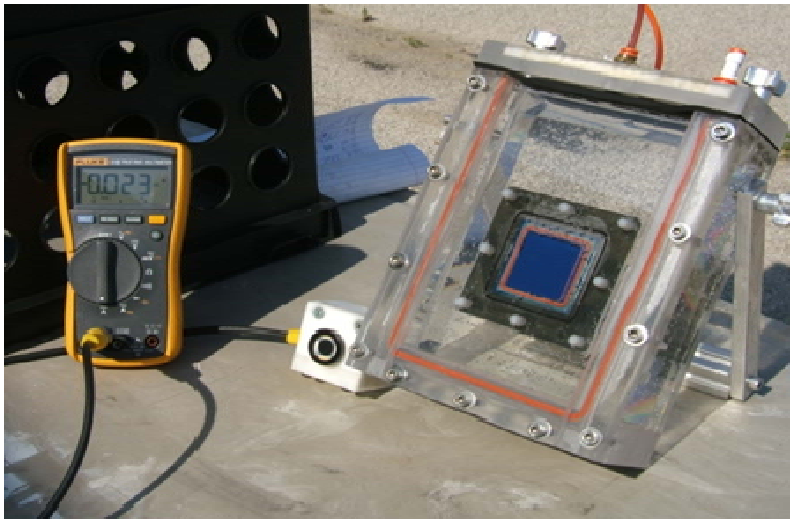

Figure 37: PEC module case during an outdoor test.

The PEC prototype module was tested outdoors and the light intensity was monitored using a Si-photodiode (see Fig. 36 above). Vigorous gas evolution (see Fig. 37 below) is observed during sunny periods and the amounts of oxygen and hydrogen generated are collected separately using graduated cylinders.

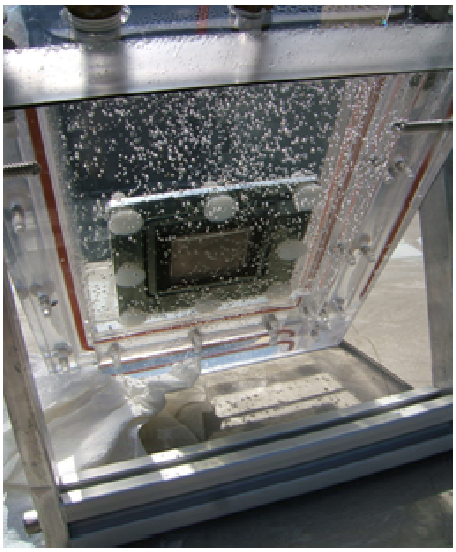

Figure 38: Backside of PEC electrode with Pt-catalyst on stainless steel showing vigorous H_2-evolution during outdoor testing.

During this outdoor test, it became evident that some of the gas generated was trapped underneath the lid of the plastic container and at the rim of the PEC sample holder. Therefore not all the gas generated could be collected and measured. Even with that, we were able to obtain an averaged STH efficiency ~2% during the six hours of runtime. The PEC electrode sample showed a LLVOC value of ~1.7V before and after the test and no visible signs of corrosion were observed.

For a follow-up test the PEC sample placement was changed using a sample holder without any O-ring edge seal. The sample edges were protected by using a clear coating. The PEC module was kept open and the gas generated was collected by using a funnel which leads the gas towards the graduated cylinder. With this setup, we were expecting to reduce the amount of gas being trapped. In this case oxygen and hydrogen gas generated were not separated (see Figs. 38 & 39).

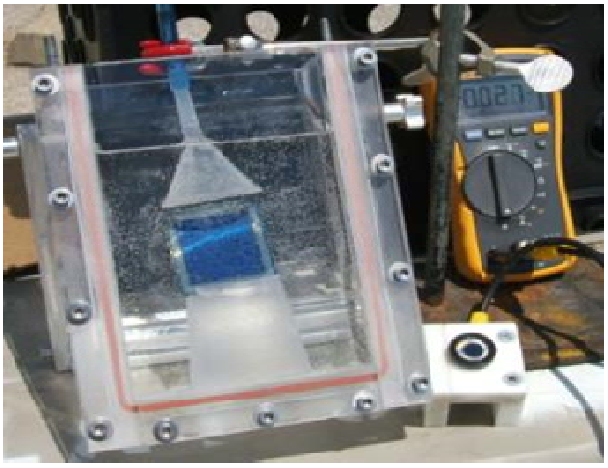

Figure 39: Modified PEC prototype set-up during outdoor testing.

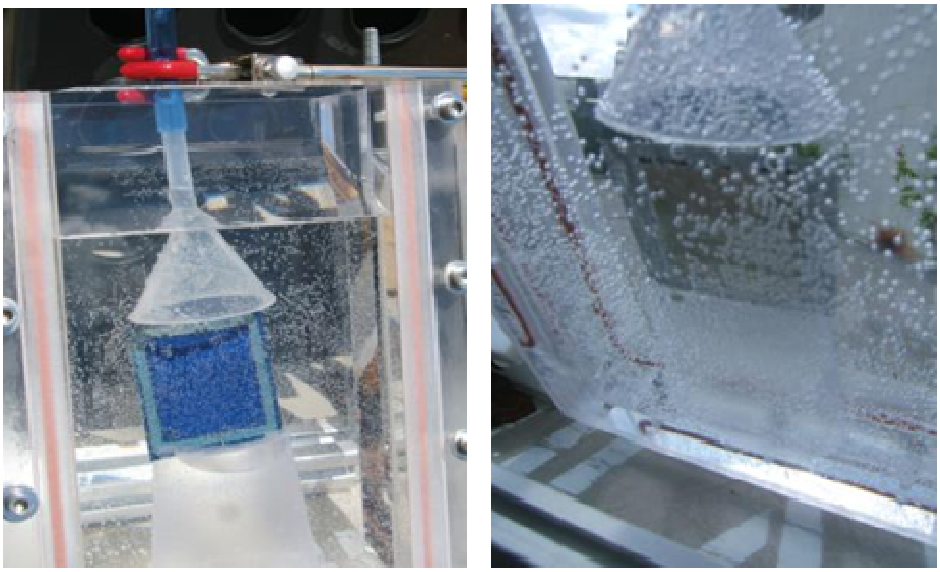

Figure 40: Oxygen evolution at the front (left) and hydrogen evolution at the back (right) of the PEC electrode.

Again, vigorous gas evolution on the front and back of the PEC electrode was observed during sunny periods of the test. The STH efficiency data are summarized in Table 11. The averaged STH efficiency of the test (~6 hrs) was ~2.5% and the highest values obtained during sunny periods is ~3.1%.

Table 11: STH efficiency data for outdoor test;

time / hrs	total time / hrs	ml H_2	ml H_2 total	STH %	total STH %	weather conditions
0.58		7.3		2.92		sunny
	0.58		7.3		2.92	
0.40		5.3		3.08		sunny
	0.98		12.6		2.98	
1.00		12.0		2.79		sunny
	1.98		24.6		2.88	
1.00		12.6		2.92		sunny
	2.98		37.2		2.90	
1.00		10.2		2.37		sunny, some clouds
	3.98		47.4		2.76	
1.00		6.7		1.56		rain, clouds
	4.98		54.1		2.52	
1.00		11.2		2.60		sunny, some clouds
	5.98		65.3		1 2.53	

The sample shows a LLVOC value of ~1.7V for both before and after the test, and no visible signs of corrosion were observed.

In order to better compare different samples side by side and to speed up the testing process, we have designed a multiple sample testing set-up as shown in Fig. 40 below.

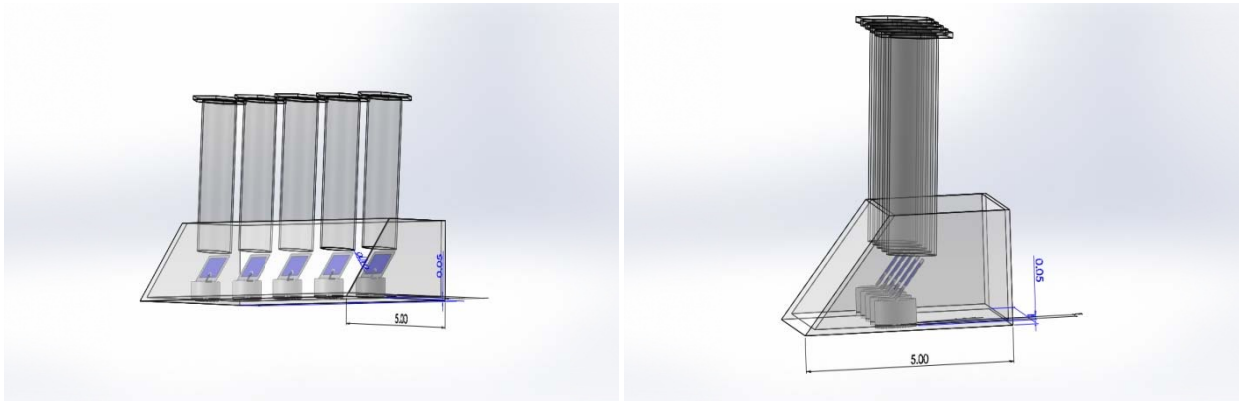

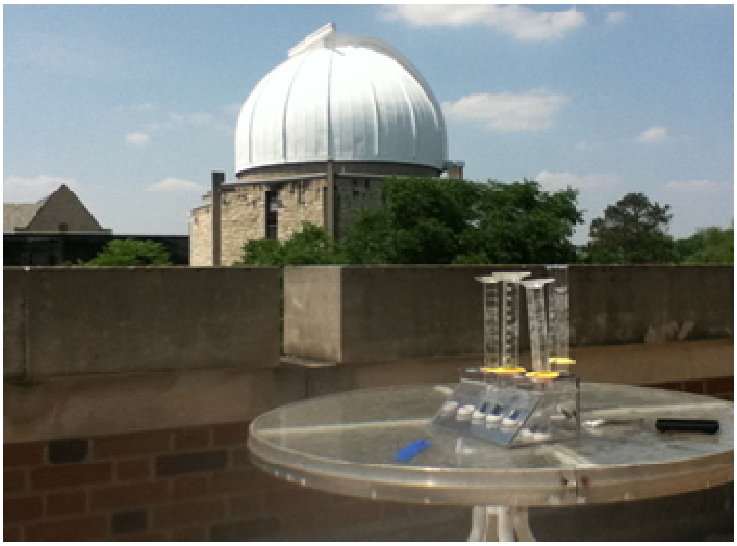

Figure 41: Schematic of the multi-sample PEC testing system (above), and (below) the actual unit in operation outside the Physics Building at the University of Toledo.

4.5. Further Development of H_2-evolution catalyst:

We have experimented with different kinds of catalysts for H_2-evolution. In this section, we will describe some of the procedures and results in details.

Pt catalyst material (Pt: ~6μg/cm^2) is electroplated onto stainless steel or Ni-foil substrates. This preparation relies on the formation of Pt-islands distributed over the substrate surface providing catalytic activity for H_2-generation. A solution of $H_2PtCl_6 \cdot 6H_2O$ is used as electrolyte. In order to coat 4"x4" samples, a plating set-up featuring a horizontal alignment of the electrodes is used (see Fig. 41). The stainless steel substrate is placed at the bottom of the plating container and a graphite foil used as counter electrode floats on the electrolyte (see Fig. 42).

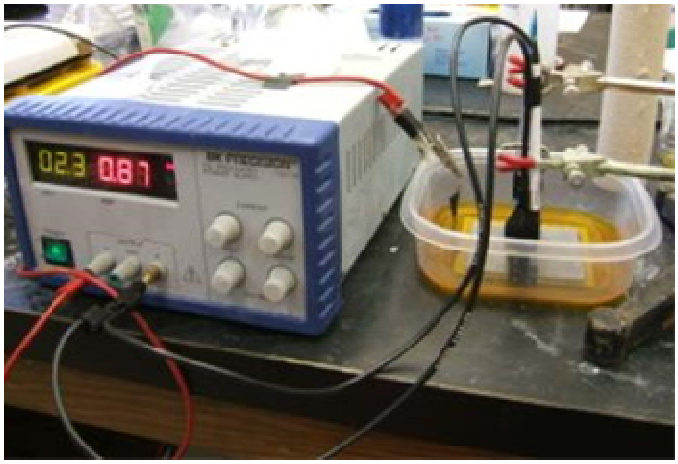

Figure 42: Set-up used for fabricating Pt-catalyst on 4"x4" stainless steel substrates;

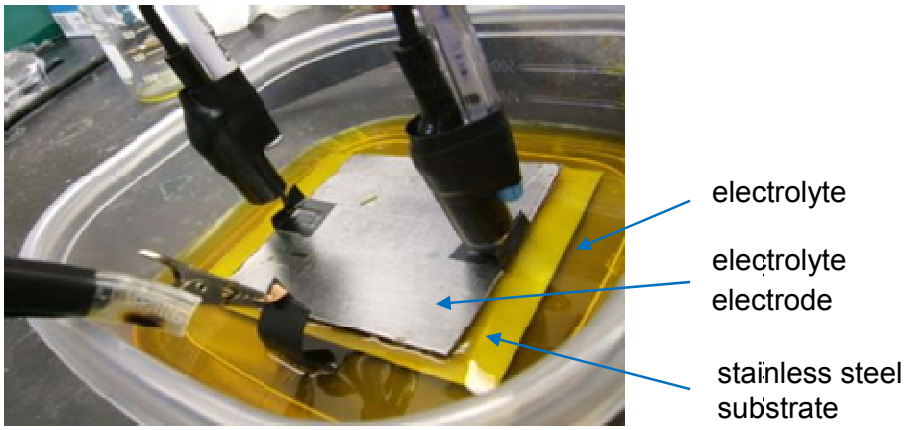

Figure 43: Electrode configuration for Pt-catalyst plating;

Hydrogen evolution reaction (HER) catalyst materials have a substantial impact on the STH efficiency and durability of immersion type PEC systems. We have developed five different types of HER catalyst. They are electroplated Platinum, Ruthenium, electroplated smooth Ni and porous Nickel, and sintered Nickel. While noble metals such as Platinum and Ruthenium are very good HER catalyst, Nickel is considered a low cost option for commercial scale PEC systems for hydrogen generation. Platinum was plated from an H_2PtCl_6 solution and Ruthenium was plated from a $RuCl_3$ solution. Smooth Nickel was plated from a $NiCl_2/NiSO_4$ solution. To obtain porous Ni, we co-deposit Nickel and Zinc from a $NiCl_2/NiSO_4/ZnCl_2$ solution and then leach out Zinc, which will leave a porous Ni coating. Sintered Nickel is obtained by annealing Nickel powders in a mixture of other metal powders acting as filler which then are leached out, leaving a porous Nickel structure behind. The HER catalyst sheet is then attached to the backside of tf-Si based PEC electrodes which use Co_3O_4 as TCCR coating.

Table 12 summarizes the initial STH efficiency values obtained for PEC electrodes using these five different HER material. The highest initial STH efficiency of 5.7% has been obtained using plated Ruthenium as HER catalyst followed by plated Platinum providing a STH efficiency of 5.6%. The STH for electrodes with Ni HER are somewhat lower: 4.1% for plated porous Nickel, 3.0% for sintered Nickel and 1.5% for plated smooth Nickel catalyst materials. In comparison, the PEC electrode without any HER catalyst (last one in Table 12) has the lowest

STH efficiency and worst durability, which indicates that a HER catalyst, although on the backside of photo-electrode, is essential.

Table 12: Comparison of different hydrogen generation catalyst:

HER catalyst	Initial STH efficiency	Operating hours w. STH efficiency >1%
Plated Platinum	5.6%	42 hrs
Plated Ruthenium	5.7%	37 hrs
Plated smooth Nickel	1.5%	80 hrs
Plated porous Nickel	4.1%	170 hrs
Sintered Nickel	3.1%	480 hrs
No HER catalyst	1.2%	8 hrs

Although the highest STH efficiency values were obtained using Platinum and Ruthenium as HER catalyst materials, the PEC system using Nickel as HER catalysts demonstrate much better durability (480hours). Figure 42a shows STH efficiency versus operation time for PEC electrodes with different HER catalyst materials.

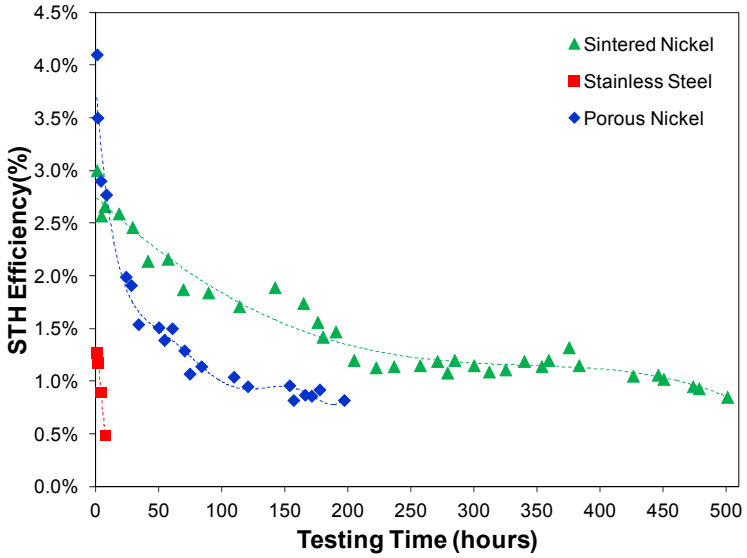

Figure 42a: STH efficiency versus operation time for PEC electrodes with different HER catalyst materials.

Sintered nickel as HER catalyst

When we used sintered Ni as the HER catalyst, we noticed a color change in the electrolyte which could be related to the migration of metallic materials of the sintered nickel from the counter electrode to the working electrode. Therefore, we performed a pre-treatment of the sintered nickel with it as cathode and a stainless steel sheet as anode in a KOH solution. A voltage of about 3V was applied between the nickel and stainless steel sheet, and the pretreatment lasted about 20 hours. The setup for the pretreatment is shown in Figure 43.

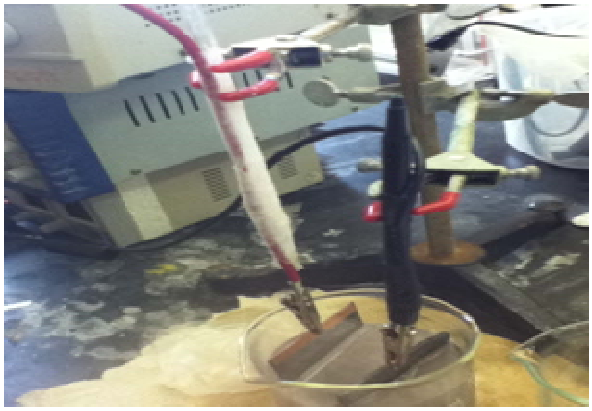

Figure 44: Setup for pre-treating the sintered nickel

Figure 44 is the images of the sintered nickel and the stainless steel sheet after being treated for about 20 hours. It is seen that the stainless steel turned to be brown after the treatment as . The PEC cell with the pretreated sintered nickel ran about 480 hours with STH efficiency above 1%, as indicated in Figure 45; while STH efficiency of the un-pretreated one drops below 1% after running only about 4 hours, and its silicon side turned to be brown quickly. This indicates that the pre-treatment of the sintered Ni greatly improves the PEC performance.

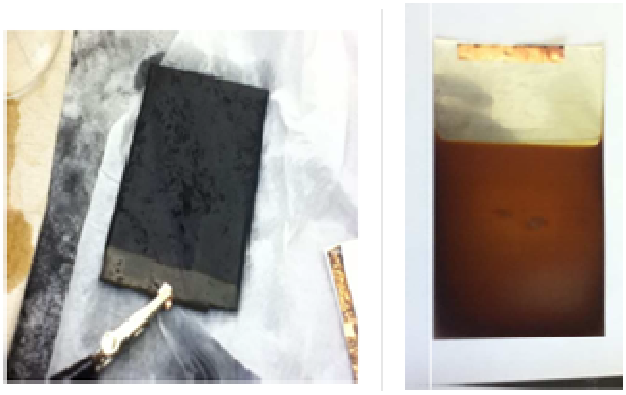

Figure 45: Images of the sintered nickel and stainless steel after being treated for 20 hours

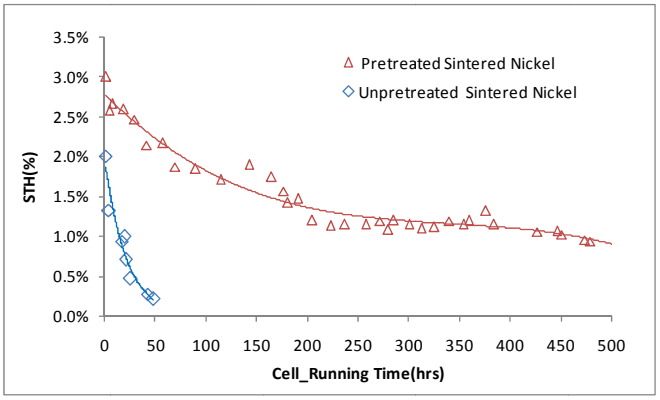

Figure 46: STH efficiencies and lifetime over time for PEC electrodes with pretreated and not-pretreated sintered nickel as HER catalyst.

PEC electrode using plated Ru as hydrogen evolution catalyst

Ruthenium (Ru) is considered a viable candidate for a hydrogen evolution catalyst. We have used the following procedures to make Ru plating for hydrogen generation catalyst. Aqueous solutions of Ruthenium-chloride ($RuCl_3$) and Ruthenium-nitrosyl-sulfate $(Ru(NO))_2(SO_4)_3$ were used as plating electrolytes. Stainless steel sheets were cleaned with a commercial degreaser and these substrates were etched with HCl before plating the catalyst. Plating from a $(Ru(NO))_2(SO_4)_3$ solution which is commonly used for plating decorative Ru coatings did not yield sufficient Ru-deposits: the concentration of the $(Ru(NO))_2(SO_4)_3$ solution was varied between 0.01–0.1 mol/L, the plating time was varied between 1-7 min and the current density was varied between 0.01 A/cm^2 - 0.02 A/cm^2. Finally, by using a 0.1 mol/l $RuCl_3$ solution at a current density of 0.02 A/cm^2 and a plating time of 3min, we were able to obtain good catalytic Ru-deposits.

Fig. 46 depicts the experimental set-up used for electroplating of Ru-catalyst and, Fig. 47 shows the plated Ru-catalyst forming a uniform coverage on the stainless steel surface.

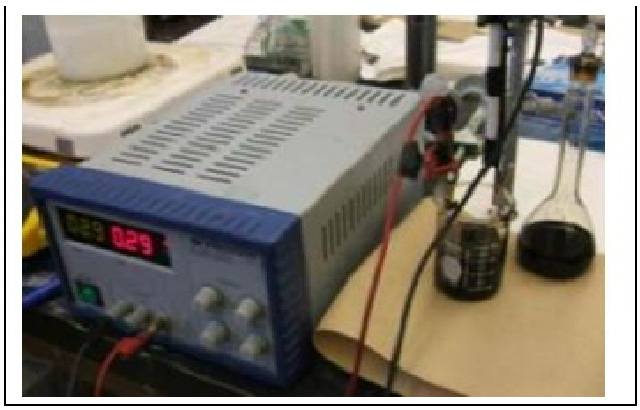

Figure 47: Set-up for electroplating of Ruthenium used as hydrogen evolution catalyst;

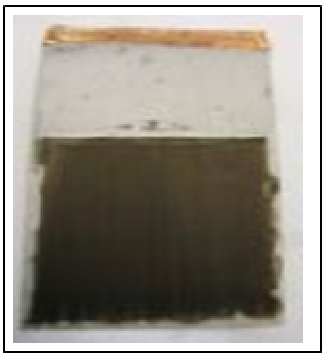

Figure 48: Plated Ru-catalyst on etched stainless steel substrate;

A PEC electrode with plated Ru-catalyst attached to the back-side was tested in KOH/H_3BO_3 for 6 test days for about 7 hours each day. Vigorous gas evolution was observed during test day 1-4 (see Fig.48).

Fig. 49 depicts the averaged STH eff. data vs runtime obtained during the test. The initial STH eff. at the beginning of the day is ~5.3%. The STH eff. degradation during test day 1 - day 4 is not significant. It recovers when the samples is not exposed to intense light such that the STH

efficiency starts at about the same value at the beginning exposure to light on the following day. Noteworthy is, that the PEC electrode shows comparable hydrogen generation during the first four days of exposure to light. The initial STH eff. value observed for the 5th test day is comparable to the initial value. However, the STH eff. shows a significantly steeper and irreversible degradation during this test day. On the 6th test day the initial STH eff. was found to be ~3%, which is much lower and the values decreased to ~1% after ~4 hrs into the test. The sample was removed from the set-up and visual inspection revealed significant development of spot corrosion on the sunny side of the PEC electrode. Again, exposure of the a-Si to the electrolyte caused by TCCR and ITO corrosion by the electrolyte has caused shunting of the device and low room light-VOC values of ~0.1 V - 0.2 V are observed.

The PEC electrode generated ~655 ml of hydrogen in ~37 hrs which indicates an averaged STH eff. of ~4.1%.

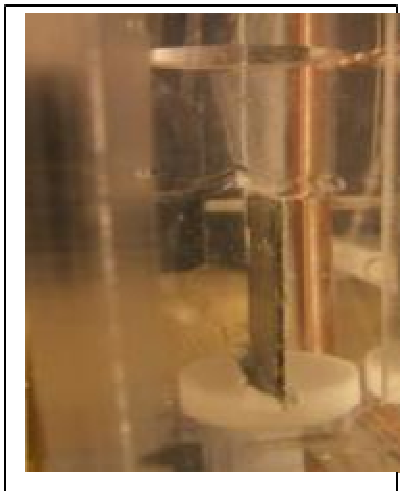

Figure 49: PEC electrode with Ru-catalyst attached to the back-side under operating conditions at the light soaking set-up with a stadium lamp;

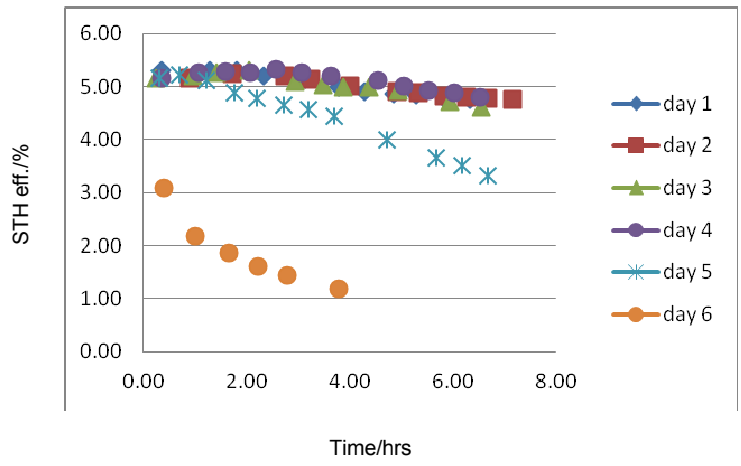

Figure 50: STH eff. vs. runtime for PEC electrode with plated Ru as hydrogen evolution catalyst;

STH efficiency measured using indoor stadium lamp set-up

According to Z.Chen et al., J. Mater. Res., Vol. 25, No 1, 2010, the STH efficiency is determined using the expression:

$$STH = \frac{(mol\ of\ H_2\ per\ second) \times (237\ kJ\ per\ mol\ (\Delta G\ for\ H_2))}{\left(P_{total}\frac{mW}{cm^2}\right) \times (Area\ of\ cell\ (cm^2))}$$

where the illumination power density P_{total} for the experimental set-up should be close to 100 mW/cm^2 which is one-sun illumination. For the stadium-light set-up used for our experiment this requirement cannot be met as the illumination power density provided is much lower and the light uniformity is impacted by the parabolic shape of the lamp (see Fig. 50). In order to get an estimate for STH efficiency value which takes the lower light intensity into consideration, we measured the light-intensity in a 3.5" x 3.5" area around the location of the PEC electrode during operation. The PEC electrodes tested have an area of 2.5" x 2.5". The actual averaged illumination power density P_{total} was determined to be about 74 mW/cm^2. Reported STH efficiency data in the previous sections of this report are calculated for P_{total} = 100 mW/cm^2, assuming a linear response in H production as a function of light intensity in the 74 -100 mW/cm^2 range. The measurement using a stadium lamp may lead to a lower measured STH efficiency value as the three component cells within the triple-junction solar cells are optimised for AM1.5 spectrum and stadium lamp does not provide a spectrum as AM1.5.

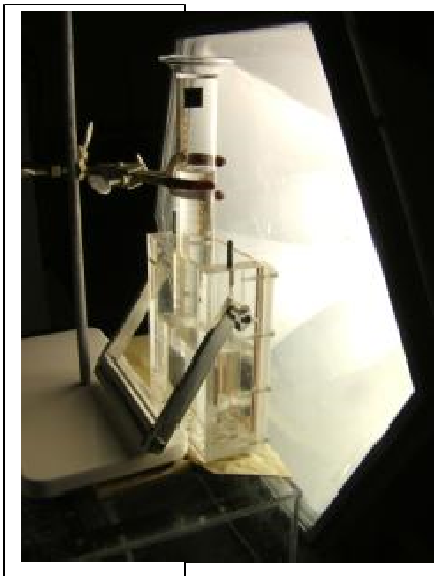

Figure 51: PEC prototype module container under operating conditions at stadium lamp set-up;

Table 13 below summarizes the initial STH eff. values obtained using the stadium light as the illumination source for a variety of electrolyte solutions we studied during this research. We achieved higher STH efficiency with the Pt or Ru as hydrogen generation catalyst in our standard KOH/H_3BO_3 electrolyte.

Table 13: STH efficiency for various catalysts

catalyst	electrolyte	STH efficiency P=100mW/cm^2
Pt (large area)	KOH/H_3BO_3	5.26%
Pt	KOH/H_3BO_3	4.37%
Pt	KOH/H_3BO_3/gelatin	4.61%
Pt	KNO_3	3.94%
Pt	KNO_3/EDTA	3.55%
Ni (sintered)	KOH/H_3BO_3	3.68%
Ru	KOH/H_3BO_3	5.31%

Cyclo-voltamtric evaluation of different hydrogen generation catalysts:

We have conducted Cyclo-voltametric measurements to characterize the hydrogen and oxygen evolution catalysts. These measurements also help us to understand the corrosion stability of PEC electrodes in different electrolytes.

Electrodes and materials were tested in a three electrode configuration using a Voltalab®-setup (see Fig. 51). A $Hg/Hg_2Cl_2/Cl^-$ (SCE: +0.2682 V vs. NHE) electrode is used as reference electrode and Pt-mesh serves as the auxiliary electrode. The measurements are performed in a KNO_3 solution and in KOH/H_3BO_3 which is used as electrolyte in immersion-type PEC systems.

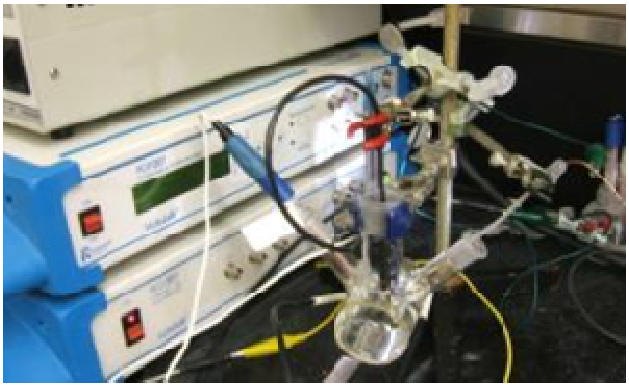

Figure 52: Voltalab set-up: three electrode configuration used for cyclo-voltametric measurements in electrolyte;

Hydrogen evolution catalysts

Plated Pt, plated Ni and sintered Ni are used as HER catalyst materials for hydrogen generation in PEC systems. Electrodes were fabricated from these materials (see Fig.52) and, from etched stainless steel, respectively.

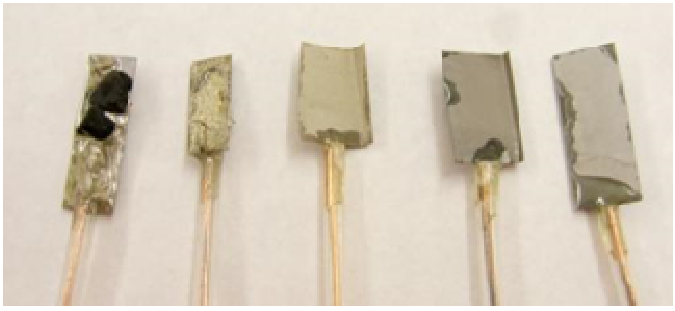

Figure 53: Electrodes made from hydrogen evolution catalysts (from left to right): sintered Ni, plated Ni ($ZnCl_2$ precursor), plated Ni (NH_4Cl precursor); plated Pt, etched stainless steel;

The electrodes were used as working electrodes for CV-measurements conducted in KNO_3 and KOH/H_3BO_3. Fig.53-Fig.55 compares the CV-measurements revealing the catalytic performance of the materials in these electrolytes.

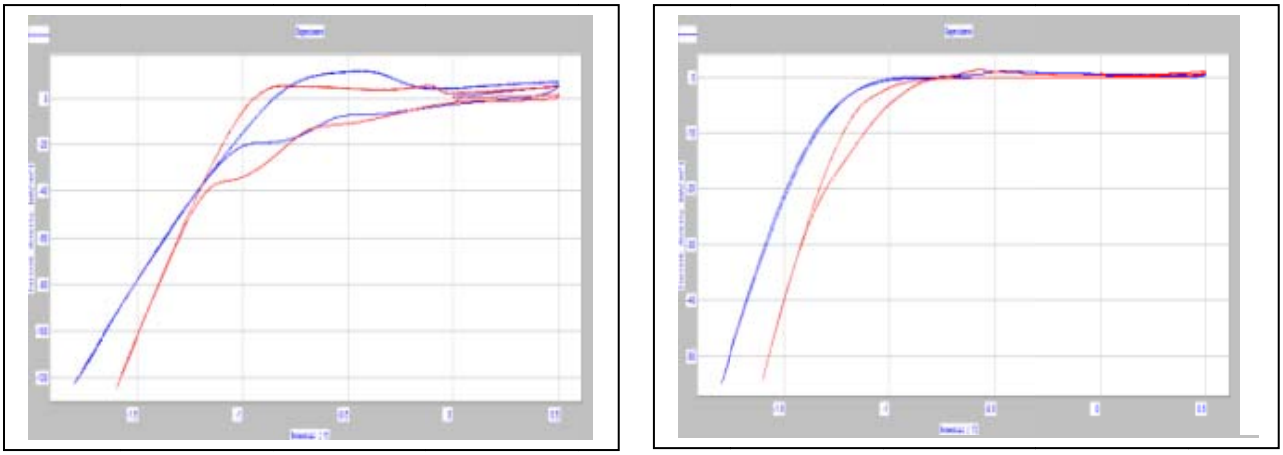

Figure 54: CV-measurement for plated Pt (left) and sintered Ni (right) performed in KNO_3 (red) and KOH/H_3BO_3 (blue);

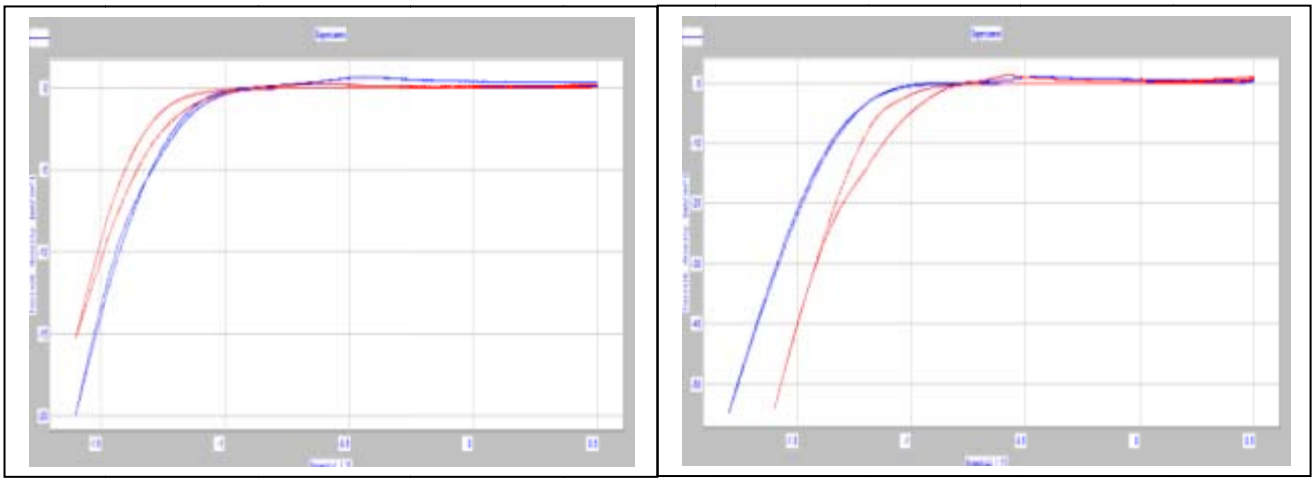

Figure 55: CV-measurement for plated Ni ($ZnCl_2$) (left) and plated Ni (NH_4Cl) (right) performed in KNO_3 (red) and KOH/H_3BO_3 (blue);

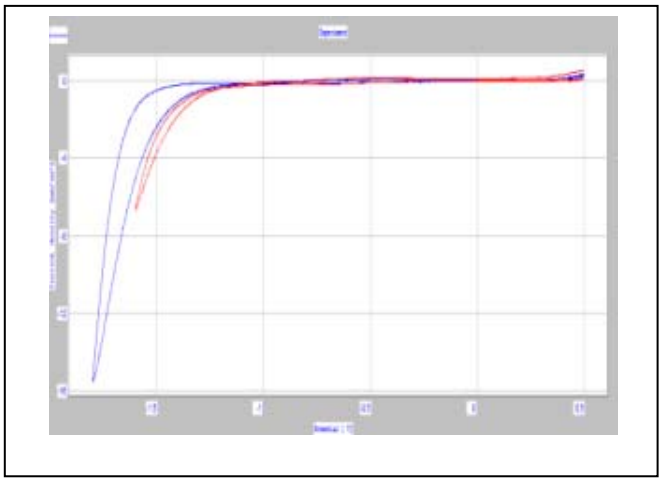

Figure 56: CV-measurement for etched stainless steel performed in KNO_3 (red) and KOH/H_3BO_3 (blue);

The data indicate that plated Pt shows comparable catalytic performance in KNO_3 and in KOH/H_3BO_3. For sintered Ni, plated Ni (NH_4Cl precursor) and etched stainless steel the hydrogen evolution occurs in KNO_3 at lower voltages than in KOH/H_3BO_3 suggesting that these materials should perform better as hydrogen evolution catalysts in KNO_3. On the other hand, plated Ni ($ZnCl_2$ precursor) should be a superior hydrogen catalyst in KOH/H_3BO_3 than in KNO_3.

Fig. 56 compares the CV readings for hydrogen evolution catalyst materials measured in KNO_3 suggesting superior performance for plated Pt compared to all other materials investigated. Stainless steel is an inferior hydrogen evolution catalyst in this study, as expected. Noteworthy is that all Ni electrode samples show comparable catalytic performances which are inferior compared to plated Pt but superior compared to etched stainless steel.

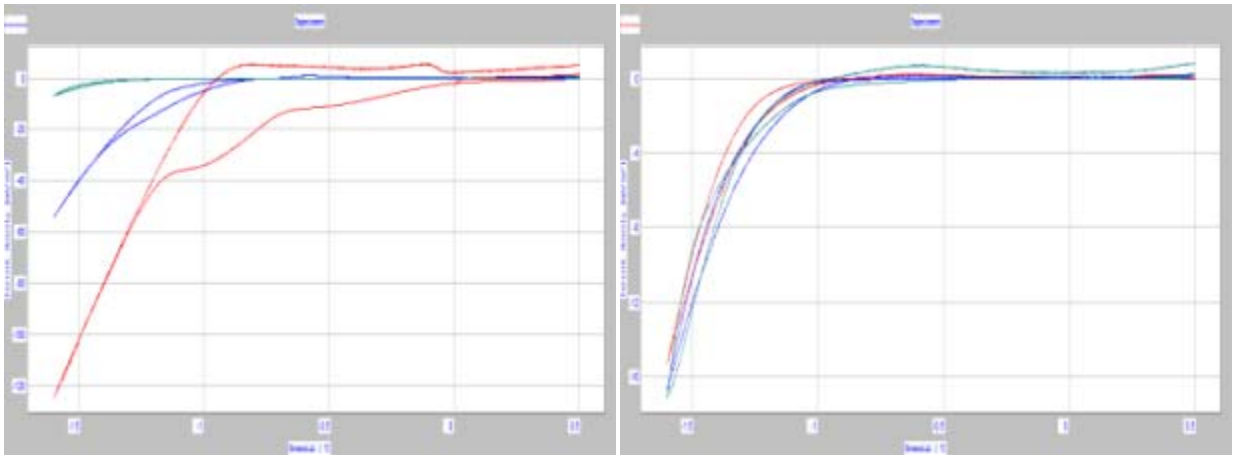

Figure 57: CV-measurements in KNO_3: left: plated Pt (red), plated Ni (NH_4Cl precursor) (blue), stainless steel (green); right: plated Ni ($ZnCl_2$ precursor) (red), plated Ni (NH_4Cl precursor) (blue), sintered Ni (green);

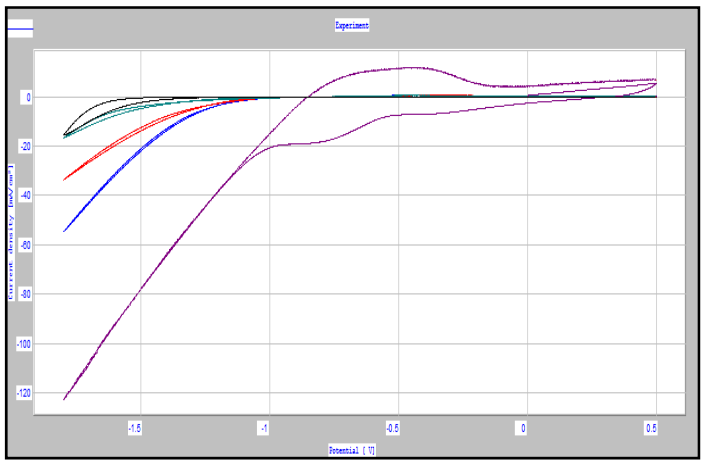

Figure 58: CV-measurements in KOH/H_3BO_3: plated Pt (purple), plated Ni (NH_4Cl precursor) (blue), plated Ni ($ZnCl_2$ precursor) (red), sintered Ni (green) and stainless steel (black);

Fig.57 compares CV-measurements for all catalysts studied regarding their performance in KOH/H_3BO_3. Again, plated Pt shows superior catalytic performance compared to all other materials investigated and, etched stainless steel behaves as an inferior catalyst. However, sintered Ni shows a similar performance compared to etched stainless steel. Plated Ni (NH_4Cl) and plated Ni ($ZnCl_2$) show small differences in performance suggesting a superior catalytic activity for plated Ni (NH_4Cl).

4.6. Cyclic-voltametric study of TCCR layer as oxygen evolution catalysts

TCCR layer deposited as a top layer at the "sunny" side of PEC electrodes are acting as oxygen evolution catalysts. These materials need to be corrosion resistant in electrolytes used for operating PEC systems. CV measurements allow investigating materials regarding their catalytic properties for oxygen evolution and, these measurements are supporting the evaluation of the expected long-term performance of materials in different electrolytes.

Electrodes were fabricated using a-Si solar cell material where the top layer is ITO and from a-Si material which has a Co_3O_4 coating deposited onto the ITO layer (see Fig.58). The edges of the samples are embedded in a non-conducting epoxy preventing electrolyte exposure during measurement.

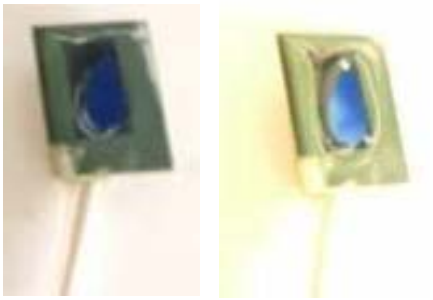

Figure 59: Electrodes made from a-Si solar cell material: electrodes where top layer is ITO (left) and electrode where Co_3O_4 is deposited onto ITO (right);

CV measurements were conducted using these electrodes in KNO_3 solution and in KOH/H_3BO_3. The measurements are compared to data obtained from electrodes made from ITO coated glass samples (TEC15). Fig. 59-Fig. 60 show the CV measurements for all electrodes obtained for ten cycles for each measurement in both electrolytes.

The CV measurements shown in Fig.59 suggest that ITO on a-Si and Co_3O_4 deposited onto ITO on a-Si are generating oxygen in KOH/H_3BO_3 at a much lower voltage than in KNO_3. This suggests that these catalysts perform much better in a borate electrolyte than in a KNO_3 solution. For each CV-measurement ten cycles were run. The difference between each cycle compared to the initial cycle and the overall shift of the CV data is used as an indicator for corrosion stability of the materials when operating in a particular electrolyte. The data indicate that ITO on a-Si might be affected by corrosion when operating as oxygen evolution catalyst in KOH/H_3BO_3: the CV data shift significantly for each run. A minor shift in the data is observed when the electrode is run in KNO_3. On the other hand, Co_3O_4 deposited onto ITO on a-Si seems to exhibit superior corrosion stability in KOH/H_3BO_3 compared to ITO on a-Si. Again, a small shift is observed when this electrode is run in KNO_3.

Fig.60 shows the CV measurements obtained for ITO deposited onto glass (TEC15). The oxygen evolution seems to occur at comparable voltages when operating these electrodes in KNO_3 or KOH/H_3BO_3. However, a significant shift in CV data is observed for each cycle measured: this indicates that ITO on glass is severely affected by corrosion when run in a borate electrolyte and, non-negligible corrosion is observed in KNO_3.

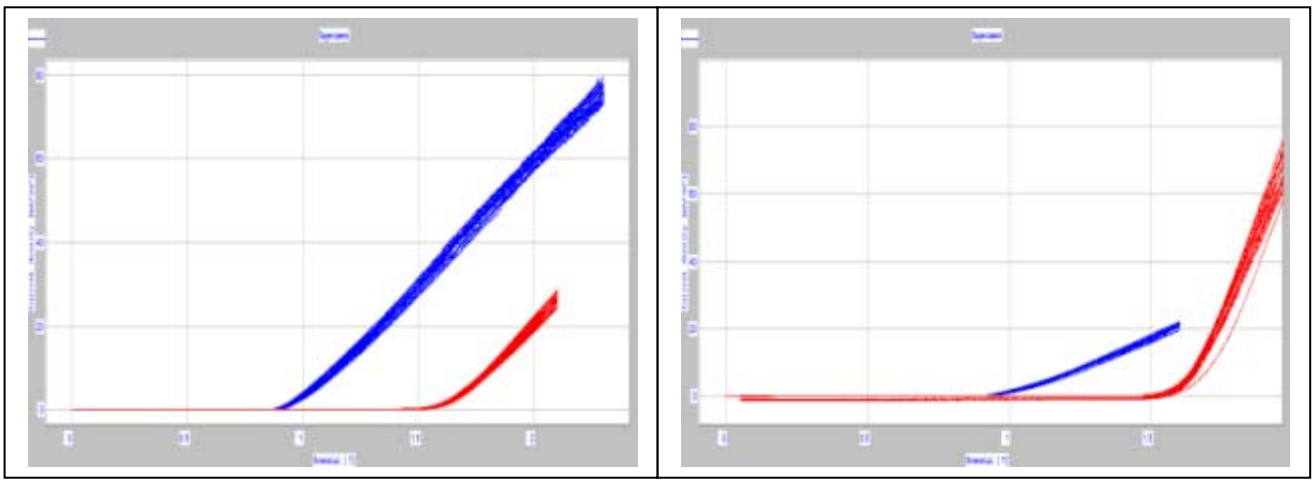

Figure 60: CV-measurement for a-Si with ITO top layer (left) and a-Si with Co_3O_4 deposited onto ITO (right) performed in KNO_3 (red) and KOH/H_3BO_3 (blue);

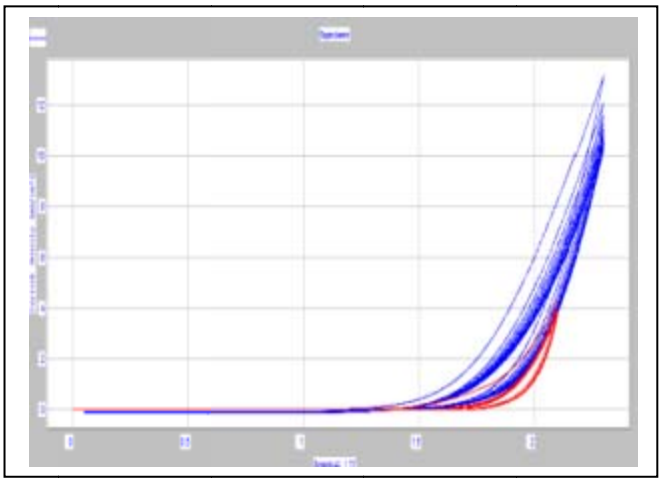

Figure 61: CV-measurement for ITO coated glass (Tec15) performed in KNO_3 (red) and KOH/H_3BO_3 (blue);

Fig. 61 compares all oxygen evolution catalysts studied regarding their performance in KNO_3 and KOH/H_3BO_3. The measurements show that ITO on a-Si and Co_3O_4/ITO on a-Si generate oxygen at a comparable voltage when run in both electrolytes. ITO on a-Si seems to have superior catalytic performance compared to Co_3O_4/ITO on a-Si when run in KOH/H_3BO_3 but, in this case ITO on a-Si is more affected by corrosion. Co_3O_4/ITO on a-Si is less affected by corrosion in both electrolytes and out-performs ITO on a-Si when run in KNO_3. Noteworthy is that the generation of oxygen is inhibited when using ITO on glass as a catalyst: water splitting occurs in both electrolytes at much higher voltages compared when using TCCR electrode samples on a-Si substrates; the CV-measurements for ITO on glass are indicating over-potential issues for oxygen evolution. Overall, the CV measurements confirm that using Co_3O_4 as TCCR in PEC electrodes provides sufficient corrosion stability in KOH/H_3BO_3 while Co_3O_4 is a suitable oxygen evolution catalyst.

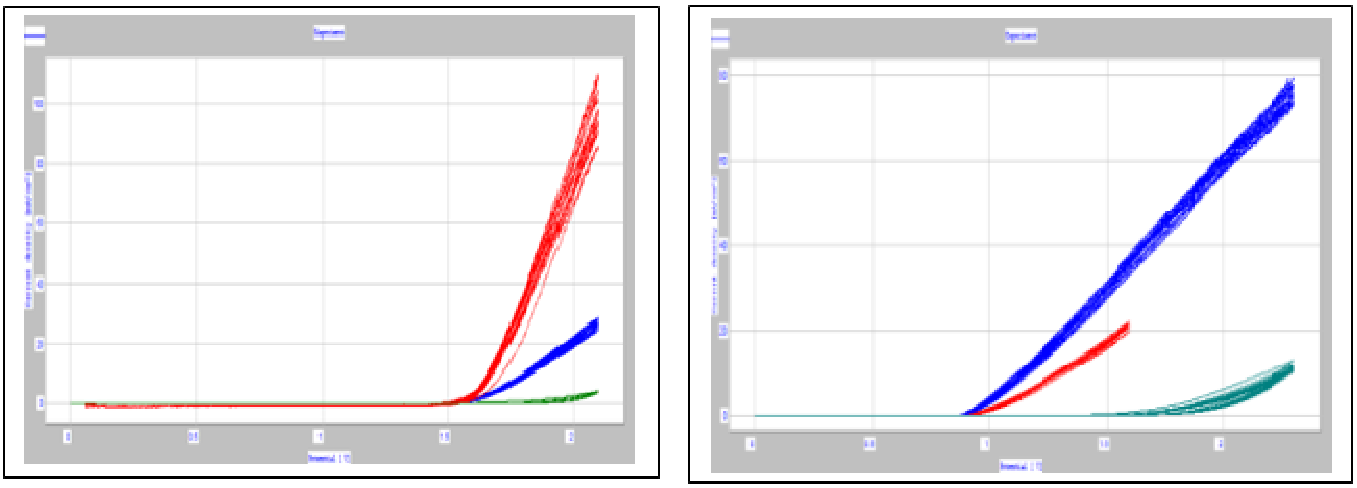

Figure 62: CV-measurements in KNO_3 (left) and KOH/H_3BO_3 (right): Co_3O_4/ITO on a-Si (red), ITO on a-Si (blue), ITO on glass (green);

4.7. A Novel Design for Immersion Type PEC Cells

Triple junction a-Si/a-SiGe/a-SiGe solar cell is an ideal material for making cost-effective Photoelectrochemistry (PEC) system which uses sun light to split water and generate hydrogen. It has the following key features:

- It has an open circuit voltage (V_{oc}) of ~ 2.3V and has an operating voltage around 1.6V. This is ideal for water splitting. There is no need to add a bias voltage or to inter-connect more than one solar cell.
- It is made by depositing a-Si/a-SiGe/aSi-Ge thin films on a conducting stainless steel substrate which can serve as an electrode. When we immerse the triple junction solar cells in the electrolyte and illuminate it under sunlight, the voltage is large enough to split the water, generating oxygen at the Si solar cell side and hydrogen at the back, which is stainless steel side. There is no need to use a counter electrode or make any wire connection.
- It is being produced in large rolls of 3ft wide and up to 5000 ft long stainless steel web in a 25MW line roll- to-roll production machine, therefore it can be produced at an extremely low cost.

However, the a-Si thin film solar cell is not very stable in the electrolyte which is usually acidic or basic. It would be corroded by the electrolyte, especially under working conditions. In order to develop a PEC system with the triple junction a-Si solar cells, we need to develop a coating which can be applied onto the solar cell surface, and which has the following features: 1) Transparent, so that the light can pass through the coating and reach the solar cells, 2) Conducting, so that the voltage generated by the solar cell under sun light can be applied to the electrolyte-electrode interface and generate oxygen, 3) Corrosion Resistant, so that it can protect the solar cell surface, not being corroded in the electrolyte, and 4) can be deposited onto the solar cell surface at 200^{o}C or lower, since the solar cell would be damaged if the temperature is higher than 200^{o}C. In addition, it would be very helpful that it can also acts as an oxygen evolution catalyst (OER).

After many years of research with many different kinds of material, we have developed a very promising TCCR coating material, which is the sputtered Co_3O_4 material. At 70nm thickness or lower, it has a transparency of 95% or better. It can be sputtered at lower than 200^{o}C. It also acts as a good oxygen catalyst. We have made PEC electrode using the triple junction a-Si solar cells, with Co_3O_4 coating at the Si side, and hydrogen generation catalyst attached at the stainless side. In the KOH/H_3BO_3 electrolyte, we were able to obtain a solar to hydrogen conversion efficiency (STH) about 5.7% and a running time about 480 hrs, which are very promising results.

However, what we have observed is that with time, the STH efficiency would decrease and eventually, after about 480 hours, the electrode surface would suffer severe corrosion and the system would stop working. It seems that the Co_3O_4 coating does have some protection effects, however, at ~70nm, the surface coverage might be sparse and it can still be corroded away with time. We could increase its thickness to increase the corrosion protection effect. However, the transparency would suffer and thus the solar energy would be under-utilized and STH would decrease.

We have come up with a novel design which would address this problem and which would lead to a PEC electrode which can generate hydrogen effectively and have a good durability.

In this brand new design, we would separate the solar cell surface into two types of regions, Region 1 and Region II. For Region I, we would coat the surface with some corrosion-resistant transparent protective layer ("CRTP Layer"), which does not need to be electrically conducting. There are many materials we can use, for example, clear coat, SiO_2 coating, etc. For region II, we would coat the surface with corrosion-resistant conducting catalytic layer ("CRCC Layer"), such as Co_3O_4 material. In this design, Region II does not need to be transparent, it only needs to have good electrical conductivity and acts as good oxygen generating site. Since there is no need to be transparent, we can make much thicker Co_3O_4 coating, not being limited by the 70nm thickness. Effectively, Region I will act as solar energy absorbing and electrical voltage generating sites, and Region II will act as oxygen generating site with Co_3O_4 as the oxygen generating catalyst.

As shown in Figure 62 below, the front surface facing light is covered in some areas with corrosion-resistant transparent protective layer ("CRTP Layer", or "Region 1") and in some other areas with corrosion-resistant conducting catalytic layer ("CRCC Layer", or "Region 2") for the evolution of oxygen. A transparent conductor layer adjacent to the front surface (right below it) helps to transport photo-generated holes from the CRTP area to the CRCC area at the front surface. The back surface of the photo-electrode is covered with a corrosion-resistant conducting catalytic(CRCC) layer for the evolution of hydrogen. The photovoltaic stack, under light through the CRTP layer, generates sufficient voltage to drive water electrolysis at the CRCC layers at the front and back surfaces. An example of such photovoltaic stack is a stainless steel (SS)/metal reflector/TCO/a-Si n-layer/a-SiGe i-layer/a-Si or nc-Si p-layer/ a-Si n-layer/a-SiGe i-layer/a-Si or nc-Si p-layer/ a-Si n-layer/a-Si i-layer/a-Si or nc-Si p-layer/ITO. Such stack allows oxygen generated at the CRCC layer near the front surface and hydrogen near the CRCC layer at the back surface. In order to have efficiency water splitting, it is desirable that a greater area of the front surface is covered with CRTP material and a small area of the front surface is covered with CRCC material. (Figure 62 and Figure 63 below).

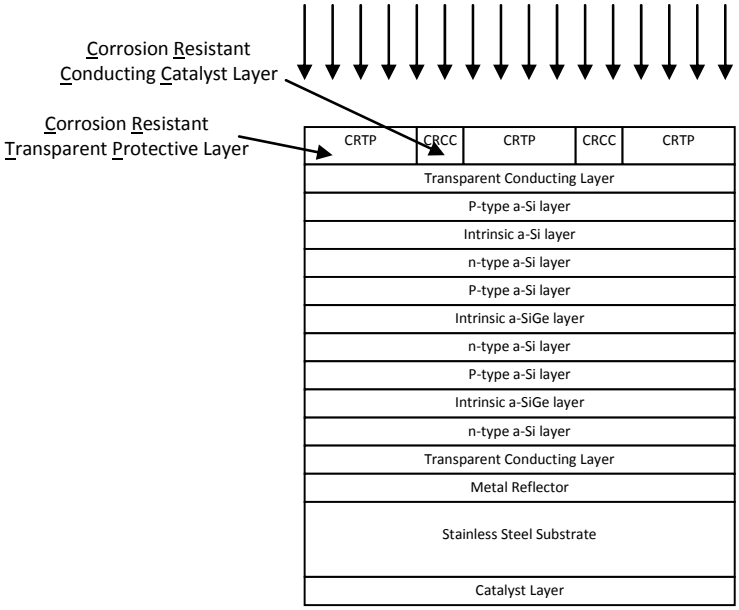

Figure 63: The schematic of the photo-electrochemical(PEC) electrode with the novel design of alternating CRCC and CRTP coating**.**

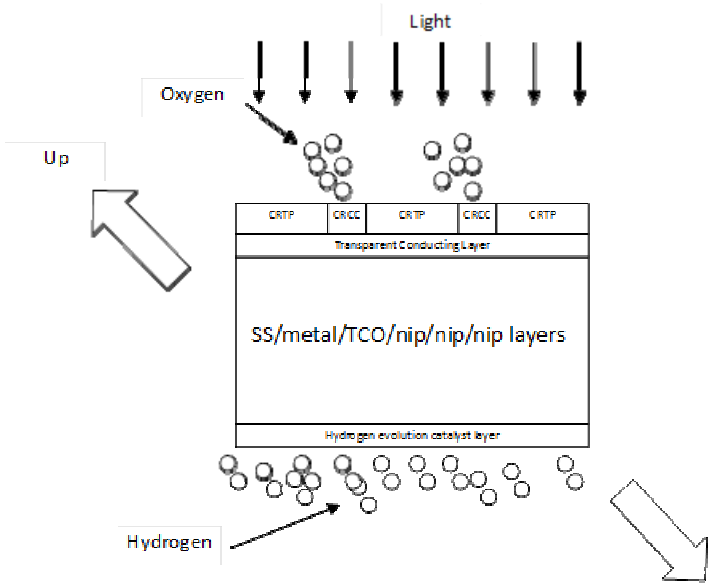

Figure 64: A schematic illustrating the Photo-electrochemical(PEC) system, with the novel electrode design of alternating CRCC and CRTP coatings, under illumination and generating hydrogen and oxygen gas.

We have filed two provisional patent applications based on this CRCC/CRTP design. Figure 64 shows a PEC electrode with CRCC/CRTP design. The silver lines are Co_3O_4-coated regions (CRCC), and the blue regions are for light absorption (CRTP). The ratio between the areas of CRCC and the CRTP regions can be adjusted to optimize the PEC performance.

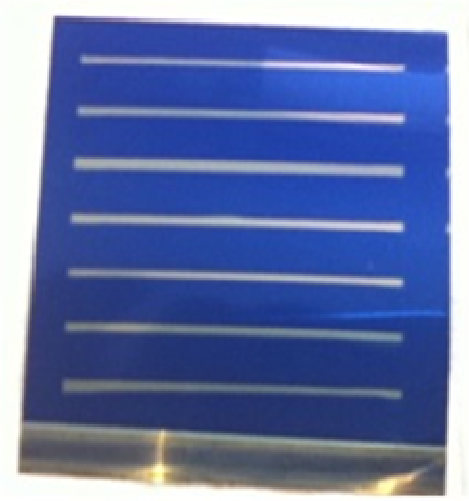

Figure 65: A PEC electrode with CRCC/CRTP design. The silver lines are Co_3O_4-coated regions (CRCC), and the blue regions are for light absorption (CRTP). The ratio between the areas of CRCC and the CRTP regions can be adjusted to optimize the PEC performance.

We have made significant effort experimenting with this design. In the following sections, we will discuss our experimental results in details. In the first set of approach, we tried to use Ni/Pt or Pt coating to make the CRCC layer and use automotive clear coat as the CRTP layer. In the

second set of approach, we tried to use Co_3O_4 as the CRCC layer and use clear coat or sputtering SiO_2 as the CRTP layer.

Development of a Pt/Ni plated layer as CRCC

We investigated coating of Pt electrode as CRCC layer on top of Co_3O_4 coated a-Si triple-junction solar cell as OER catalyst, using H_2PtCl_6 as electrolyte (pH ~ 1) and with a Pt-mesh as the counter electrode. It is found that corrosion of Co_3O_4 starts after 90 seconds of electro-deposition. Similar plating process on the stainless steel back side as the HER catalyst was successful. When pH level was increased to ~ 6, minimal corrosion would occur. We explored the plating of Pt onto Co_3O_4 coated a-Si with varying plating current densities and varying plating times. A typical plating condition used is 8 mA/cm^2 for 60 sec. In order to form Pt coating in certain areas for CRCC and expose certain other areas for the application of CRTP, Kapton tapes are applied to areas to prevent Pt plating. A clear coating used in automotive industry is used to create the CRTP region. Certain overlap of CRCC and CRTP areas are designed into the process to avoid undercut corrosion. The effort in generating CRCC/CRTP structure using plated Pt is challenged with device shunting issues as the plating process corrodes the TCO layer and the a-Si device. We then explored the use of a plated Ni as a buffer layer prior to the plating of Pt layer. We investigated plating of Ni films on Co_3O_4 coated a-Si device using $NiSO_4/NiCl_2$ electrolyte with a pH-value of ~3. A typical plating conditions used is 20mA/cm^2 current and with 30 -180 sec. Again, Kapton tapes are used to pre-define areas for plating so that clear coat can be applied to create CRTP regions. So the device structure in the CRCC region is SS/a-Si triple cell/ITO/ Co_3O_4/Ni/Pt. Many sets of PEC electrodes with such a structure were fabricated and studied. The results show that Pt/Ni coated device is more stable than Pt coated device, with an initial STH efficiency of 3.7%. The performance drops down to 50% value after approximately 5 hours of operation. It is interesting to notice that after the sample is kept overnight in dark, the STH efficiency is recovered almost back to its initial value (See Figure 65). This repeats for five consecutive days. The mechanism for the degradation of STH efficiency under light and the recovery of efficiency in dark needs to be further understood.

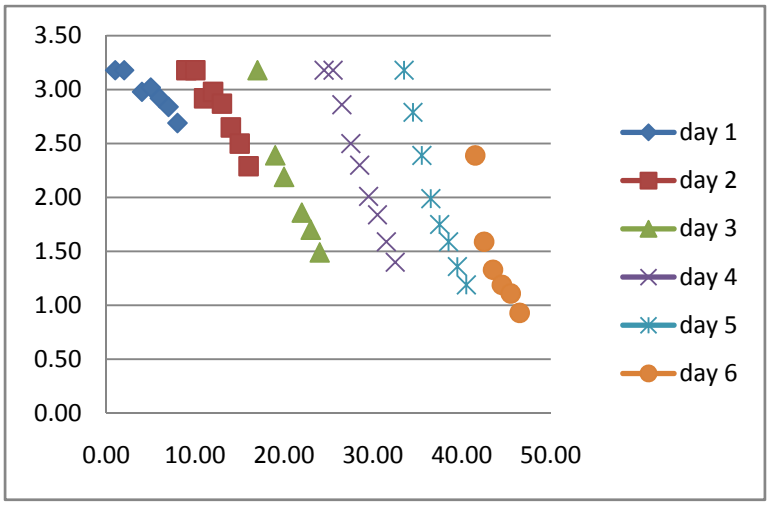

Figure 66: STH efficiency (%) as a function of PEC hydrogen production time (in hours) for a CRCC (electroplated Ni/Pt) / CRTP (ClearCoat) device, showing the recovery of its degradation when the sample is placed in dark.

Development of Co_3O_4 as the CRCC layer

As electroplating an OER catalyst layer exposes the semiconductor under corrosive environment, a vacuum coating process is used to deposit CRCC layer using sputter deposition. In this approach, we explored the use of a thick Co_3O_4 layer as the OER catalyst. Such a thick Co_3O_4 is deposited on top of a thin Co_3O_4 layer. A thick Co_3O_4 layer is acceptable even though its transparency is not high, since only partial area of the device front surface is covered with the thick Co_3O_4 layer. An automotive clear coat, with a thickness of around 0.5 mm, is used as the CRTP layer. A Kapton tape is used to define the areas for clear coat coverage. Alternatively, a sputter deposited SiO_2 layer is used as the CRTP layer. Certain overlap of CRCC and CRTP areas are designed into the process to avoid undercut corrosion.

Specifically, we deposited Co_3O_4 layers with a thickness in the range of 500nm and 1500 nm as the CRCC layer, over the 70nm Co_3O_4 coating that covers all areas, using magnetron sputter deposition with a power density of around 100W over a 3" round sputter target. Various devices with such a Co_3O_4 (CRCC) and Clear Coat (CRTP) combination were fabricated. Initial results show an initial STH efficiency of 3.5% and the performance degraded down to its 50% value after 55 hours. Studies of the degraded samples showing a change of color in the Clear Coat CRTP layer, suggesting the lifetime of the Co_3O_4 layer may be much longer.

In order to have a stable CRTP layer, we used magnetron sputtering process to deposit SiO_2 layer. This is done for both CRCC layers made using electroplated Ni/Pt layers and sputter deposited Co_3O_4 layer. For CRCC (Ni/Pt)/CRTP(SiO_2) combination, the initial STH efficiency is around 3.5%, and the STH efficiency drops to 50% in around 12 hours, representing an improvement from CRCC (Ni/Pt)/CRTP(ClearCoat). It is also observed that the STH efficiency get recovered to 90% of its initial value after the sample is kept in dark overnight.

A device structure with CRCC (Sputtered-Co_3O_4)/CRTP (Sputtered-SiO_2) was also explored. Two approaches were studied: (1) first SiO_2, then Co_3O_4 (the "SiO_2/Co_3O_4" device); and (2) first Co_3O_4, then SiO_2 (the "Co_3O_4/SiO_2" device). Kapton tapes were used to mask out the area during sputtering so that the deposition does not occur in the unwanted areas. The Kapton tapes are applied in such a way to allow certain overlap of Co_3O_4 and SiO_2 layers to avoid undercut corrosion. The Co_3O_4/SiO_2 device shows less durability, with the device fails after around 30 hours of PEC operation. The SiO_2/Co_3O_4 device shows an interesting increase in STH efficiency during the first 250 hours of run time, followed with a drop after 300 hours (Fig. 66). Further studies are needed to understand these observations.

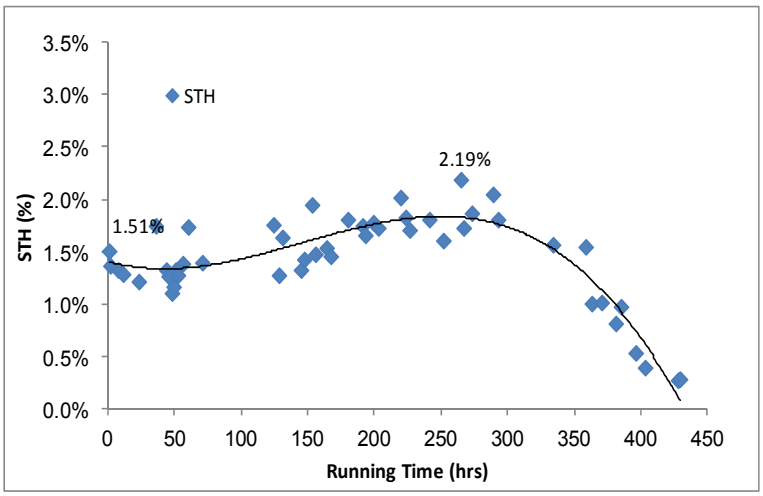

Figure 67: STH efficiency (%) as a function of PEC hydrogen production time (in hours) for a CRTP (SiO2) / CRCC (Co3O4), showing an increase in STH efficiency during the first 200 hours of operation.

Use of TiO_2 as CRTP layer

We have previously investigated TiO_2 as TCCR material. However, the conductivity of TiO_2 limits the performance of PEC device. In this study, TiO_2 is used as CRTP layer, where the conductivity is not a requirement due to the unique CRCC/CRTP design. After various base line depositions on various substrates and various deposition conditions, device with CRCC (Sputtered-Co_3O_4) / CRTP (Sputtered-TiO_2) is fabricated. The device has shown improved stability, with performance at 50% level at ~ 40 hours and with> 1% STH even after 100 hours.

4.8. Substrate type Photoelectrochemical(PEC) modules

The objective of this task is to develop a substrate-type photo-electrochemical cell for hydrogen generation. In such a PEC cell, a triple-junction amorphous silicon photo-electrode deposited on a conducting substrate is integrated into a PEC cell in which the hydrogen and oxygen compartments are both behind the photo-electrode and are separated by a membrane. Areas of research activities include: Development of improved encapsulation materials and process, Optimization of grid configuration and installation process, Investigation of effect of various cell dimensions in the oxidation and reduction compartments, Design of improved membrane holder to prevent hydrogen and oxygen from intermixing, and study of various electrolyte inlet and gas/electrolyte outlet configurations.

Under this task, we have:

- Developed an encapsulation process for substrate-type cells in large area. Figures 67a shows the encapsulation system that MWOE designed, developed and constructed. These encapsulation systems may be used to fabricate substrate-type PEC panels of the sizes of 2ft x 3ft for the mid-size laminator and 3ft x 8ft for the large-size laminator. Figure 67b shows some dummy solar panels (without semiconductor layers) encapsulated using these laminators.
- Developed a grid configuration and installation process, in which a grid pattern was generated using a computer controlled inkjet nozzle mounted on an X-Y stage.

- Fabricated a small-area (4" x 12") substrate-type PEC panel (Figure 67c) that shows a hydrogen generation rate of 5.9 cc/min under 92% sunlight intensity, corresponding to a STH efficiency of 4.3%
- MWOE has also fabricated large area superstrate type PEC modules and constructed a large area outdoor testing center, as shown in Fig. 68.

(a) (b) (c)

Figure 68: (a)Mid-size (2ft x 3ft) and large-area (3ft x 8ft) laminators that can be used for the encapsulation of substrate-type PEC panels; (b) Solar modules (dummy modules without semiconductor coatings) encapsulated using the laminators; (c) Small area (4"x12") substrate-type PEC panel with 5.9 cc/min hydrogen generation rate under 0.92 sun intensity.

Figure 69: Outdoor testing center for superstrate type PEC modules and hydrogen collection setup.

4.9. Atomic Layer Deposition to Make CRCC/CRTP Layers

Our novel PEC device design, as illustrated in Figure 69a, decouples the requirements for transparent conducting and corrosion resistant (TCCR) coatings. This design provides wide selection of CRCC and CRTP materials that have the potential to meet the requirements for PEC cell stability.

Our collaborator South Dakota State University (SDSU) performed optical modeling of the new PEC device design using Macleod Thin Film Optics. The transparent conducting layer underneath the CRTP layer is ITO, which is a standard material in thin film silicon solar cells. ITO has a refractive index about 2.2. Therefore, the CRTP layer would result in low reflectance (hence desirable higher absorption) if its refractive index n meets the condition $n = (n_{ITO} * n_{air})^{1/2} \approx 1.48$. Silicon oxide films have a refractive index close to this value. Thus, the simulation used SiO_2 as the CRTP layer in the novel design and the baseline was a single Co_3O_4 transparent CRCC coating (Fig. 69b). In both structures, the minimum reflectance was designed to be at 550 nm, corresponding to the highest photon flux in the solar spectrum. The simulated reflectance spectra are depicted in Fig. 70. The results show that the novel design can greatly reduce reflection loss; a detailed analysis indicates that the average reduction in reflectance is over 10%. Therefore, even if the CRCC film is not transparent and take up to 10% surface area, the optical absorption will not be lower than the conventional design with a single transparent CRCC layer.

Analyzing the performance of a variety of TCCR coatings we tested previously, we noted that they exhibited similar degradation trend. This phenomenon implies that there might be a common mechanism. We suspect that the pinholes and/or grain boundaries in the sputtering deposited CRCC layer might be the root reason(s). A study we plan to conduct is to use Atomic Layer Deposition (ALD) to fabricate pinhole-free CRCC or TCCR layer. SDSU is establishing an ALD system that will be used to perform this research. Fig. 71 shows images of this ALD system currently under installation, to be used to study the grain growth behavior of the ITO, CRCC, and CRTP films.

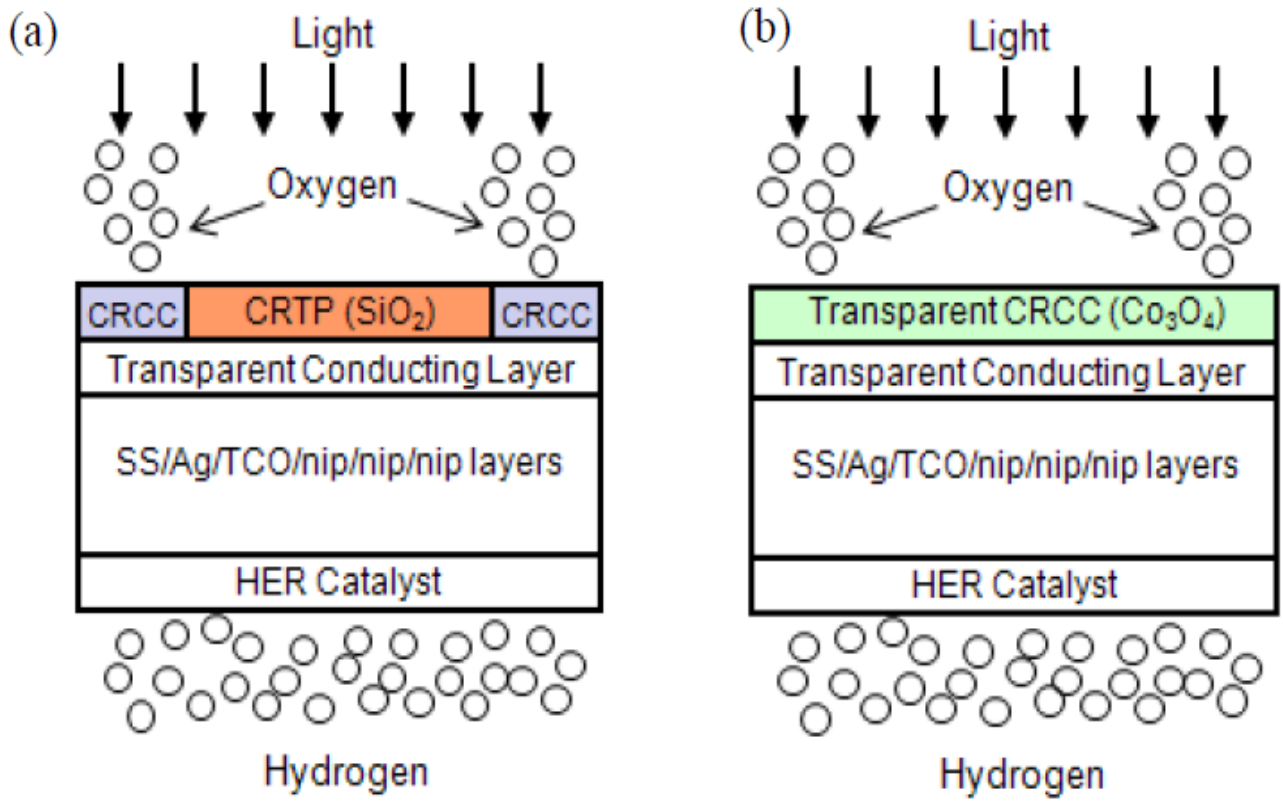

Figure 70: (a) A novel PEC device design that includes separated CRCC and CRTP coatings. (b) A conventional PEC device with a single CRCC layer.

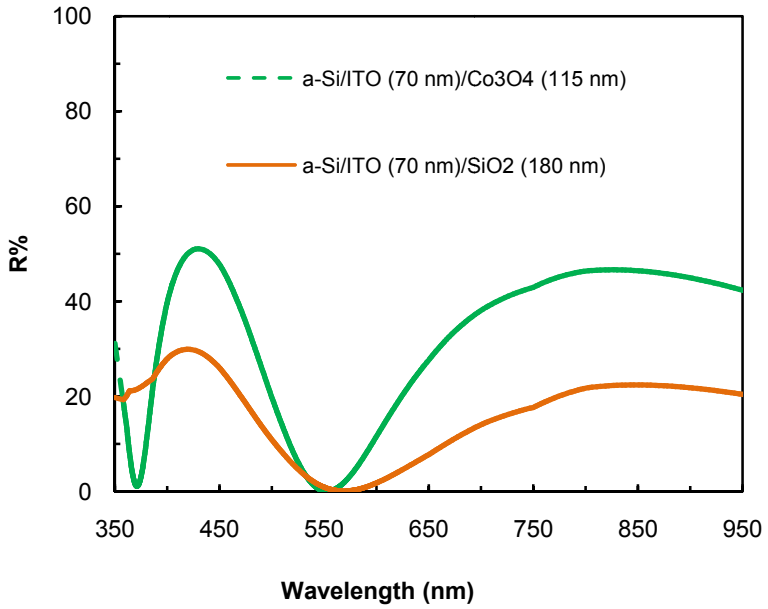

Figure 71: Simulated reflectance spectra of the novel PEC design (e.g. a-Si/ITO/SiO_2) in comparison with conventional device structure (e.g. a-Si/ITO/Co_3O_4)

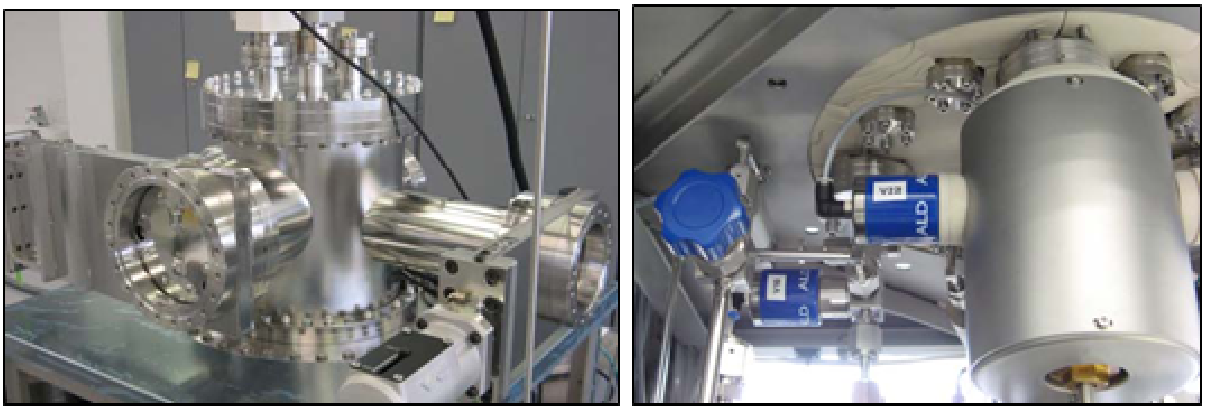

Figure 72: Photograph images of an ALD system under installation at SDSU to be used to grow dense and pin-hole free catalyst and protective layers.

Study of indium tin oxide (ITO) thin film as the TCCR coating

Indium tin oxide is usually used as the transparent and conducting (TCO) top layer of a-Si solar cells. Our earlier studies show that ITO films deposited using a sputter deposition do not show sufficient electrochemical stability in acidic or basic solutions. It is believed that the chemical instability is to some extend associated with the grain boundaries in a ITO material and is therefore dependent on the crystallinity and the structure morphology of the materials. During this period, we studied more fundamental properties of transparent and conducting ITO films in order to gain better understanding of electrochemical stability of ITO films for use as a TCCR layer in a PEC cell.

SDSU group performed comprehensive study on the electronic characteristics and the grain growth process of indium tin oxide (ITO) thin films using high resolution scanning probe techniques, namely electrostatic force microscopy (EFM) and Kelvin probe force microscopy (KPFM). The study focused on the effects of substrate temperature and sputtering gas mixture, two most critical parameters for transparent conductive oxide film growth. Two types of ITO films were compared, which were deposited using radio frequency magnetron sputtering in pure argon or 99% argon + 1% oxygen, respectively.

Figure 72(a-m) shows the corresponding topographic and EFM images of ITO thin films deposited at different substrate temperatures and gas mixtures. At 0% oxygen the films deposited without any substrate heating showed smooth morphology having grain size ranging from 15-25 nm with root mean square (rms) roughness 1.22 nm. With increase in the substrate temperature, both the grain size and rms roughness increased. The average grain size was 35 nm and 47 nm for 150°C and 220°C substrate temperature, respectively. This was primarily due to grain growth promoted by higher temperature as a thermodynamically favored process. However, in the case of 1% oxygen shown in Figure 72 (h-j) the grain growth mechanism observed was quite different. Films grown at room temperature with 1% O_2 showed bigger grain size than the one grown in pure Ar. With increase in the growth temperature the grain size increased but saturated at above 150°C with the average grain size about 37 nm. This was most possibly due to the complete oxidation of the indium tin oxide and the passivated grain boundaries inhibited further growth of the grains.

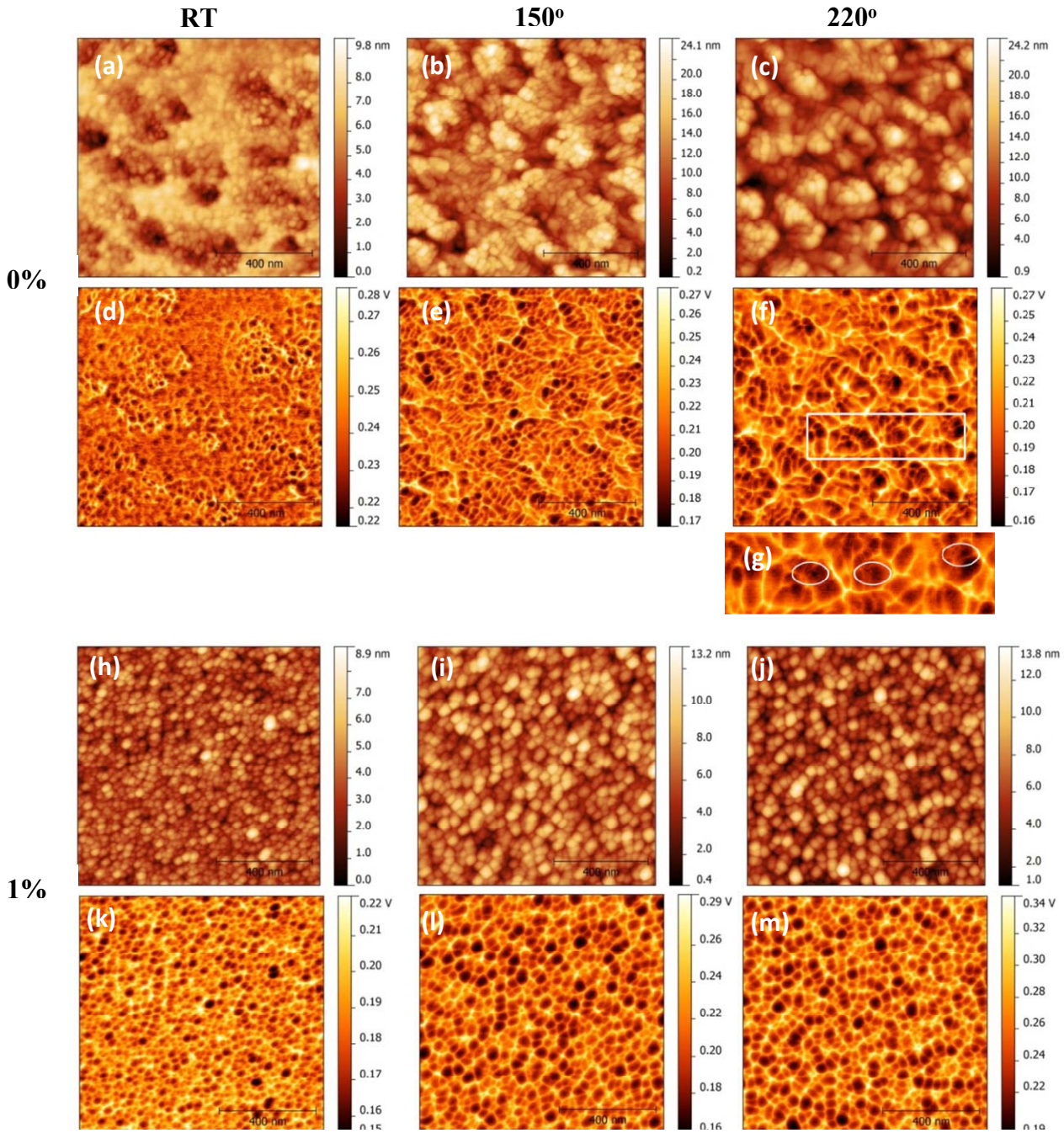

Figure 73: Topography (a-c, h-j) and EFM (d-f, k-m) images of ITO thin films deposited at different concentrations of O_2 and heating temperatures. (g) shows the zoomed in part of (f). The scale bar in each figure is 400 nm.

The EFM images confirmed higher electrostatic force at the grain boundaries in all samples, while the samples prepared with 1% O_2 exhibited still higher electrostatic force than the ones prepared in pure Ar. The grain boundaries were structural defects and hence acted as centers for charge accumulation under local electric field, in this case, when an electrically biased tip was brought closer to the sample. Such grain boundaries were electrically active and acted as potential barriers for charge transport. Hence when the biased tip probed over the grain boundary it

experienced higher coulombic force and therefore an increase in the amplitude of the tip was observed. In the case of films grown at 220°C without introducing oxygen, inactive grain boundaries were seen in Figure 72(g) shown in white circles. These inactive grain boundaries were structural defects but were not electrically active. This was an interesting behavior possibly due to the growth of smaller grains within a bigger grain, which was more thermodynamically relaxed and hence did not act as potential barrier. Such inactive grain boundaries were not observed in other films deposited at different conditions.

Examine the EFM images shown in Figure 72, it was noted that the surface potential difference for the ITO film deposited at room temperature without oxygen was much smaller than the other samples. This raised the uncertainty that whether or not that potential difference represented grain and grain boundary. In order to further understand the micro-structural evolution of the ITO films grown with and without oxygen, KPFM measurement was performed based on the fact that the work function of the grain and grain boundary should be distinct.

Figure 73(a-i) shows the topographic and corresponding KPFM images together with the topography and surface potential line profiles of the ITO thin films deposited in Ar. The room temperature film showed no specific contrast or topographic correlation, indicating highly amorphous nature, which was evidenced from the origin of the sharp peaks in the surface potential profile shown as the blue line in Figure 73(g). These peaks were higher and more frequent than the noise peaks associated with slower servo feedback in the KPFM mode. The above discussed results implied that the ITO film deposited at room temperature without oxygen was dominated by amorphous phase that has high density of surface states. When the growth temperature increased, a distinct correlation between the topography and the KPFM images could be seen. The grains showed a higher surface potential compared to the grain boundaries. In the case of the 150^{o}C samples, the grain boundaries showed an average 25-30 meV surface-potential drop, while in the case of 220^{o}C samples, the potential difference between the grain and grain boundaries reduced to 10-15 meV. Increasing the substrate temperature thereby improved the electronic quality of the grains and grain boundaries. Also the electrically inactive grain boundaries mentioned in the EFM images for the 220^{o}C sample were not seen in the KPFM images, either.

Figure 74(a-i) shows the topographic and corresponding KPFM images together with line profiles of ITO thin films deposited with 1% oxygen. The ITO film grown with 1% oxygen at room temperature showed a specific topographic correlation unlike the room temperature grown film without oxygen gas. This correlation provided evidence of promoted crystallization with the inclusion of oxygen gas in sputtering at low temperatures. All the films showed ~20 meV surface-potential difference between the grain and grain boundary. Relating the topographic and KPFM information it could be deduced that grain growth in ITO occurred through defective interfaces. Both indium oxide and tin oxide were *n*-type semiconductors due to the presence of oxygen vacancies. With the introduction of oxygen gas during sputtering these defects were considerably reduced leading to passivated grains. The passivated grains inhibited further grain growth even at elevated temperatures.

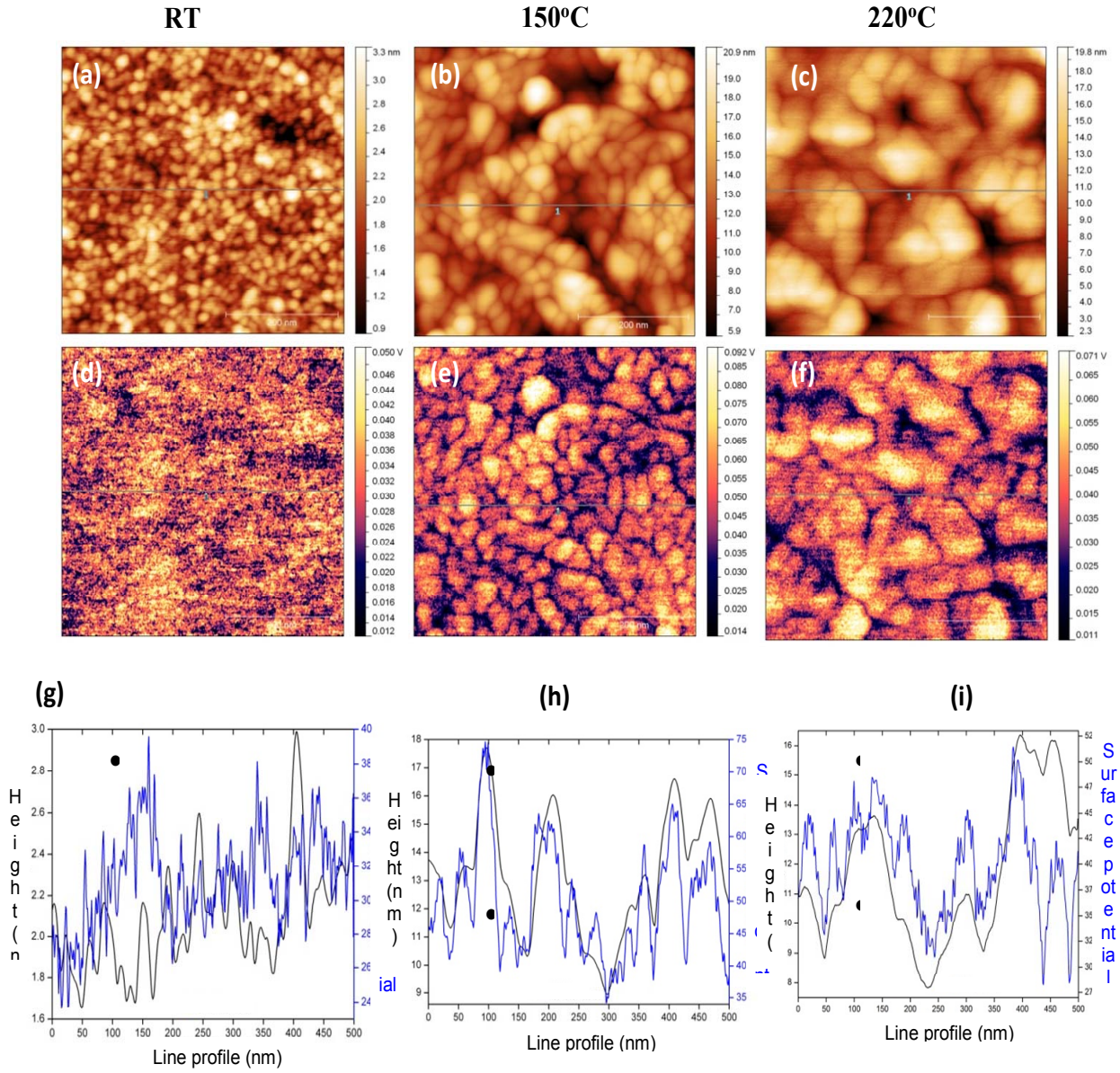

Figure 74: Topography (a-c) and KPFM (d-f) images of ITO thin films deposited with 0% O_2. (g-i) show the coresspoding height and surface potential line profiles in the topographic and KPFM images. The scale bar in each figure is 200 nm.

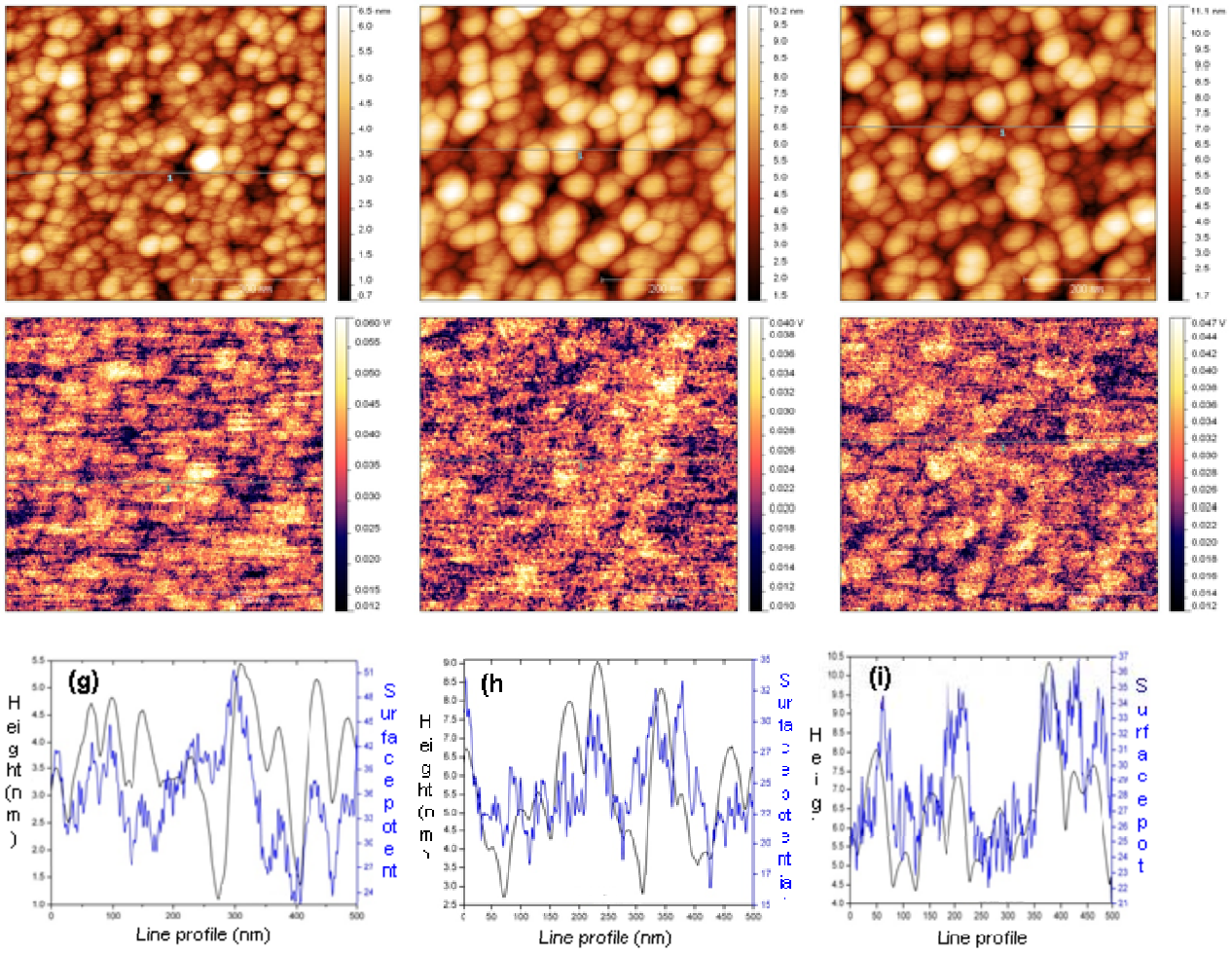

Figure 75: Topography (a-c) and KPFM (d-f) images of ITO thin films deposited with 1% O_2. (g-i) show the corresponding height and surface potential line profiles in the topographic and KPFM images. The scale bar in each figure is 200 nm.

Further the sheet resistance of the ITO films was measured using four point probe method and plotted versus the substrate temperature as shown in Figure 75. In both cases the sheet resistance of the films decreased with the increase in the substrate temperature. The films deposited in Ar showed lower sheet resistance (approximately 10 Ω/□ for 200 nm thick films deposited at 220°C substrate temperature). The films deposited with 1% oxygen showed an order of magnitude higher sheet resistance. In particular, the room temperature deposited sample with 1% oxygen had a sheet resistance in the order of kilo ohms per square and hence was not shown in Figure 75. This sample was expected to have higher carrier mobility than the sample deposited in pure Ar if only considering its crystallinity. Since the electric conductivity was proportional to the product of carrier mobility and carrier concentration, these results implied that oxygen greatly reduced the carrier concentration and/or created significant potential barrier at the grain boundaries. Both EFM and KPFM results indicated that the ITO films deposited in 1% oxygen at 150°C and 220°C had similar grain size and surface potential; the decrease in the sheet resistance

at higher temperature was therefore mainly due to increased crystallinity that promotes carrier mobility.

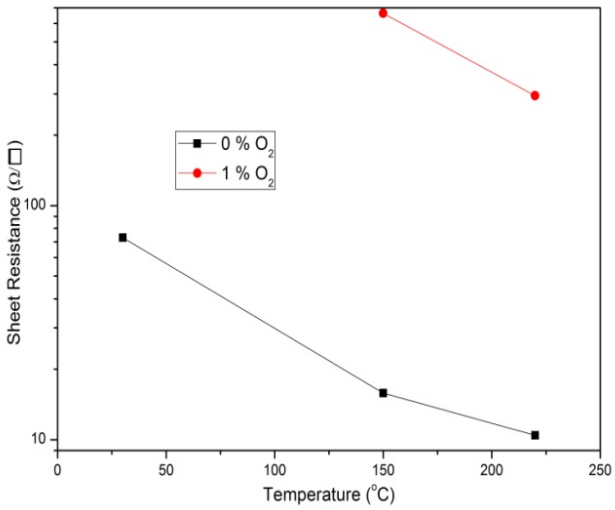

Figure 76: Variation of sheet resistance with substrate temperature**.**

The optical transmittance spectra of the ITO films are shown in Figure 76. The films deposited in pure Ar showed significant blue shift of the transmittance at increased substrate temperature. On the other hand, the films deposited in 1% O_2 exhibited little blue shift when the substrate temperature varied from 25°C to 150°C and further increase the substrate temperature to 220°C did not enhance short wavelength transmittance. Recall the above mentioned EFM and KPFM results regarding the grain size of the ITO films deposited in Ar or 1% O_2, one could conclude that the grain boundaries were responsible for scattering and absorbing the short wavelength light.

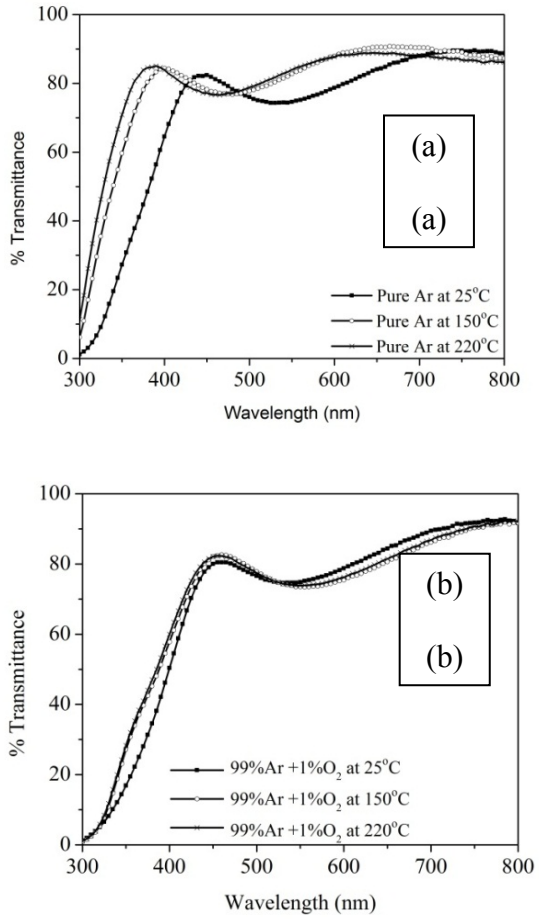

Figure 77: Transmittance spectra of ITO films at different substrate temperatures in (a) pure argon, and (b) 99% argon and 1% oxygen gas environment.

Plasma treatment of transparent conducting oxide thin films

Transparent conducting oxide (TCO) film on top of a-Si solar cell is critical to the PEC cell performance. To improve the conductivity of the TCO films, high-temperature deposition or annealing is generally required. However, this process temperature is limited by the a-Si cell; a low temperature favors the conservation of the solar cell performance. To address this dilemma, we conducted research on using low-temperature plasma to modulate the properties of TCO films. Our hypothesis is that hydrogen plasma can efficiently reduce TCO film and promote the carrier concentration and consequently the conductivity. We also assume that oxygen can eliminate defects and improve transmittance.

Our study included the following steps.

1) Prepare ZnO thin film using a solution process at different temperatures (200°C, 300°C, 400°C, and 500°C).
2) Perform H_2 and O_2 plasma treatment of the samples.
3) Characterize the structure, optical, and electrical properties of the TCO films.

Fig. 77 below shows the transmittance spectra of ZnO films prepared at different temperatures. A noticeable change occurred after 300°C. Further increase the process temperature to over 400°C did not lead to changes in the transmittance.

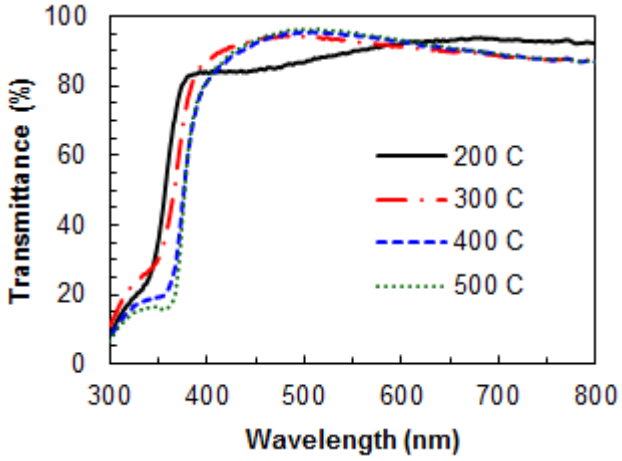

Figure 78: Optical transmittance of ZnO thin films prepared at different temperatures.

Fig. 78 shows the XRD results of the ZnO films prepared at different temperatures. At temperatures below 300°C, the films were almost amorphous. The ZnO (002) peak at 34.320 degree started to appear at 300°C, but is very weak. Once reaching 400°C, the peak became intensive, indicating good crystallinity. In an extreme case of 500°C, the (002) peak was very sharp.

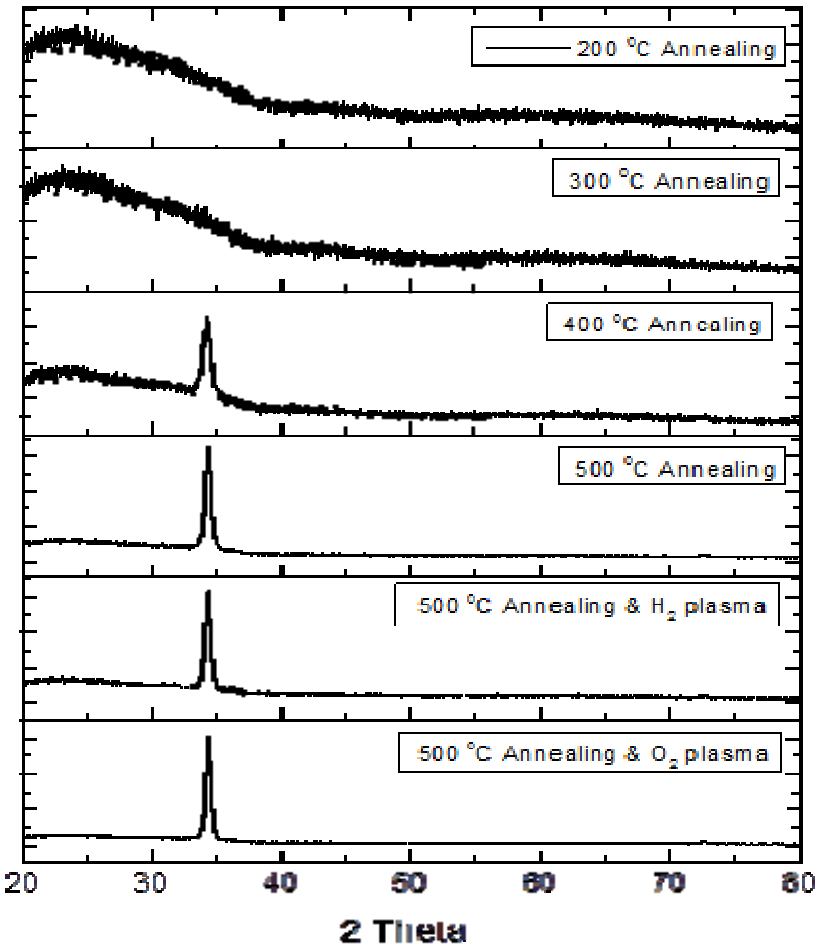

Figure 79: XRD spectra of ZnO thin films prepared at different temperatures and treated with different plasmas.

Treating the ZnO films with hydrogen and oxygen plasmas did not alter the crystallinity. Thus, it was deduced that the plasma treatment only caused small variation in the carrier concentration and defect density.

The optical transmittance spectra (Fig. 79) after the plasma treatment showed interesting variation. Oxygen plasma led to small change in the spectra as compared with the as-deposited ZnO films, while hydrogen plasma caused significant change in the samples prepared at temperatures below 300°C. Our interpretation for these characteristics was that organic precursors still existed in the amorphous ZnO films prepared at low temperatures. Hydrogen plasma reduced the organic precursors, leaving behind carbon in the ZnO films, which therefore had low transmittance. Plasma treatment of TCO films or TCCR films opens a new area of study as many of the films desire to be deposited at higher temperature while the underlying a-Si solar cell material suffer degradation at high temperatures.

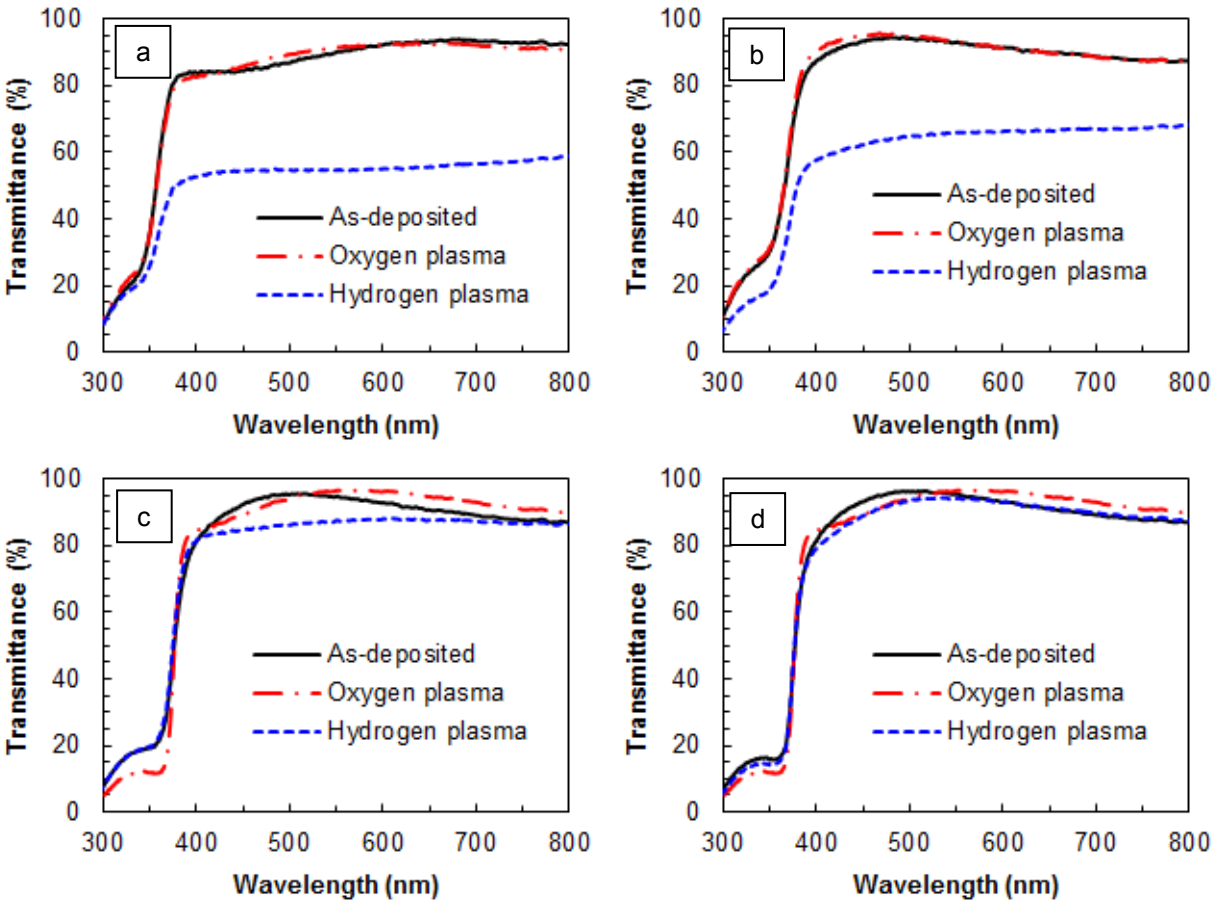

Figure 80: Optical transmittance spectra of ZnO films prepared at different temperatures and treated with oxygen and hydrogen plasmas. (a) 200° (b) 300°C, (c) 400°C, and (d) 500°C.

It is worth noting that the solution-based ZnO thin films required relatively high temperatures that would not be suitable for a-Si solar cells. However, this research provided clear guidance on the roles of different plasmas. It opens a potential research topic that combines a variety of plasma treatment to modulate the TCO film properties. Based on the same principle, the plasma treatment can be readily applied to other TCO films that can be prepared at low temperatures to enhance the conductivity without compromising the transmittance.

4.10. Fabrication of solar cells for collaboration with MIT/Sun Catalytix and JCAP/Caltech

In the device fabrication area, research efforts are focused on two areas: 1) fabrication of wide bandgap a-Si:H single-junction solar cells that is desirable for use as the top junction of a triple-junction photoelectrode; and 2) fabrication of solar cells for collaboration with Nathan Lewis Group at Caltech/JCAP.

In the first area, the effort was in the fabrication of single-junction, wide bandgap a-Si:H solar cells which is desirable for use as the top junction of a triple-junction cell. Process gas, containing a high concentration of hydrogen, mixed with smaller amount of SiH_4 is used. A relatively lower deposition temperature is also used. A p-type nanocrystalline silicon doped layer, made with a process gas mixture of SiH_4, BF_3 and H_2, is deposited on top of the wide-bandgap a-Si:H layer to achieve a high open circuit voltage.

Figure 80 shows I-V curve for such a wide bandgap a-Si:H top-junction component cell. It shows a high V_{oc} of 0.994V, J_{sc} of 9.889 mA/cm^2, FF of 0.656, and an efficiency of 6.44%, without the use of a back-reflector. Such a solar cell is highly desirable for use as the wide-gap top cell in a triple-junction PEC electrode.

We also deposited middle and bottom component cells that would match the performance of the above described wide bandgap top cell. Figure 81 and Figure 82 shows I-V curves for the middle and bottom cells. The middle cell has V_{oc} at 0.806V, J_{sc} at 14.2 mA/cm^2, and FF at 0.613; while the bottom one has V_{oc} at 0.634, J_{sc} at 21.1 mA/cm^2, and FF at 0.586. These high-performance component cells (top, middle and bottom component cells) are expected to form triple-junction photoelectrode with high solar-to-hydrogen conversion efficiency.

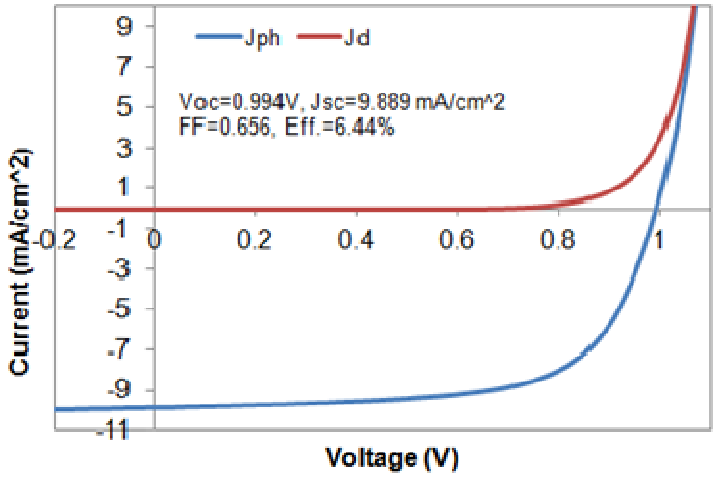

Figure 81: I-V curve for the a-Si top component cell

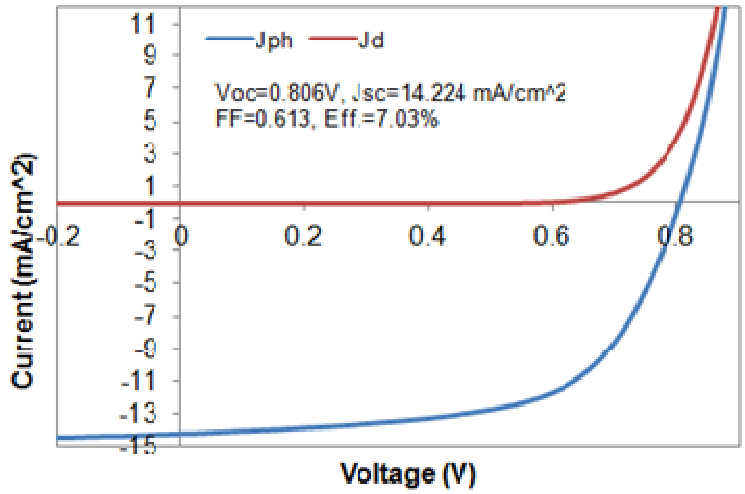

Figure 82: I-V curve for the a-SiGe middle component cell

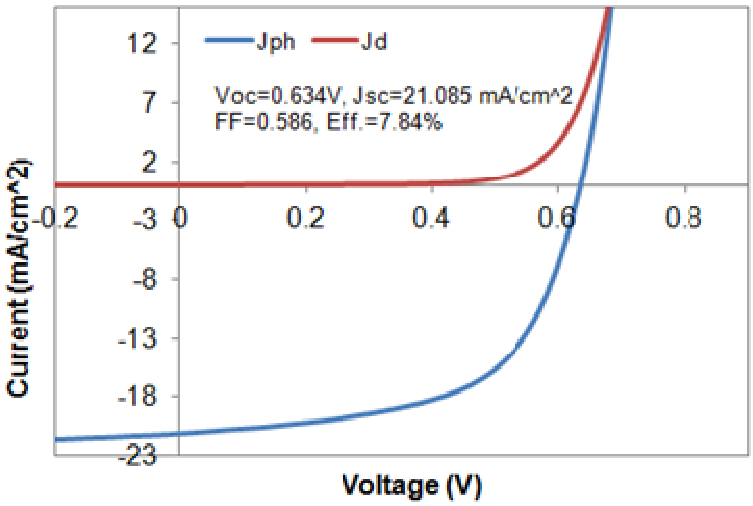

Figure 83: I-V curve for the a-SiGe bottom component cell

Twelve samples, approximately 3.5”x4” in size, were prepared and supplied to Nathan Lewis Group at Caltech for PEC production research. The structure of these solar cells are: SS/Al/ZnO/(a-Si-n)/(a-SiGe (1.4eV)-i)/(nc-Si-p)/ (a-Si-n)/(a-SiGe (1.6eV)-i)/(nc-Si-p)/ (a-Si-n)/(a-Si (1.8eV)-i)/(nc-Si-p)/ITO.

A collaborative research was performed by MWOE, Xunlight, Dr. Dan Nocera's group at MIT and Sun Catalytix. Under this DOE-funded collaboration, MWOE and Xunlight fabricates triple-junction solar cells with the structure of SS/Al/ZnO/(a-Si-n)/(a-SiGe (1.4eV)-i)/(nc-Si-p)/ (a-Si-n)/(a-SiGe (1.6eV)-i)/(nc-Si-p)/ (a-Si-n)/(a-Si (1.8eV)-i)/(nc-Si-p)/ITO. The samples are then treated with a propriatary photo-assisted electrochemical shunt passivation process, which converts the ITO nearby areas with potential electrical shunt into insulator thereby isolating the electrical shunts. Several series of samples were provided to MIT/SunCatalytix for the growth of cobolt oxide and other catalytic materials. It was observed that when proper catalytic materials are coated, the MWOE/Xunlight produced photoelectrodes exhibit high solar-to-hydrogen efficiency and appropriate stability. This collaborative research was published in Science and was highlighted in

Time Magazine as one of the major innovations of the year. The article in Science (29 September 2011 issue) "Wireless Solar Water Splitting Using Silicon-Based Semiconductors and Earth-Abundant Catalysts", describes the development of solar water-splitting cells comprising earth-abundant elements that operate in near-neutral pH conditions, both with and without connecting wires. The MWOE/Xunlight made cells consist of a triple junction, amorphous silicon photovoltaic interfaced to hydrogen and oxygen evolving catalysts made at MIT and SunCatalytix from an alloy of earth-abundant metals and a cobalt|borate catalyst, respectively. The devices described herein carry out the solar-driven water-splitting reaction at efficiencies of 4.7% for a wired configuration and 2.5% for a wireless configuration when illuminated with 1 sun of AM 1.5 simulated sunlight. Fuel-forming catalysts interfaced with light-harvesting semiconductors afford a pathway to direct solar-to-fuels conversion that captures many of the basic functional elements of a leaf. A video of hydrogen production by MWOE/Xunlight produced PEC cell is shown in MIT web site: http://video.mit.edu/watch/the-artificial-leaf-9750/. This video shows a MWOE PEC cell similar to those shown in Fig. 28 above.

Under the "artificial leaf" collaboration, MWOE/Xunlight coated 12 active and functional layers of semiconductor, metal and TCOs, and MIT/SunCatalytix coated OER and HER catalysts layers. This work will not be possible without the major contribution made by MWOE/Xunlight under this DOE-funded program.

4.11. Techno-economic analysis of our PEC system

We have performed the techno-economic analysis of our immersion type PEC system using the H2A model provided by DOE. Below are the assumptions and results of this analysis.

System Description:

We used the H2A spreadsheet to model MWOE's PEC solar hydrogen generation system. The a-Si triple junction PV cells, coated with appropriate corrosion resistant catalysts material and/or protective coatings, are in direct contact with the electrolyte and produce oxygen gas on the anode side and hydrogen gas on the cathode side. As shown in Figure 83 below: circulation pumps are used to maintain electrolyte concentration and to provide filtration. The evolved hydrogen is compressed, water is allowed to condense, and the stream is passed through an intercooler system to provide cool, dry H_2 at 300 psi at the factory gate.

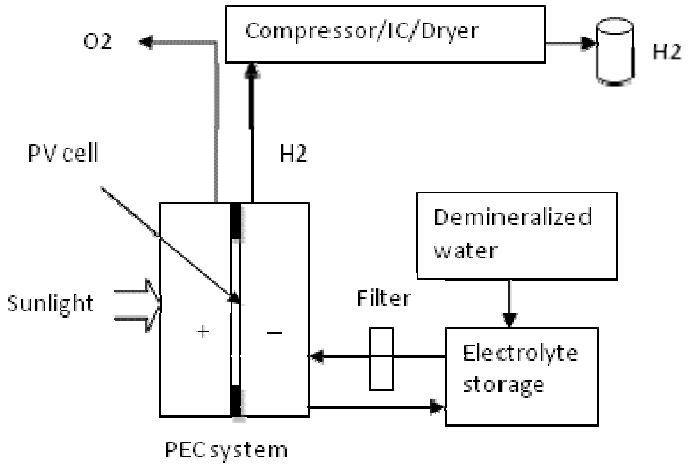

Figure 84: Process flow for H_2 generation

Costs and Assumption:

The current variable manufacturing costs of triple-junction solar cells on stainless steel substrate is in the range of $\$25/m^2$ (assuming full production of a 25MW plant) and many technology improvement roadmap and the use of alternative materials will lead to a reduction of variable manufacturing cost down to about $\$15/m^2$ (with expanded capacity). We expect that the corrosion-resistant catalytic coatings and durable protective layers will add some additional cost, but no more than $\$15/m^2$, for a total PEC electrode cost of < $\$30/m^2$. The electrode will be contained in a polymeric housing. The cost of the housing, electrical terminals, etc. is expected to be approximately $\$10/m^2$, which is a reasonable assumption given the packaging costs of current commercially available PV panels. (For example, current 8% a-Si modules are reported to have a manufacturing cost around $0.5/Watt, corresponding to a panel cost of $\$40/m^2$ for a fully encapsulated and framed panel with junction box and all other functional components).

We anticipate that some electrodes will require refurbishment/catalyst regeneration every

two years, at a cost of $6/m^2 (i.e. 20% of the PEC electrode cost).

We also assume a 10% solar-to-hydrogen conversion efficiency and 1825 hours of standard sunlight per year. Land costs are taken to be $500/acre, and 50% coverage is assumed due to the use of tilt structures. The plant is designed for 1 ton/day (1 TPD) and costs have been scaled to 50 tons/day using a "learning factor" of 0.78 (supported by Williams et al 2007). Balance of system costs are based on Type 3 PEC example system in a report by Directed Technology with a projected reduction in installation costs due to modular design.

Results:

This calculation demonstrates that when scaled upthe 1 TPD system will be able to produce hydrogen at a cost of approximately $5/gge with an electrode lifetime of 2 years before refurbishment. As listed in Table 14, scaling the system by a factor of 50 using a 0.78 learning factor, to 50 TPD, is projected to reduce costs to under $2/gge, thus meeting DOE's goal.

Table 14: H2A Model Parameters and Results

Parameter	Year 3 (1TPD)	Ultimate Case (50 TPD)
Solar to Hydrogen Conversion Ratio	10%	10%
Plant Size	1 TPD	50 TPD
PEC Electrode Cost	$30.00/m^2	$12.80/ m^2
PEC refurbishment/Catalyst Regeneration Cost	$6.00/ m^2	$2.56/ m^2
Catalyst Replacement Schedule	2 years (expected)	2 years
Balance of Plant Cost	$2.8 million	$1.2 million/1 TPD base
Cost of Hydrogen	$4.97/gge	$1.95/gge

Detailed analysis

We have carried out some detailed calculation to study what are the major factors in determining the final hydrogen generation cost. Some more conservative scenarios were studies for a sensitivity analysis. For example, in one of the more conservative approaches, we set the following assumption: the cost of the PEC electrode with catalyst coating is increased to $40/m^2; and the cost of the housing, electrical terminals, etc. is increased to approximately $12/m^2; Land

costs are increased to $3000/acre [Applied Energy 88 (2011) 3524–3531, Ryan Davis, Andy Aden, Philip T. Pienkos], and 50% coverage is assumed due to the use of tilted structures; the balance of system costs such as piping, control system and compressor/ condenser/cooler are widely used industry equipment, and their cost are adapted from the report by Direct Technology [Report to DOE: Techno economic Analysis of Photoelectrochemical (PEC) Hydrogen Production, Submitted by Direct Technologies Inc].

We assumed that refurbishment/catalyst regeneration is scheduled every two years, at an increased cost of $\$8/m^2$ (i.e. 20% of the PEC electrode cost). The plant is designed for 1 ton/day (TPD) and costs have been scaled to 50 tons/day using a "learning factor" of 0.78 (supported by Williams et al 2007).

Using DOE H2A model, the final H_2 production cost is $2.23/gge based on the more conservative assumptions described above. The model calculation had shown that 72.9% of H_2 generation cost is resulted from direct capital cost, and 25.7% from operation and maintenance. The reference year for financial input in DOE H2A model is 2007, the resulting H_2 generation costs is presented in year 2009 US dollars.

As shown in Figure 84 below, the cost of PEC cells accounts for about 37% of total direct capital costs, which is about $2.2M for a plant of 1 TPD production scale. The second most costly item is installation, and most of it is for PEC reactors installation. The installation cost not only depends on the total installed wattage, but also on the number of panels installed. If the STH efficiency is improved by 10%, it is expected that installation cost will drop roughly by 10% because the number of PEC reactors is reduced by 10%. The rest of capital cost allocation is shown in Figure 84.

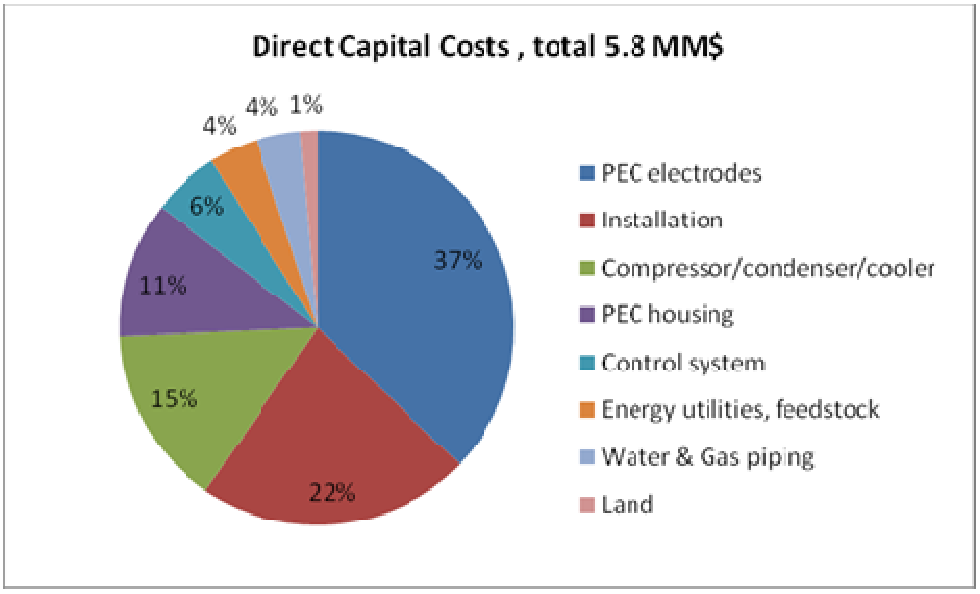

Figure 85: The capital cost allocation for a flat PEC array (for a production scale of 1TPD).

Sensitivity Analysis

We did a sensitivity analysis of hydrogen generation cost based on replacement cost, plant life, installation cost, land, PEC housing and PEC electrodes. As shown in Fig. 85, it seems that

the cost of the PEC cells (including cells and housing) has bigger impact on the Hydrogen generation cost than the replacement schedule and land costs. When PEC electrode cost increases from \$40/m^2 to \$60/m^2, the hydrogen generation cost is increased from \$2.23 to \$2.69 per gge. Therefore it is important to develop PEC electrodes with lower cost. As a part of PEC reactor, PEC housing cost is also critical to lower final cost. Polymeric housing price is expected to be lower than \$12/m^2, with a larger scale plant.

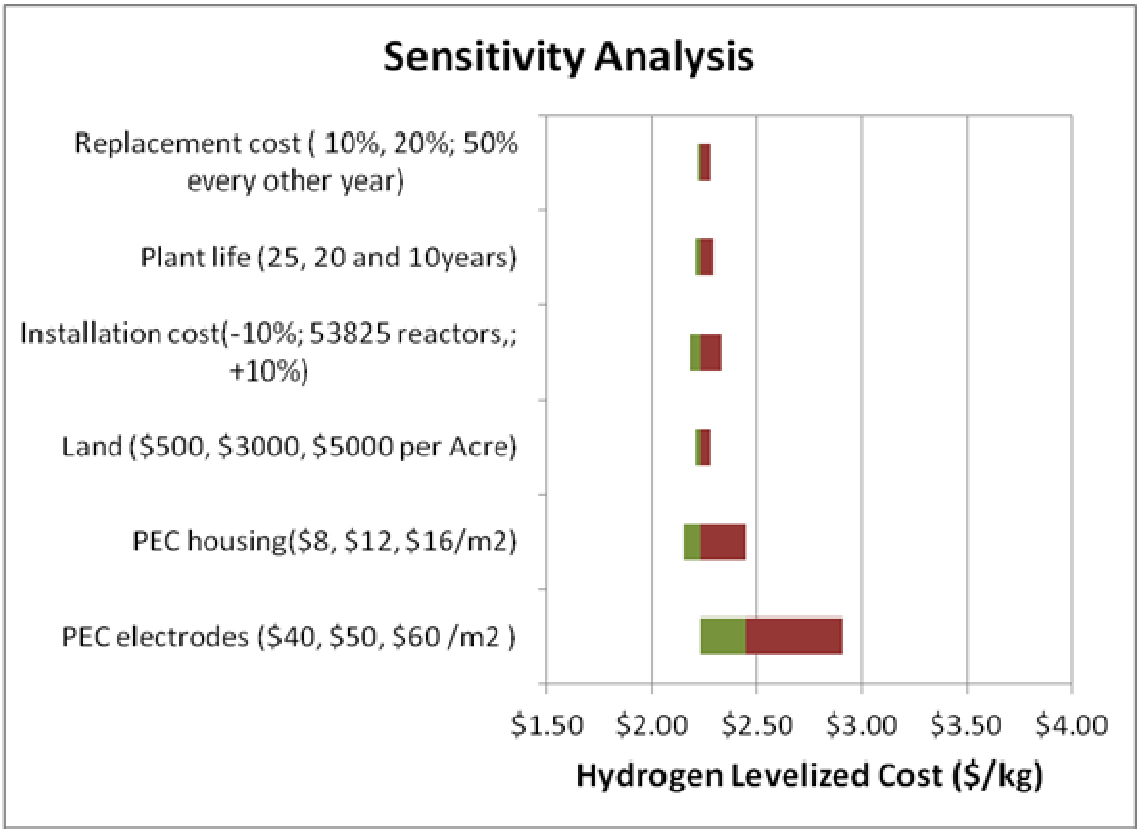

Figure 86: Sensitivity analysis of variable factors on hydrogen generation cost

In summary, we have accomplished the following goals and objectives of this project.

- We have carried out extensive research on TCCR material and developed high quality TCCR materials, for example, Co_3O_4, with extended stability up to 1,000 hours; it can be deposited at 250 °C or lower; at 70nm, it has a transparency ≥ 90%, and a voltage drop ≤0.15V across the TCCR layer for the TCCR/PV-cell stack under typical PEC device operating conditions.
- We have carried out extensive research on the hydrogen generation and oxygen generation catalyst materials and developed highly promising catalyst material.
- We have developed procedures for the fabrication of PEC cells from production-grade a-Si triple junction solar cells. We were able to achieve an initial direct Solar-to-Hydrogen (STH) conversion efficiency of 5.7%, which is, to the best of our knowledge,

the highest ever achieved for direct STH efficient for PEC system made using low cost thin film materials without electrical bias.

- We have successfully transferred the sputtering method to coat Co_3O_4 on solar cells from lab to a proto-type 2 MW roll-to-roll production machine and were able to make PEC electrode on a 91cm wide web.
- We have designed various types of immersion-type PEC modules, with electrode size vary from 2"x2" to 4"x4"; and carried out extensive outdoor testing.
- Using Department of Energy (DOE)'s H2A model, we have performed preliminary techno-economic analysis of the immersion-type PEC system based on the concept design. The result indicates that with 50 TPD production scale, generation cost of $2/gge is achievable.
- During the course of this project, four PCT patent applications and two provisional patent applications have been filed.
- We have worked with many outside industry and university labs, contributed triple-junction solar cells for the collaborative PEC research, and provided technical support to facilitate the progress of the overall PEC field.
- We have studied immersion type PEC cells in which one of the voltage-generating junctions is a semiconductor-electrolyte rectifying junction, which is deposited on two semiconductor junctions to produce sufficient voltage for water splitting.
- We have studied substrate-type PEC cells in which only the SS substrate was in direct contact with electrolyte.